

## ABSTRACT

Title of Document: A HYBRID TESTING PLATFORM FOR  
REALISTIC CHARACTERIZATION OF  
INFRASTRUCTURE SENSOR  
TECHNOLOGY

Michael William Mercado,  
Master of Science, 2011

Directed By: Professor Yunfeng Zhang, Department of Civil  
and Environmental Engineering

In America's transportation infrastructure, maintaining safe and serviceable bridges is of paramount importance to America's transportation officials. In order to meet the increasing demands for information-based maintenance and repair of civil infrastructures such as highway bridges, an increasing number of structural health monitoring sensors and other non-destructive evaluation (NDE) devices have begun to be implemented on these structures. Before these health monitoring sensors can be implemented on a large scale, they must first be validated and characterized in a controlled environment. This thesis proposes and demonstrates the use of a hybrid testing platform to create a more realistic testbed to evaluate these structural health monitoring sensors for steel bridges. The details of this hybrid testing platform are discussed including the effects of ramp time, stress level, complexity of the virtual model, fatigue, and high temperature testing. The accuracy and practical implementation of this hybrid testing platform are also addressed.

A HYBRID TESTING PLATFORM FOR REALISTIC CHARACTERIZATION OF  
INFRASTRUCTURE SENSOR TECHNOLOGY

By

Michael William Mercado

Thesis submitted to the Faculty of the Graduate School of the  
University of Maryland, College Park, in partial fulfillment  
of the requirements for the degree of  
Master of Science  
2011

Advisory Committee:  
Professor Yunfeng Zhang, Chair  
Professor Chung C. Fu  
Professor M. Sherif Aggour  
Dr. Y. Edward Zhou

© Copyright by  
Michael William Mercado  
2011

# Dedication

To my loving parents: Bill and Janice Mercado  
and my siblings: Christopher, Ryan and Caitlin.



## **Acknowledgements**

The research performed in this thesis was supported and funded through the Eisenhower Fellowship Program through the Federal Highway Administration and Civil Engineering Department at the University of Maryland

My sincerest gratitude goes to Dr. Yunfeng Zhang, my research faculty advisor, for his constant advice, encouragement, and direction throughout the course of this research.

Special thanks also goes to Linjia Bai and Zhou Changjiang for their time and help in constructing the test setup.

Thank You

# Table of Contents

Dedication .....	ii
Acknowledgements.....	iii
Table of Contents .....	iv
List of Tables .....	v
List of Figures.....	vi
Chapter 1: Introduction.....	1
1.1 Problem Statement.....	1
1.2 Hybrid Testing .....	2
1.3 Fatigue in Steel Girder Bridges.....	4
1.4 Research Objective .....	6
1.5 Outline of Thesis.....	7
Chapter 2: Prototype Structure.....	8
2.1 Yellow Mill Pond Bridge.....	8
2.2 Test Specimen Details.....	9
2.3 Weigh In Motion Data .....	12
2.4 Loading Models .....	13
Chapter 3: Hybrid Testing Methodology.....	26
3.1 General Description .....	26
3.2 Virtual Component.....	29
3.3 Physical Component .....	35
3.4 Loading the Prototype Structure .....	37
3.5 Openfresco .....	40
Chapter 4: Hybrid Testbed for Sensors Characterization .....	48
4.1 Overview .....	48
4.2 Hybrid Testing Results .....	49
4.3 Ramp Time.....	62
4.3 Model Type.....	70
4.4 Force Level .....	75
4.5 Experimental Drift .....	79
4.6 Step and Ramp Loading of the Dead Load .....	84
4.7 High Temperature Testing .....	88
Chapter 5: Conclusion and Future Work .....	126
5.1 Conclusions.....	126
5.2 Future Work.....	129
Appendix A: WIM Data.....	131
Appendix B: MATLAB Code.....	133
Appendix C: Derivation of Scale Factors .....	137
Bibliography .....	141

## List of Tables

Table 3- 1: Comparison of Actual to Virtual Models.....	32
Table 4- 1: Comparison of Stiffness from Hysteresis Plots.....	53
Table 4- 2: Test Duration for Truss Model at Various Ramp Times.....	65
Table 4- 3: Test Duration for Refined Mesh Model at Various Ramp Times .....	68
Table 4- 4: Max Force and Deflection for Each Model Type.....	74
Table 4- 5: Summary of Max Force and Displacement at Various Loading Factors .	77
Table 4- 6: Experimental Drift for Various Model Types .....	82

## List of Figures

Figure 1- 1: Typical Fatigue Crack in Steel (Fisher, 1998) .....	5
Figure 2- 1: Rounded Cover Plate End for Yellow Mill Pond Bridge (Fisher, 1981)	16
Figure 2- 2: Fatigue Cracks at Cover Plate Detail (Fisher, 1981) .....	16
Figure 2- 3: Test Specimen Design Drawing.....	17
Figure 2- 4: Completed Test Specimen .....	18
Figure 2- 5: Test Specimen During Arc Welding.....	18
Figure 2- 6: Close-up of Test Specimen Weld.....	19
Figure 2- 7: Attachment Head.....	20
Figure 2- 8: Combined Test Specimen and Attachment Head .....	21
Figure 2- 9: Assembled Test Specimen .....	22
Figure 2- 10: Day 1 Yellow Mill Pond Bridge Weight in Motion Data.....	22
Figure 2- 11: Day 2 Yellow Mill Pond Bridge Weight In Motion Data.....	23
Figure 2- 12: Day 3 Yellow Mill Pond Bridge Weight In Motion Data.....	23
Figure 2- 13: Average Yellow Mill Pond Bridge Weight In Motion Data.....	24
Figure 2- 14: AASHTO Fatigue Truck (AASHTO, 1990).....	24
Figure 2- 15: Laman and Nowak Fatigue Truck (Laman and Nowak, 1996).....	25
Figure 2- 16: Yellow Mill Pond Discrete PDF and CDF.....	25
Figure 3- 1: Schematic illustration of Hybrid Testing scheme .....	42
Figure 3- 2: Girder Plan View Showing Virtual and Physical Components .....	42
Figure 3- 3: Schematics of Hybrid Testing Software Framework .....	43
Figure 3- 4: Virtual Model #1: Truss Element Model (Elevation View) .....	43
Figure 3- 5: Quad Element (Mazzoni, 2009).....	44
Figure 3- 6: Virtual Model #2: Quad Element Model .....	44
Figure 3- 7: Interface between Lower Flange and Cover plate (Takamori, 2000) .....	45
Figure 3- 8: Test Specimen (Physical Component) .....	45
Figure 3- 9: Sample Load History for Node 4 .....	46
Figure 3- 10: Individual Truck Loading .....	46
Figure 3- 11: Complete Loading History.....	47
Figure 3- 12: OpenFresco Flow Diagram (Schellenberg, et al., 2009).....	47
Figure 4- 1: Yellow Mill Pond Bridge Physical Test Specimen.....	94
Figure 4- 2: Strain Gage Locations on Test Specimen .....	94
Figure 4- 3: Force Applied to Test Specimen During Hybrid Test .....	95
Figure 4- 4: Close-up of Loading from Single Fatigue Truck.....	95
Figure 4- 5: Hysteresis of Physical Test Specimen .....	96
Figure 4- 6: Hysteresis of Test Specimen in OpenSees.....	96
Figure 4- 7: Hysteresis of Purely Virtual Finite Element Model.....	97
Figure 4- 8: Force Scaling Between Physical and Virtual Components.....	97
Figure 4- 9: Location of Midspan Deflection and Test Specimen in Virtual Model..	98
Figure 4- 10: Midspan Deflection of OpenSees Model .....	98
Figure 4- 11: Comparison of Virtual to Experimental Force Results.....	99

Figure 4- 12: Comparison of Virtual to Experimental Deflection Results .....	99
Figure 4- 13: Comparison of Strain to Force Measurements.....	100
Figure 4- 14: Strain Gage Force versus Measured Force .....	100
Figure 4- 15: Truss Model Force History for 0.1 Second Ramp Time.....	101
Figure 4- 16: Comparison of Ramp Times for Truss Model .....	101
Figure 4- 17: Truss Model Total Time to Complete Test vs. Ramp Times.....	102
Figure 4- 18: Refined Mesh OpenSees Model.....	102
Figure 4- 19: Refined Mesh Model Force History for 0.1 Second Ramp Time .....	103
Figure 4- 20: Comparison of Ramp Times for Refined Mesh Model.....	103
Figure 4- 21: Comparison of Oscillations at Different Ramp Times.....	104
Figure 4- 22: High Oscillations at Ramp Time of 0.02 Seconds .....	104
Figure 4- 23: Force Instability at Ramp Time of 0.01 Seconds.....	105
Figure 4- 24: Refined Mesh Model Total Time to Complete Test vs. Ramp Times	105
Figure 4- 25: Truss Model Force History .....	106
Figure 4- 26: Truss with Mass Model Force History.....	106
Figure 4- 27: Refined Mesh Model Force History.....	107
Figure 4- 28: Refined Mesh with Mass Model Force History .....	107
Figure 4- 29: Mass Effects on the Force Histories .....	108
Figure 4- 30: Truss Model Midspan Deflection .....	108
Figure 4- 31: Truss with Mass Model Midspan Deflection.....	109
Figure 4- 32: Refined Mesh Model Midspan Deflection.....	109
Figure 4- 33: Refined Mesh with Mass Model Midspan Deflection .....	110
Figure 4- 34: Mass Effects on the Deflection History .....	110
Figure 4- 35: Comparison of Max Midspan Deflection for Each Model Type .....	111
Figure 4- 36: Test Setup with Supporting W-Beam .....	111
Figure 4- 37: Force History Comparison at Different Scale Factors .....	112
Figure 4- 38: Max Force vs Scale Factor.....	112
Figure 4- 39: Displacement History Comparison at Different Scale Factors .....	113
Figure 4- 40: Max Displacement vs Scale Factor.....	113
Figure 4- 41: Displacement Response to 30 Constant Trucks for Truss Model.....	114
Figure 4- 42: Max Displacement for Truss Model at Constant Loading.....	114
Figure 4- 43: Disp. Response to 30 Constant Trucks for Refined Mesh Model.....	115
Figure 4- 44: Max Displacement for Refined Mesh Model at Constant Loading ....	115
Figure 4- 45: Strain History for 30 Constant Trucks for Truss Model .....	116
Figure 4- 46: Strain History for 30 Constant Trucks for Refined Mesh Model .....	116
Figure 4- 47: Max Strain Truss Model at Constant Loading.....	117
Figure 4- 48: Max Strain Refined Mesh Model at Constant Loading .....	117
Figure 4- 49: Effect of Ramp Loading on Truss Model .....	118
Figure 4- 50: Closeup of Ramp Loading for Truss Model .....	118
Figure 4- 51: Effect of Instantaneous Dead Loading on Model with Mass.....	119
Figure 4- 52: Effect of Ramp Loading on Model with Mass.....	119
Figure 4- 53: Close-up of Ramp Loading on Model with Mass .....	120
Figure 4- 54: Environmental Chamber Front View .....	120
Figure 4- 55: Environmental Chamber with Front Door Removed.....	121
Figure 4- 56: Heat Control System for Environmental Chamber .....	121
Figure 4- 57: Air Circulation Vent in Environmental Chamber .....	122

Figure 4- 58: Force in Test Specimen as Temperature Increases .....	122
Figure 4- 59: Effect of Temperature on Force Applied .....	123
Figure 4- 60: Close-up of Temperature Effect on Force History.....	123
Figure 4- 61: Location of Strain Gages in Environmental Chamber .....	124
Figure 4- 62: Strain Gage Readings as Temperature Increases .....	124
Figure 4- 63: Effect of Temperature on Strain Data .....	125

# Chapter 1: Introduction

## *1.1 Problem Statement*

In America's vast infrastructure, maintaining safe and serviceable highways and bridges is of paramount importance to America's civil engineers. Many of the structures and facilities in this infrastructure network were constructed several decades ago and now require substantial monitoring and maintenance to ensure that these structures continue to function safely. This is evident through the American Society of Civil Engineers, which estimates that \$10.5 billion is spent annually to repair and maintain bridges (ASCE report card 2009). In order to meet this increasing demand to monitor these structures, a wide variety of health monitoring sensors are beginning to be employed throughout these structures.

While the use of structural health monitoring (SHM) techniques to assess the condition of structures is still in its infancy, a wide variety of sensors are beginning to be used on several high profile structures throughout the United States such as the Golden Gate Bridge (Koerner, 2003; Kim, 2007). With the advancement in micro-electronic-mechanical-system (MEMS) and wireless sensor technology, the costs to manufacture and implement SHM systems has decreased and has led to the possibility of widespread use of such SHM systems throughout America's infrastructure network (Chang, 2003).

Before sensors for SHM can be implemented on a large scale, they must first be validated, characterized and calibrated in well-controlled lab environment. Salt

spray, large environmental temperature variation, corrosion, and moisture are all potential factors that may impact the performance of a sensor during its lifespan; as such the performance characteristics of these sensors must be realistically evaluated before they can be implemented in the field. The sensor data collected from such characterization tests also provide essential information for structural condition diagnosis and prognosis for predicting remaining useful life of infrastructures. However, currently, there is very few (if there is any) reported testbed for evaluating and characterizing infrastructure sensors in a well-controlled load environment that can simulate the traffic-induced load actions realistically.

Often these sensors are directly placed in the field and evaluated based on how they perform to actual field and load conditions. The advantage of this method of evaluation is that the real loads encountered in the field are applied, however, this method of evaluation lacks control over test variables that exists in a controlled lab environment and as such the test results are often confusing because of environmental noise and too many influencing factors. A hybrid testing technique offers the potential for a realistic controlled lab setting in which realistic loading and environmental conditions are applied. Thus, a hybrid testing platform presents a promising facility for realistically assessing and characterizing SHM sensors.

## ***1.2 Hybrid Testing***

The conventional method to test large scale structural systems has been to fabricate the large structural components or subassemblies and test these elements in a large-scale structural testing facility. For example: To evaluate the fatigue behavior of a steel girder cover plate, the entire girder with cover plate would be fabricated and

then tested in a large-scale testing setup. While this method of testing may be appropriate for validating certain components of the structure, it is very costly as an entire structural assembly must be fabricated and tested. Furthermore, large structural testing facilities are limited to a small number of locations across the United States in the sense of equipment and technician capabilities.

In some structural problems, there may exist a small portion of the structure that cannot be readily modeled using the geometries and mechanics of materials for the structural elements. For example: welded connections, repaired sections, connections and fuse elements for seismic resistance would be difficult to model without physical testing. However, larger, simpler components in the structural system such as W-beams, truss members, and columns are relatively easy to model based on the mechanics of these members. Since the behavior of many simpler structural elements in the system is well known, while the behavior of some complex components of the structure such as welded connections is difficult to predict, why test the whole structural system when it is only a small portion of the structural system whose behavior is unknown?

The hybrid testing method presents an alternative testing technique to the conventional large scale structural testing method. The hybrid testing method involves physically testing the portions of a structure whose behavior is difficult to model such as a welded connection or repaired section, while modeling/simulating the remainder of the structure. During testing the loads are specified in the simulated model, transferred and physically applied to the test specimen (welded connection, repaired section, etc.), and the response of this test specimen is then fed back to the

simulated model of the entire structural system. Thus the hybrid testing technique presents the possibility of large scale structural testing without having to fabricate large portions of the structure. Another advantage of hybrid testing is the ability to apply any arbitrary form of external load to the concerned structure.

Since the hybrid testing method is ideal for testing large-scale components in a complex structural system, it presents the ideal platform for characterizing and validating sensor technology for SHM. Furthermore, since the physical testing portions of the hybrid testing technique are conducted in a laboratory setting, certain characteristics of the tested sensors can be evaluated by controlling certain variables in the lab. This presents the possibility for evaluating sensors in different environmental conditions (hot and cold temperature, humidity, salt spray, etc.) during the testing process. Overall, the hybrid testing method provides a platform for developing a testbed for testing large-scale structural components under realistic load conditions and evaluating SHM sensors. A more detailed description of the hybrid testing method can be found in Chapter 3 titled “Hybrid Simulation Methodology”.

### ***1.3 Fatigue in Steel Girder Bridges***

One of the major concerns in aging steel highway girder bridges is the development of fatigue cracks in the steel girders. Fatigue is a progressive, localized failure as the result of repeated stresses at levels that are usually far less than the tensile strength of the material (ASM, 1975). Typically after several decades of repeated stresses caused by thousands of loading and unloading cycles, fatigue cracks begin to form in fatigue critical regions of steel girders. For highway bridges, this constant loading and unloading is caused by the passage of trucks across the bridge.

AASHTO estimates that over the 75 to 100 year life of a bridge, over 100 million trucks pass over these highway bridges (AASHTO Fatigue Specifications, 1990).

The fatigue growth of a structural element has three phases. The first is the crack initiation by initial fatigue damage. This is followed by the propagation of the crack as the member continues to be loaded and unloaded. Finally, after a sufficient number of load cycles, the member fractures (Boresi, 2003). A typical image of a fatigue crack can be seen in the figure below:

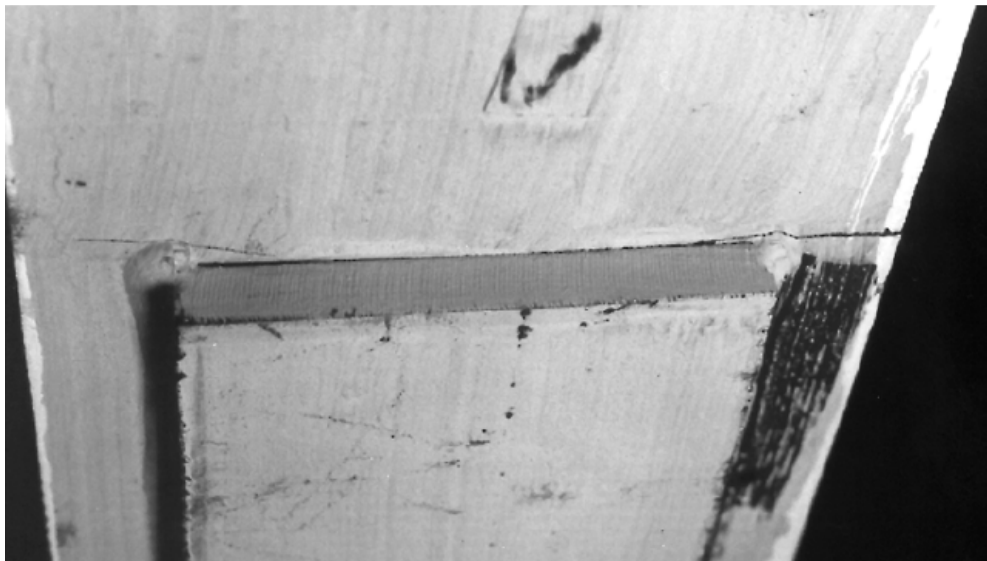


**Figure 1- 1:** Typical Fatigue Crack in Steel (Fisher, 1998)

The crack initiation begins at locations where inherent defects in the steel are formed in the fabrication or installation process. Within the microstructure of the steel, micro-cracks exist, which after a large number of stress cycles grow in size until they are visible to the human eye. These fatigue cracks can also be formed by discontinuities in the welded portions of a steel structure. Groove welding or fillet welding that does not fully penetrate the steel plates they are joining or if a lack of fusion occurs between the weld materials can cause discontinuities in the weld which can later develop fatigue cracks after many loading cycles (Fisher, 1998).

In order to identify fatigue in existing steel bridges, inspection of steel highway girder bridges is typically conducted on a biennial basis and is limited to hands on inspection of the visible portions of the bridge. Since the inspections are biennial, after a fatigue crack forms on a steel girder, it can be several months before an inspection crew identifies the crack (Dexter, 2005). However, the use of SHM system with online sensors presents the possibility to continuously monitor steel girders between regular inspection cycles.

Conventional testing of structural elements for fatigue usually involves large scale fabrication of the structural elements (such as fabricating entire W-beams) due to scale sensitivity and loading these elements using a repetitive constant amplitude sinusoidal force for thousands of load cycles. While this method of testing may be appropriate for evaluating a large structural subassembly with several fatigue details, it is not cost-effective if the primary goal is to validate and characterize sensors such as for fatigue detection. Furthermore, the conventional fatigue test of a repetitive constant amplitude load does not accurately simulate the actual variable loads on the structure. An alternative approach to validate and characterize fatigue sensors would be to use a hybrid testing platform where the large scale components with fatigue details from the structure of interest would need to be fabricated. Furthermore, hybrid testing presents the possibility of simulating more realistic loading and environmental conditions through testing in a controlled lab environment.

#### ***1.4 Research Objective***

The goal of this research is to demonstrate how a hybrid testing platform can be utilized to validate and characterize sensors, particularly for SHM purpose. This

hybrid testing platform will be demonstrated on a typical highway steel girder bridge with cover plate fatigue detail. An existing bridge with known structural defects that required structural health monitoring will be modeled and utilized in demonstrating the hybrid testing platform. Various parameters involved in the hybrid testing method will be evaluated including the effects of hydraulic ramp time, stress level, fatigue loading, and complexity of the virtual model. Finally, it will be demonstrated through the controlled lab environment in the hybrid testing how sensors can be validated under various environmental conditions by using a temperature chamber.

### ***1.5 Outline of Thesis***

This thesis has been organized into five chapters beyond this introduction. Chapter 2 will describe the prototype structure used in the hybrid testing and the actual existing bridge and load history this prototype was modeled after. Chapter 3 will discuss the general methodology of the hybrid testing technique and how the prototype structure is simulated using the hybrid testing method. Chapter 4 will describe the experimental setup and results for the hybrid testing of the Yellow Mill Pond Bridge, the parametric study of the parameters used in the hybrid testing, and the controlled environment testing results for validating sensors under various environmental conditions. Finally, the conclusions and future work will be presented in Chapter 5.

## **Chapter 2: Prototype Structure**

### ***2.1 Yellow Mill Pond Bridge***

To demonstrate implementing the hybrid testing method to develop a testbed for evaluating structural health monitoring (SHM) techniques and sensors, an existing bridge with known fatigue details was selected as a prototype structure for this study and portions of the bridge was fabricated for the test specimen in the hybrid testing. The existing bridge that this prototype structure was modeled off of is the Yellow Mill Pond Bridge in Bridgeport, Connecticut. The Yellow Mill Pond Bridge carries the Connecticut Turnpike (I-95) and was constructed in 1958. The bridge carries three lanes of traffic in each direction and consists of 14 simple spans that typically have lengths of 100 feet. Given the major interstate traffic that travels over this bridge, the girders of the bridge are subject to constant loading and unloading cycles from thousands of trucks on a daily basis.

All of the girders used throughout the Yellow Mill Pond Bridge are hot-rolled WF-beams with cover plates on both the compression and tension flanges. What is unique about these cover plates, however, is the end details. All cover plate ends on this bridge are not tapered but rather have corners that are rounded to a radius of 3" (see Figure 2-1 at the end of this chapter).

Since the ends of the cover plates on the Yellow Mill Pond Bridge were rounded instead of being tapered, large stress concentrations built up at the weld toe at the ends of the cover plate. Given the high volume of truck traffic on this bridge,

this girder configuration made it possible for fatigue cracks to form at the toe of these welds. Bridge inspections in 1970 showed that fatigue cracks had formed at twenty-two of the cover plate details at the location of the weld toe (Fisher, 1981). Many of these fatigue cracks had even propagated into the lower flange and web of the rolled W-beam sections (see Figure 2-2). After discovering the fatigue cracks in these cover plates, several of the beams were replaced and all of the cover plate welds were retrofitted in 1976 using air hammer peening and gas tungsten arc remelting (Takamori, 2000).

After the fatigue cracks were found on the Yellow Mill Pond Bridge, strain gauges were subsequently installed on the girders. As a result, a large amount of data was collected on the stress ranges these girders encountered. Due to the fatigue crack prone weld details and large amounts of strain data collected, the Yellow Mill Pond Bridge is an excellent candidate for demonstrating the use of the hybrid test method for evaluating SHM techniques and sensors on steel highway girder bridges and is used as the model bridge in the hybrid testing throughout this thesis.

## ***2.2 Test Specimen Details***

A hybrid testing setup involves two components: a large-scale but local portion of the structure that is fabricated and physically tested (test specimen) and the usually larger, remainder of the structure that is modeled numerically in a finite element model. In the case of the Yellow Mill Pond Bridge, the girders have standard W-beam sections and are simply supported; thus the girders can be modeled very easily in a finite element program using the mechanics of these girders. However, at the cover plate ends where fatigue cracks are known to have formed, this portion of

the girders is very difficult to model numerically, since fatigue cracks and failures fall outside any linearly elastic assumptions that can be made for the girders. As a result, a test specimen based on the 5'-0" section of the lower flange and cover plate at the locations where the fatigue cracks were found was chosen to be the test specimen for the hybrid testing. The rest of the girder is modeled virtually using the finite element software OpenSees (this software is discussed in depth in the following chapter).

The first 2'-6" of this test specimen is the lower flange of a typically interior girder in one of the simple spans. The second half (2'-6") of the test specimen is the lower flange with a cover plate. Thus at the center of the test specimen is the rounded cover plate end with the weld detail that has known fatigue issues. A three view drawing of the test specimen can be seen in Figure 2-3.

Note that due to the capacity of the test frame and servo-hydraulic actuator used for the test, the cross section dimensions of the test specimen were scaled to 60% of the actual as-built dimensions. One of the major advantages of the hybrid testing method is that a large portion of the structure is modeled numerically in a finite element software. Since this software communicates with the test specimen via controller during testing, the stresses generated from the virtual model can be scaled down and applied to the test specimen, and the response of the test specimen scaled back up to the full scale virtual model. Thus, even though the test specimen has been scaled down, the full scale response of the entire structure can still be modeled using this hybrid testing method.

The construction of the test specimen was made to emulate as close as possible the actual construction methods used to fabricate the girders in the Yellow

Mill Pond Bridge. To create the weld, a professional welder was hired and arc welding was used to create a 3/8" weld between the cover plate and lower flange of the test specimen. Images from the construction and the final test specimen can be seen in the following Figures 2-4 through 2-6.

Since the test specimen is the lower flange and cover plate of the girder, the stress variation from the bending moments is relatively constant across the flange cross section (since the bending stress varies as  $\sigma = M \cdot c / I$  where  $c$  is the distance from the shear center and the thickness of the flange is small compared to the depth of the girder). As a result, the test specimen will be loaded axially in the physical testing.

In order to attach the test specimen to the axial loading actuators, an attachment head was designed to transfer the axial loads from the actuators to the test specimen. At the end of this attachment head, a 1/2"-diameter threaded rod extends from the attachment head to the axial loading actuator. A 3-view drawing of the attachment head, a combined drawing of the attachment head and test specimen, and photo of the test specimen in the testing setup can be seen in Figures 2-7 through 2-9.

The threaded rod serves two purposes in the test setup. Since the area of the threaded rod is much less than the test specimen, it has a much lower stiffness and thus amplified axial elongation compared to the test specimen. Due to the limited resolution of the displacement sensors (LVDT) in the MTS servo-hydraulic actuator, measuring the axial deformation of the test specimen at small load levels pose technical difficulty in feeding precise load values to the virtual model; therefore, the threaded rod is used as a displacement amplifier that will yield a greater value of the displacement in the actuator and subsequently more precise load data for feedback to

the virtual model in the hybrid testing. Additionally, the threaded rod acts as a "fuse element" which will fracture or buckle if any unexpected issues arise during testing, thus preventing damage to the test specimen or the actuators.

### ***2.3 Weigh In Motion Data***

The prototype bridge structure described in the previous sections was the Yellow Mill Pond Bridge in Bridgeport, Connecticut. In order for the hybrid test method to accurately simulate the conditions on the bridge, the loading applied to the model must also accurately simulate the actual loading conditions on the Yellow Mill Pond Bridge. In order to obtain realistic loading distributions for the structure, the load history for the Yellow Mill Pond Bridge over a three-day time window was obtained from the Connecticut Department of Transportation. This load history was taken from a truck weigh-in-motion station situated before the bridge and shows the loading frequency for different truck weights throughout the loading period. The weigh-in-motion reports can be found in Appendix A and have been summarized in Figures 2-10 through 2-13.

Figure 2-13 is the average of the frequencies for the various truck loadings over the three days that the weigh in motion data was provided. The bi-modal shape shown in this figure is typical for a large bridge carrying interstate traffic. The first peak in the graph represents under-loaded or lightly loaded trucks, while the second peak represents trucks loaded near the legal limit (Sivakumar, 2008). This loading frequency distribution provides a basis for determining the loading model to be applied to the hybrid testing model. Several different loading models will now be presented in the following section.

## ***2.4 Loading Models***

Several different loading configurations (models) have been proposed for fatigue tests loading on bridges. The axle configurations in these models have been determined to represent the variety of the actual axle configurations and gross weights of the trucks that travel the interstate roadway system. The foremost of these configurations is the AASHTO Fatigue Truck specified in the AASHTO Fatigue Guide Specifications (AASHTO, 1990). This axle configuration is shown in Figure 2-14. The AASHTO Fatigue Truck was developed based on weigh-in-motion (WIM) studies from over 27,000 trucks and 30 sites nationwide (Synder et al., 1985). Furthermore, the axle spacing was approximated based on the axle spacing of four and five axle trucks, which dominate the fatigue damage in bridges (Chotickai, 2004).

An alternative fatigue truck model was proposed later by Laman and Nowak which is based on a study of five steel bridges combined with simulation results (Laman and Nowak, 1996). This study found that fatigue damage in bridges was primarily caused by ten and eleven axle trucks. The axle configuration for this fatigue truck is shown in Figure 2-15.

Due to the widespread acceptance of the publications by AASHTO, the AASHTO Fatigue Truck will be used as the loading configuration for the load model for the hybrid testing throughout this thesis. Note that the AASHTO Fatigue Truck loading configuration in Figure 2-14 shows the average recommended axle weights for the fatigue truck. However, these average values can be modified based on an actual gross truck weight distribution such as in Figure 2-13 for the Yellow Mill Pond

Bridge. AASHTO recommends modifying the gross weight of the fatigue truck so that:

$$W_{eq} = \left( \sum f_i W_i^3 \right)^{1/3} \quad (\text{AASHTO, 1990})$$

This equation provides a way transforming a gross weight distribution into a constant amplitude equivalent gross weight for the fatigue truck. This equation lends itself well to fatigue testing where constant amplitude loads are applied cyclically for thousands of cycles. However, due to the nature of hybrid testing, the load distribution does not necessarily need to be simplified to a constant amplitude load (note the details of hybrid testing are described in more depth in Chapter 3).

Furthermore, hybrid testing lends itself to having a load history over time which need not be a constant amplitude truck loading. So for this prototype structure of the Yellow Mill Pond Bridge, the actual loading on the bridge can be simulated more accurately by generating trucks at different gross weights subject to the actual discrete loading distribution shown in Figure 2-13.

Based on the discrete load distribution shown in Figure 2-13, a discrete cumulative distribution function (CDF) was determined to randomly generate the gross weights of the trucks to be applied to the hybrid testing model. To check the cumulative distribution function, a set of 1,000 trucks was generated and their gross weights tabulated. A plot of this data, which shows the discrete cumulative distribution function and discrete probability distribution function (PDF) can be seen in Figure 2-16. Based on this cumulative distribution function, trucks with different gross weights will be randomly generated and applied to the hybrid testing model.

The advantage of this type of loading model is that it more accurately simulates the actual loading the bridge experiences throughout its lifespan.

Overall, the test specimen has been designed to follow the actual as-build dimensions of the bridge as closely as possible. Since the fatigue prone sections of the bridge are at the interface at the ends of the cover plates on the lower flanges of the girders, this section of the girder will be fabricated for the physical testing portion of the hybrid testing. The remainder of the structure will be modeled virtually as a finite element model. Based on the gross weight CDF, a more realistic loading pattern can be applied to the structure during the hybrid testing. Next the details of the hybrid testing are described in the next chapter.

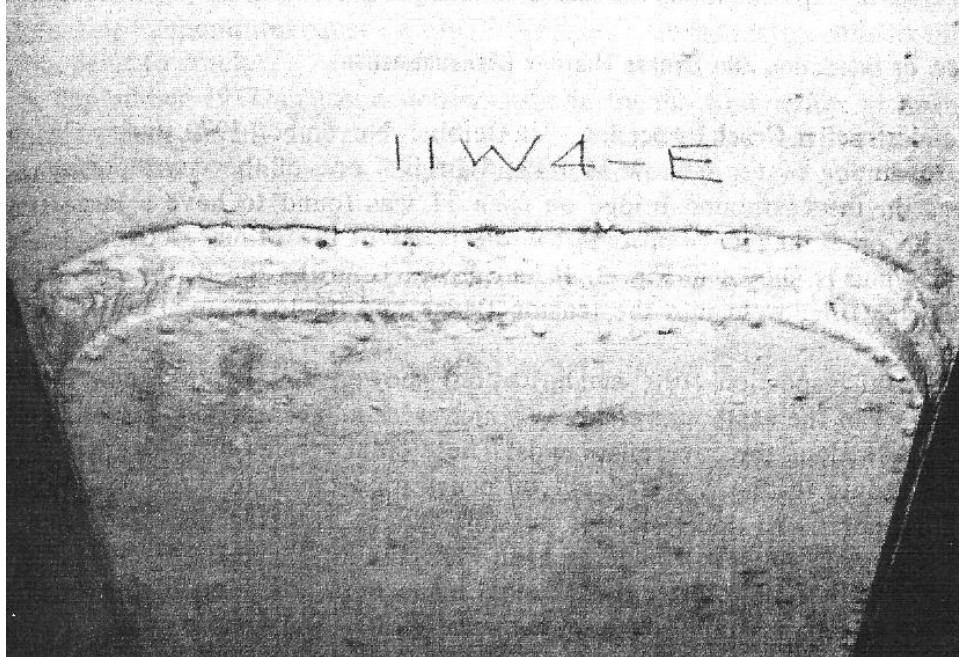


**Figure 2- 1:** Rounded Cover Plate End for Yellow Mill Pond Bridge (Fisher, 1981)

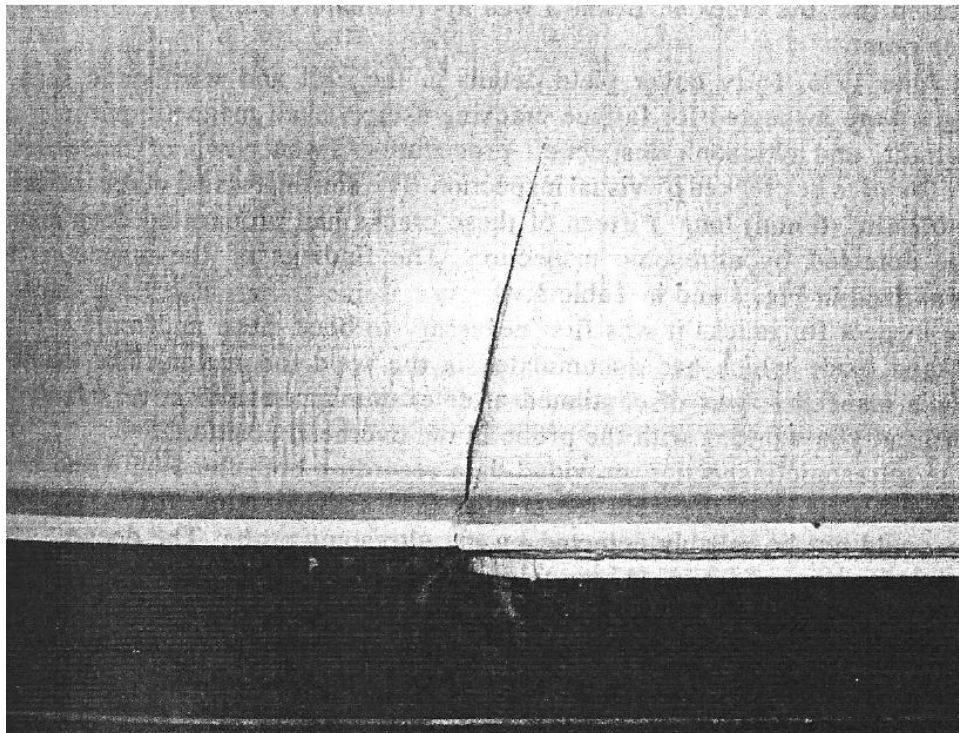


**Figure 2- 2:** Fatigue Cracks at Cover Plate Detail (Fisher, 1981)

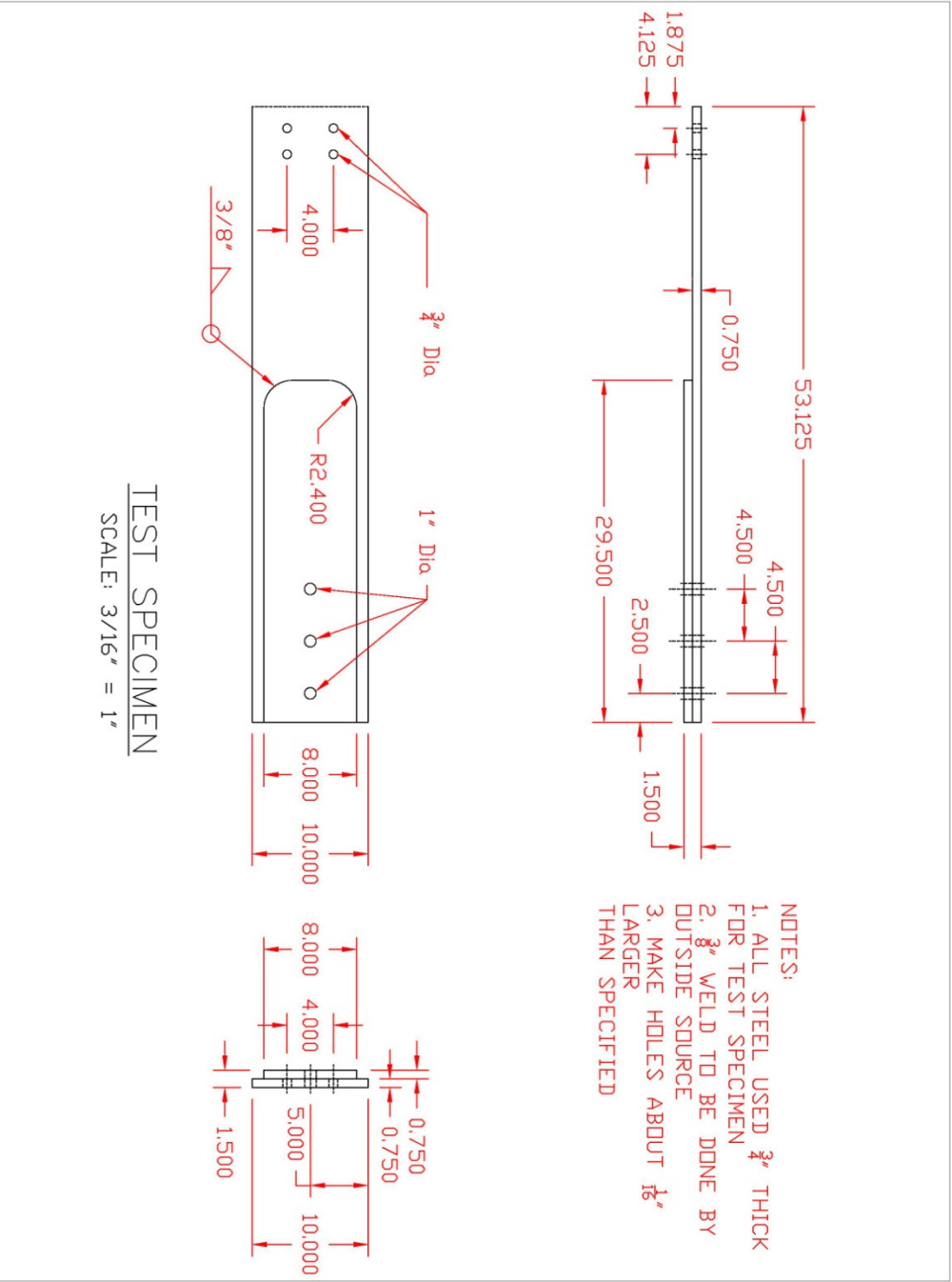


**Figure 2- 3:** Test Specimen Design Drawing



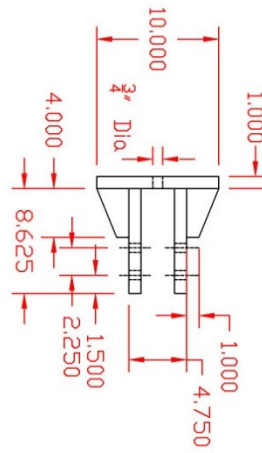
**Figure 2- 4:** Completed Test Specimen



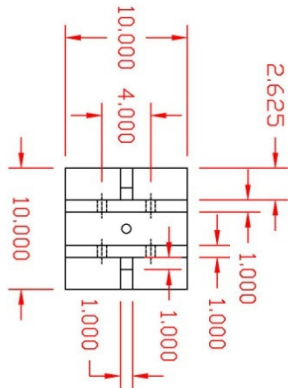
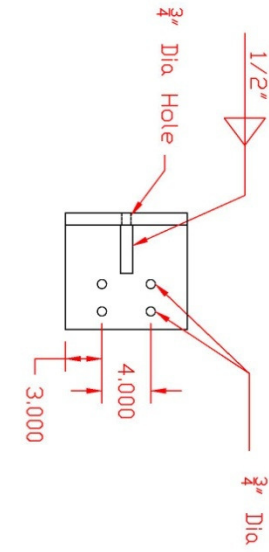
**Figure 2- 5:** Test Specimen During Arc Welding



**Figure 2- 6:** Close-up of Test Specimen Weld



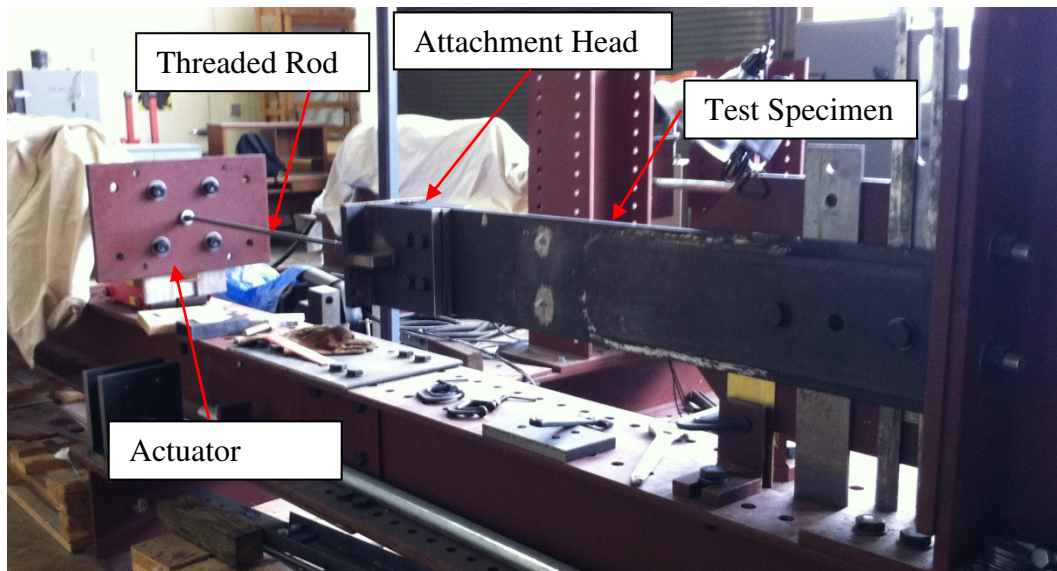
- NOTES:  
 1. ALL STEEL USED 1" THICK  
 FOR ATTACHMENT HEAD  
 2. MAKE HOLES ABOUT 1/8" LARGER  
 THAN SPECIFIED



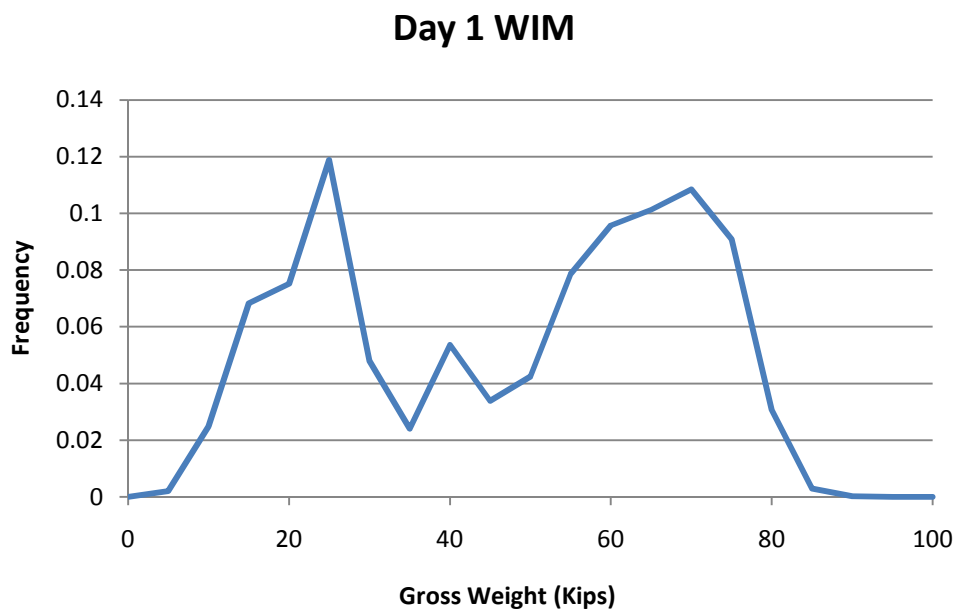
ATTACHMENT HEAD  
 SCALE: 3/16" = 1"

Figure 2- 7: Attachment Head





**Figure 2- 9:** Assembled Test Specimen



**Figure 2- 10:** Day 1 Yellow Mill Pond Bridge Weight in Motion Data

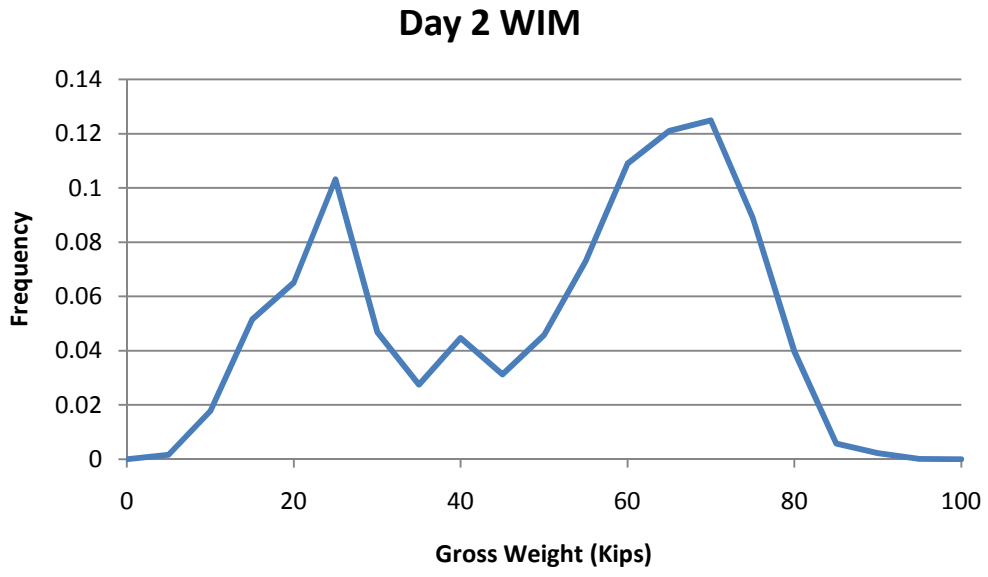


**Figure 2- 11:** Day 2 Yellow Mill Pond Bridge Weight In Motion Data

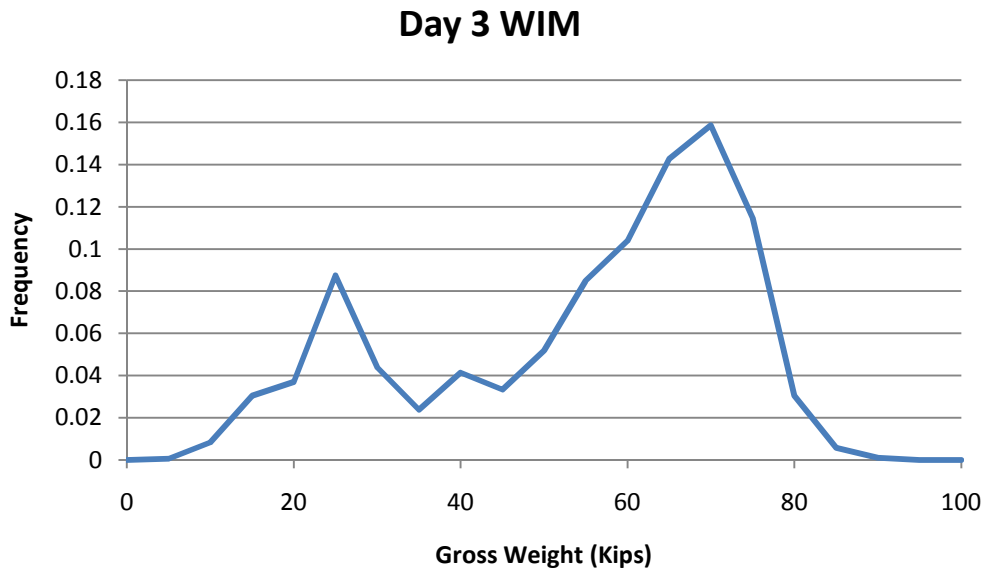


**Figure 2- 12:** Day 3 Yellow Mill Pond Bridge Weight In Motion Data

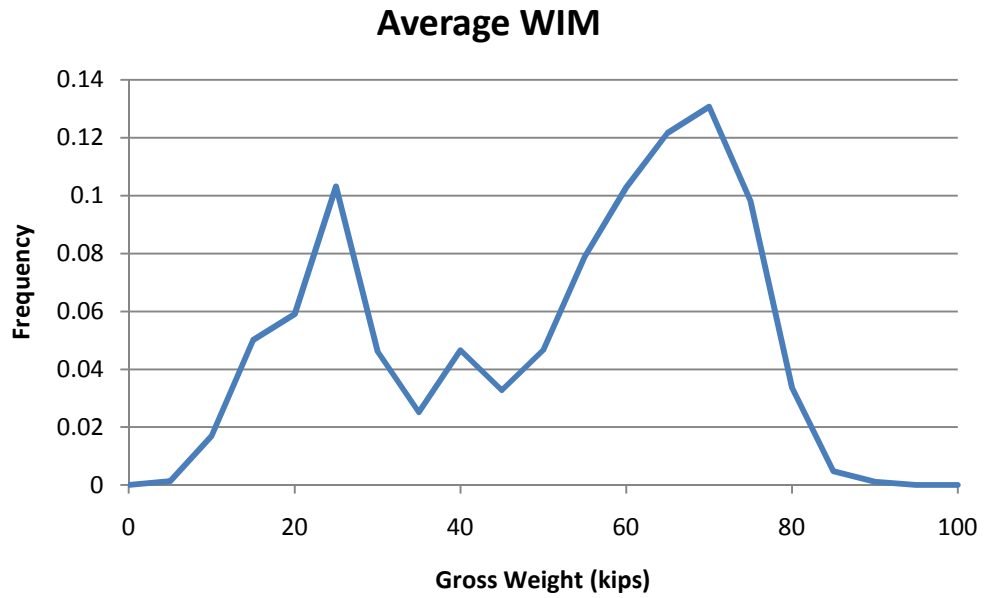


**Figure 2- 13:** Average Yellow Mill Pond Bridge Weight In Motion Data

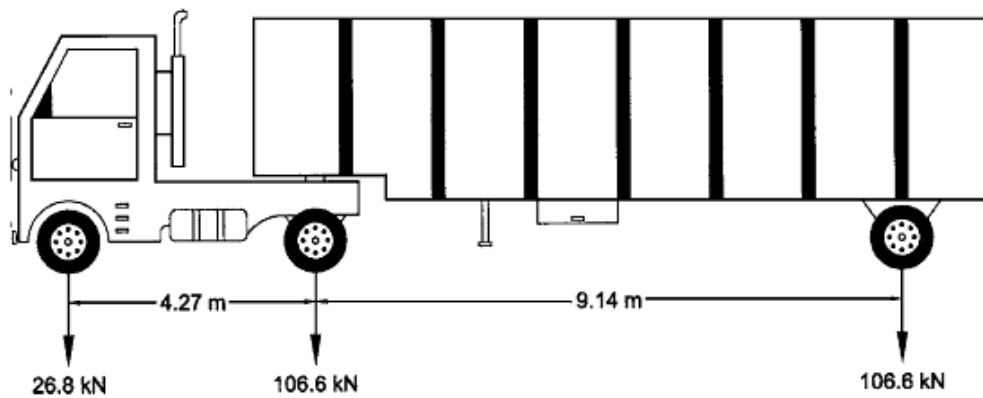


**Figure 2- 14:** AASHTO Fatigue Truck (AASHTO, 1990)

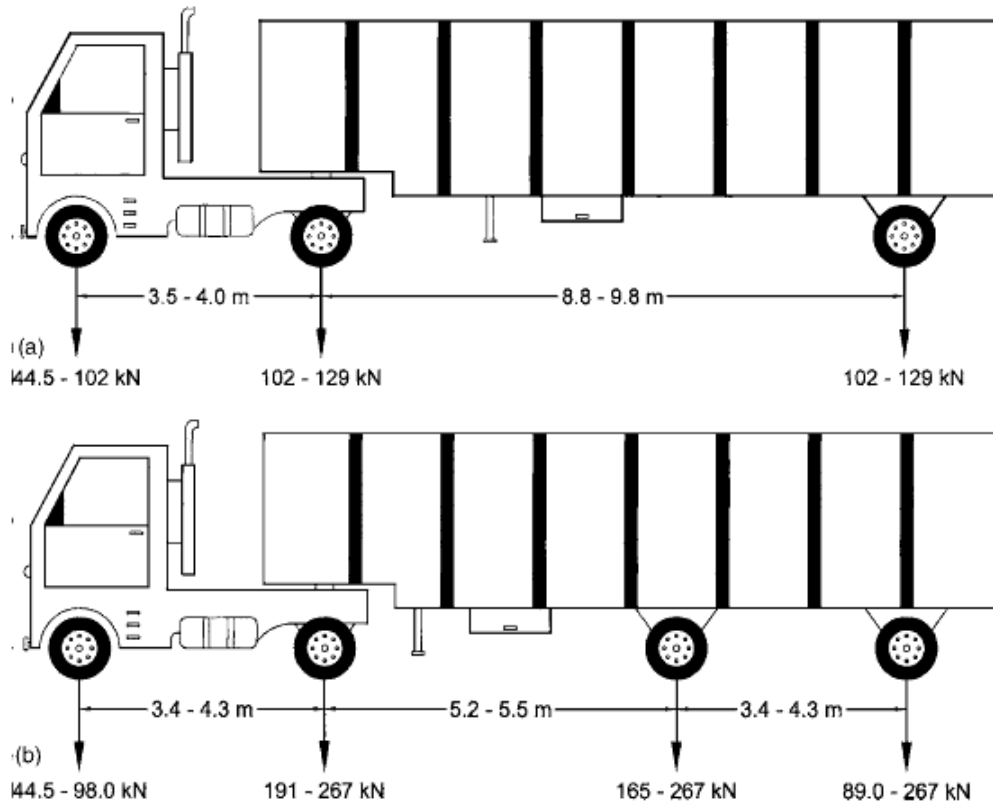


Figure 2- 15: Laman and Nowak Fatigue Truck (Laman and Nowak, 1996)

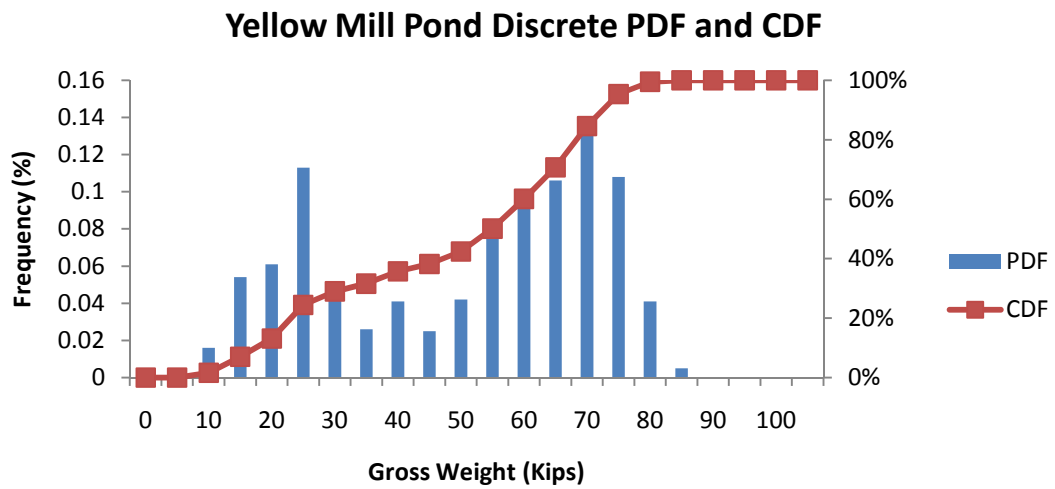


Figure 2- 16: Yellow Mill Pond Discrete PDF and CDF

## **Chapter 3: Hybrid Testing Methodology**

### ***3.1 General Description***

The conventional method of testing structural systems involves fabricating the structural system members, simplifying the loading pattern, and applying these simplified loads and measuring the response of the structure. While this method is a proven method for structural testing, it is often very costly and limited to locations that have access to large testing equipment. However, oftentimes only a portion of the structural system is of direct interest to the engineer, and typically the behavior of this portion of the structure is less known compared to the rest of the structure. Particularly in the case of fatigue, only portions of the structure are usually deemed fatigue critical, and it is these portions of the structure that are of the most interest to the engineer. Furthermore, when the loading resides in the linear range of the structural members, the behavior of most of the structural elements can usually be predicted quite accurately using basic mechanics of materials principles. Thus, it seems inefficient to fabricate entire structural systems and test them, when often only a portion of the structure is of interest.

The hybrid testing method presents a novel large scale testing alternative to overcome the shortcomings of the conventional testing methods. The basic principle of this hybrid testing method is that typically the behavior of the majority of the structural elements in a structural system can be fairly accurately modeled and predicted with currently available finite element modeling techniques. Furthermore,

often the behavior of a select localized portion of the structure cannot be accurately predicted such as a fatigue prone detail or a repair to a structural element. The hybrid testing method combines these two assertions by creating two components in the testing process.

The first of these two components is the virtual component of the testing. The virtual component consists of a finite element model of all of the elements and portions of the structure that can be easily modeled using the linearly elastic structural analysis principle. In the hybrid testing performed in this thesis, the virtual components are defined in a general purpose finite element program OpenSees (Open System for Earthquake Engineering Simulation), which was developed at the University of California, Berkeley (McKenna 1997).

The second component of the hybrid testing is the actual physical component to be tested in the lab. The physical component of the testing includes the portions of the structure that cannot be accurately modeled in the finite element software. As a result, these portions of the structure must be fabricated and will be physically tested to determine their characteristics and response to different loadings.

What makes hybrid testing unique is that it combines both of these components together simultaneously during testing. The loading patterns to the structural system are specified in the virtual model. The virtual model does the computation in which these loads are distributed to all of the structural elements; when the virtual model encounters the elements that are part of the physical test components, it transmits the load from the model to the physical testing equipment via pre-specified interface degrees-of-freedom (DOFs). Actuators then apply these

loads at interface DOFs to the physical test specimens and record their responses (displacements, stresses, etc.). These responses of the physical components are then sent back to the virtual model, and the model updates and proceeds to the next step in the computation process. The next set of loads are then applied and the cycle continues. Figure 3-1 demonstrates this sequence (all figures can be found at the end of this chapter).

The major advantage of this method of testing is that only portions of the structure whose response is not predictable with current computation techniques need to be physically tested, and the response of these test portions of the structure is measured in real time and sent back to the virtual structural model for updating the computation. Thus a relatively large scale test specimen can be used even in a test facility which does not have adequate large scale structural testing equipments (e.g., strong floor, reaction wall, reaction frames, servo-hydraulic test equipments). Nonlinear behavior of the test components can also be considered in the prediction of the structural response behavior through measurement. Another advantage of the hybrid testing is the flexibility to apply any arbitrary form of loading such as time varying environmental loads in the virtual model of the concerned structure.

As described in Chapter 2, to demonstrate the use of this hybrid testing technique for evaluating sensors and structural health monitoring (SHM) techniques, an actual existing bridge with known structural defects (fatigue issues) will be modeled (Yellow Mill Pond Bridge in Bridgeport, Connecticut). This bridge will be broken down into two components for the hybrid testing, the virtual and physical

(experimental) components. These two components are described in the following two sections.

### ***3.2 Virtual Component***

The Yellow Mill Pond Bridge was designed to be loaded within its linear range throughout its lifespan. Thus, for the steel girders which support the bridge deck, the only portion of the girder that cannot be readily modeled is the fatigue prone areas at the interface between the end of the cover plate and the lower flange. Thus, the majority of the steel girders can be modeled virtually within the OpenSees finite element software.

Since the girders for the Yellow Mill Pond Bridge are typically 100 feet in length, the hybrid simulation for this bridge will be for an interior girder with the same section properties as listed in the as-built plans (Fisher, 1981). The virtual component of this bridge will encompass all of the portions of the girder except for a 5'-0" section of the lower flange centered around the interface where the bottom cover plate terminates. This 5'-0" section will be designated as the physical (experimental) component in the hybrid simulation (see section 3.3). A schematic showing the components in the hybrid testing is shown in Figure 3-2.

To perform hybrid testing, a software framework needs to be first established to integrate the physical testing elements with the computer model. Figure 3-3 shows the architecture of such a software framework that depicts its basic components and the interrelationships. OpenFresco is one of the hybrid test software frameworks which has a modular architecture (Schellenberg et al. 2006, 2008). Each module can be modified and new ones can be added without affecting other modules. In

OpenFresco, a module is called a class, including ExperimentalElement, ExperimentalSite, ExperimentalSetup and ExperimentalControl classes. The relationship between these classes is shown schematically in Figure 3-3. During a hybrid test, the first task for the software framework is to transform the degree-of-freedom from the coordinate system of the finite element (FE) software to those of the specimens being physically tested, by considering the geometry and kinematics of the system. Subsequently, another class is responsible for communication between the laboratory control and data acquisition systems. For geographically distributed hybrid testing, another class is needed to facilitate the communication between distributed experimental sites and the master site which runs the computational software and works as the coordinator in the test.

As stated previously, the finite element software used for this hybrid testing is OpenSees (McKenna 1997). This software was originally developed for general purpose nonlinear finite element analysis of complex structures undergoing inelastic deformation. As a result, the software has a very large library of various finite elements for use in modeling the structure. OpenFresco is independent of the FE software used, meaning that any FE software that allows the addition of new elements can be used, such as Abaqus, LS-Dyna, OpenSees, Matlab, etc. For example, OpenSees can be readily used with OpenFresco because of its object oriented design methodology. Unlike a pure numerical analysis conducted in OpenSees, the difference in hybrid testing is to replace the numerical element with the ExperimentElement from OpenFresco and add the numerical integration operators (Schellenberg et al. 2006). A deeper discussion into the relationship between

OpenSees and the physical testing equipment platform is described later in section 3.5.

In order to model the Yellow Mill Pond Bridge in OpenSees, two different types of models were explored. The first of these types is a planar model based off truss elements, which can only handle axial forces and deflections. The goal of this type of model is to simplify the girder into an equivalent truss comprised of a series of truss elements, which yields the same global and local responses under moving loads from passing trucks. An image of this truss model can be seen in Figure 3-4. As Figure 3-4 shows, the girder has been simplified into a series of truss finite elements. The horizontal elements at the top and bottom chords of the truss model act as the upper and lower flange elements in the girder. The shear effects are taken by the diagonal and vertical truss members. Note the location of the physical element that is to be fabricated and physically tested in real time with the virtual model is circled in red.

In order to fine tune the proper cross sectional areas of all the truss members so that the deflection of the truss closely mimics the actual deflection (determined from analytical beam equations) of the Yellow Mill Pond Bridge girder, an iterative trial-and-error process was employed. Under any arbitrary loading the deflection of simply supported girder can be determined using the beam equations from Mechanics of Materials. A general point load was applied to the midspan of a 100' girder with the properties as specified in the as-built plans for the Yellow Mill Pond Bridge. Using the general beam equations, the deflection was then calculated at the midspan. The cross sectional areas of the truss model as shown previously in Figure 3-4, were

then modified and iterated until the midspan deflection of that truss model was within 5% of the midspan deflection of the Yellow Mill Pond Bridge girder as calculated from the beam equations. This iterative process was carried out using a MATLAB script `trussarea.m`, which can be found in Appendix B. A summary of the actual girder areas of the flanges and webs as specified in the as-built plans for the Yellow Mill Pond Bridge compared to the calculated cross sectional areas for the truss model of the bridge can be found in the following table. Note that for the truss model, flanges refer to the horizontal truss members on the top and bottom of the structure and web refers to the diagonal and vertical members.

**Table 3- 1:** Comparison of Actual to Virtual Models

	As-Built Yellow Mill Pond Bridge Girder	OpenSees Truss Model
Flanges	20.8 in <sup>2</sup>	25.5 in <sup>2</sup>
Web	23.8 in <sup>2</sup>	23.2 in <sup>2</sup>
Total Area	65.4 in <sup>2</sup>	74.2 in <sup>2</sup>

As the above table shows, the area of the flanges for the virtual model are larger than the flange areas of the actual bridge girders. This was required, since for the actual bridge girder, the stiffness against bending came from both the flanges and web. However, since the virtual model is composed of axially loaded members (truss members), the stiffness against vertical deflection came from only the cross sectional areas in the "flange" type axial members and subsequently had to be increased to properly simulate the deflections of the actual bridge girders.

The major advantage of using truss members to model the actual bridge girder resides in the computational benefits. By using truss elements throughout the model,

the number of degrees of freedom at the nodes decreases compared to using other types of elements such as beamcolumn or plate elements. Furthermore, since fatigue tests can have several thousand cycles, it is advantageous to use a computationally efficient model. Thus, by modeling the girder using truss elements, the computations between loading cycles becomes much faster and over thousands of loading cycles this results in a savings of time.

While using a truss model is computationally efficient, is not the most accurate finite element model for modeling a bridge girder. Thus, a second type of virtual model was designed for the hybrid testing consisting of quad elements (plane stress 2-D elements) for comparison purpose. Quad elements are similar in geometry to plate elements, however, they only allow translation at the four nodes at the corners (see Figure 3-5).

The quad elements were used to make up the web of the girder in the virtual model. Since the actual girder being modeled had a height of 36.5" and is 100'-0" long, the web was meshed into 500 smaller quad elements, each of dimensions 7.3" x 12". For the flanges in this virtual model, truss elements were again used similar to the virtual truss model described earlier in this section. The nodes for these truss members were placed every five feet along the top and bottom of the web. The reason for using the truss members and the five foot spacing is due to the portion of the structure that will be physically tested (the physical component). This physical component of the testing is the 5'-0" length of the bottom flange centered around the location where the cover plate terminates. Thus, a five foot spacing was necessary to match the physical test specimen. Furthermore, the testing equipments (including

reaction frames and servo-hydraulic equipments) in the structural lab for hybrid testing is set up for performing axial loading. Thus, in order for the data from the physical testing to be updated in the virtual testing, the interface between these two systems could only accommodate axial forces, which is only possible through truss finite element members. An image of this virtual model composed of quad elements for the web and truss elements for the flanges taken from the OpenSees Navigator is shown in Figure 3-6.

Beyond using quad elements to more accurately represent the web of the test structure, this second virtual model was also designed to model the dynamic effects that the bridge would undergo as trucks pass over the structure. This was accomplished by assigning material densities to the quad elements to incorporate the mass effects of these elements. Furthermore, lumped masses were added to nodes along the top and bottom flanges. These masses took into account the mass of the flanges as well as the mass of a 7 ¼"-thick concrete deck on top of the girders. These masses provide the inertial properties of the structure that are required for a dynamic analysis.

In addition to assigning masses to the elements and nodes of the structure, damping was also taken into account in this virtual model. Since the software used in the hybrid testing for the virtual model was originally designed for use in earthquake engineering, a variety of damping schemes existed in its programming library. Rayleigh damping was chosen to model the damping of the structure. A damping ratio of 1% was selected to be applied to the first two modes of the structure. This damping ratio was selected based on the materials in the structure; the girders were

constructed out of steel and there is a 7 ¼"-thick concrete deck on top of the steel girders. Thus, a damping ratio of 1% was chosen to model the structure.

As can be seen in Figure 3-6, this second virtual model for the test structure consists of significantly more nodes compared to the truss model due to the meshing with the quad elements. As a result this model is much more computationally intensive for each load cycle, and over the thousands of load cycles during the hybrid test, this type of model runs much slower, since it requires substantially more computations compared to the truss model.

Both of the previously described virtual models (truss element model and quad element model) present two different ways to model the Yellow Mill Pond Bridge virtually in OpenSees. Both of these models have advantages and disadvantages over each other in computational speed and model accuracy. However, these virtual models only comprise the first component in the hybrid testing, the virtual component. The second component of the hybrid testing involves the portions of the structure that cannot be easily modeled virtually; these portions of the structure comprise the physical component of the hybrid testing.

### ***3.3 Physical Component***

The major advantage of hybrid testing is that it incorporates both the efficiency of computer simulation with the realism of physical testing. As described in section 3.2, the majority of the Yellow Mill Pond Bridge can be accurately analyzed virtually using a finite element model. However, there is one section of the bridge that difficult to model virtually. This section is the interface between the

lower flange and the end of the cover plate. This interface is shown again in Figure 3-7.

Due to the stress concentrations that develop at the weld interface between the cover plate and lower flange, this portion of the structure is susceptible to fatigue. As a result, the response of this portion of the structure for thousands of load cycles poses significant challenges to computer simulation with currently available commercial finite element program. Thus, this portion of the bridge is preferred to be physically tested to determine the actual response of this section of the structure, and it is this portion of the structure that comprises the physical component of the hybrid testing.

As described previously, a five foot section of the lower flange, centered at the weld at the interface between the lower flange and cover plate will be used for the physical component of the testing. A five foot section was chosen for two practical reasons. First, the capacity of the testing facility available to perform this research lends itself for testing structural elements of similar size. Second, the spacing of the nodes in both of the truss and quad element virtual models were designed to fit a five foot physical test specimen, so that the response for the physical testing could be seamlessly and accurately transferred to the virtual model.

The details of this physical component of the hybrid testing were described earlier in Chapter 2. This test specimen is the physical component in the hybrid testing and will be tested simultaneously with the virtual model to determine the overall structural response of the Yellow Mill Pond Bridge. A picture of the test

specimen (physical component of the hybrid testing) in the test setup is shown in Figure 3-8.

### ***3.4 Loading the Prototype Structure***

Conventional structural testing usually involves simplifying a complex loading history to a more basic loading such as sinusoidal loads with a constant amplitude. While this method of testing is good for developing basic structural responses and general fatigue response models, for steel highway girder bridges it does not realistically simulate the actual loading history that occurs throughout the lifespan of the bridge. As was shown in section 2.3 in the Weigh-In-Motion (WIM) data, the loading on a highway bridge is of a random form following a bimodal shape (Sivakumar, 2008) in the probability distribution function.

In hybrid testing, the loads are specified in the virtual model. These loads are then transferred to all of the individual elements in the structure as well as the interface degrees-of-freedom where the physical components are connected to the virtual model. The interface loads are then transferred to the servo-hydraulic actuators via controller which apply the specified displacement (for displacement based test control) or force (for force-based test control) to the physical component (test specimen). The response of this test specimen is then measured and fed back to the virtual model via controller and the forces and displacements in the finite elements update themselves. The second load cycle then begins and the process repeats itself.

As this description shows, for hybrid testing, the external loads are usually applied to the virtual finite element model. Since they are specified virtually, detailed

load histories of an arbitrary form can be created for the hybrid testing that are more realistic in describing actual environmental loads (e.g., truck load or wind load) than constant amplitude loads. For the case of the Yellow Mill Pond Bridge hybrid test, a loading history was defined that more accurately simulated the actual truck loading with variations in the loading that followed the actual probability distribution of the trucks more closely.

As described in section 2.4, the AASHTO Fatigue Truck was selected as the loading model for the hybrid test for the Yellow Mill Pond Bridge. To create a realistic loading cycle that simulated the fatigue truck driving over the bridge, the loads at each of the nodes on the top flange were calculated based on the location of the fatigue truck on the bridge over time. A time history of the loads on each of the nodes was developed based on a fatigue truck travelling at 40 mph over the bridge. Using two programs written in MATLAB titled `createloadmatrix.m` and `yellowmillpondloadfile.m` (see Appendix B) a discrete time interval was selected, and the load on each of the nodes was calculated at each time interval as the fatigue truck travelled across the bridge. After the fatigue truck had completely crossed the bridge, a second fatigue truck was sent over the bridge and the loads on each of the nodes calculated again. Using this process and several hundred fatigue trucks, a suitable loading history was generated for the hybrid testing. An example of a typical load history at one of the nodes of the bridge structure is shown in Figure 3-9.

Figure 3-9 shows a portion of the loading history for node 4; in this case it is for the first four trucks that pass over the bridge (first 9 seconds of loading). As Figure 3-9 shows, all of the trucks do not create the same magnitude of loading. For

example truck 2 has a much smaller loading compared to truck 4. This demonstrates the probability distribution function that generates the gross weights for each of the trucks in the load history. The gross weight of each truck generated in the load history is based on the discrete probability distribution function shown in Figure 2-13. Thus, each truck that is generated for the load history has a different gross weight, and after hundreds of trucks are generated for the hybrid testing, a realistic distribution of truck weights is generated that more accurately simulates the actual loading distribution that occurs on the Yellow Mill Pond Bridge. In addition to the gross weight distribution that occurs, Figure 3-9 also shows how each truck creates three pulses as it passes over the bridge. To illustrate what each of these three pulses represent, a close-up view of the load history for truck 1 is shown in Figure 3-10.

Recall that the AASHTO fatigue truck consists of three axles (see Figure 2-14). In this loading configuration, the first axle carries only a small portion of the load, while the back two axles carry the majority of the load. This loading configuration is what creates the three pulses in the loading history for each truck that passes over a given node in the model. The first pulse is the first axle in the truck, while the second and third pulses represent the back two axles of the fatigue truck. Note that there is a time gap between each of the axles. This is because for a truck travelling at 40 mph, this is the time gap between each of the axles driving over that particular node.

In addition to the moving load due to the fatigue truck travelling over the bridge, the dead load from the self weight of the girders and concrete deck must also be taken into account in the loading. Given the tributary area of the deck above each

node and the length of the girders between each node, a constant dead load force was added to the time history developed for the live loads from the fatigue trucks. Figure 3-11 shows both of these loads. As this figure shows, the live load shown in Figure 3-9 has been bumped up by a constant dead load applied over the entire interval.

Now that the load history, virtual, and physical components of the hybrid testing have been described, the only portion of the hybrid testing methodology that needs to be clarified is how the physical and virtual components of the testing communicate with each other in real time during the testing. This is accomplished through the software component OpenFresco, which is described in the next section.

### ***3.5 Openfresco***

Both the virtual and physical components of the hybrid testing are controlled by different systems. In the case of the Yellow Mill Pond Bridge Hybrid Testing in this research, the virtual component is controlled by the OpenSees software program, while the physical component is tested using servo-controlled MTS actuators. A component is needed to bridge the two systems together so that the virtual component can communicate in real time with the physical component of the hybrid testing. The software component that accomplished this task is OpenFresco. The hardware component to facilitate this communication is an MTS FlexTest 60 controller and a driver for hybrid simulation developed by MTS.

OpenFresco is short for Open Source Framework for Experimental Setup and Control. This software was developed similar to OpenSees at the University of California, Berkeley. OpenFresco works by acting as the "middleman" between the physical testing component and the virtual component that is in the software

OpenSees. Forces from the virtual model are transmitted by OpenFresco to the testing actuators where these forces are then applied to the physical component (test specimen). The response from the physical component is then transmitted to OpenFresco which transmits the displacements and responses of the test specimen to the virtual model in OpenSees. This whole process occurs seamlessly in real time allowing the virtual model to be updated with the response of the physical component immediately after the forces are applied. A diagram showing the communication that occurs between the virtual component, physical component, and OpenFresco can be seen in Figure 3-12.

This concludes the description of the hybrid testing method. As described in the previous sections, the hybrid testing method allows complex structures to be broken down into virtual and physical components in testing based on the degree of knowledge of the mechanical behaviors of those members. The hybrid testing method combines virtual modeling of the components whose behavior can be easily predicted with physical testing of the components with behaviors difficult to simulate on computer. In the case of the Yellow Mill Pond Bridge, the girders of this bridge were broken down into virtual components for the portions of the girder within the linear elastic range and a physical component for the location on the bottom flange at the interface of the cover plate where fatigue cracks have been known to form. This physical component was detailed in the test specimen in Chapter 2. Now that the general description of the hybrid testing method and how it is applied to the Yellow Mill Pond Bridge has been described, what remains is the actual hybrid testing. The results of this testing are presented in the following chapters.

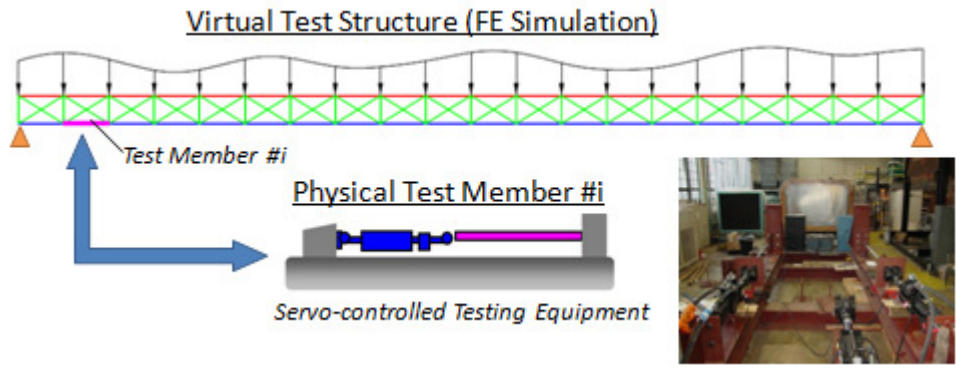


**Figure 3- 1:** Schematic illustration of Hybrid Testing scheme

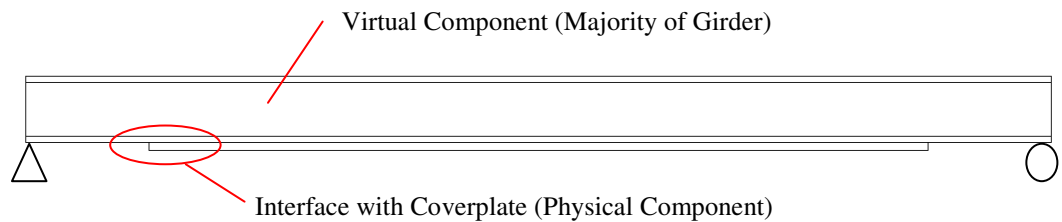


**Figure 3- 2:** Girder Plan View Showing Virtual and Physical Components

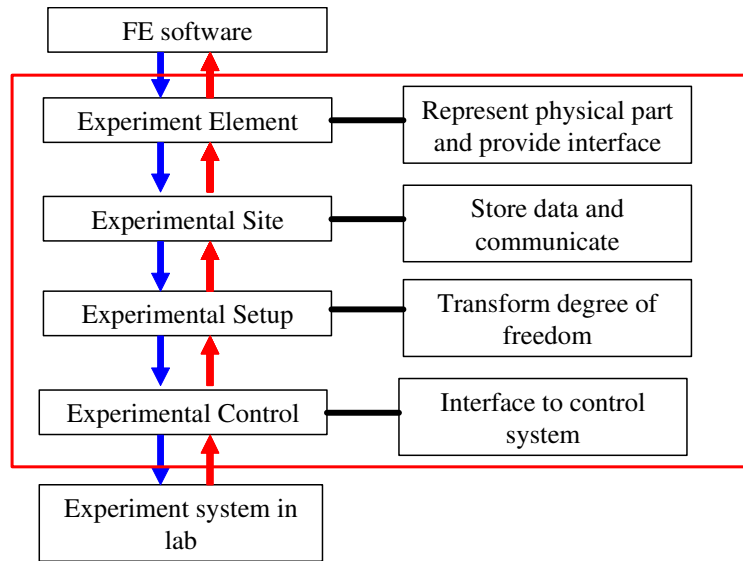


**Figure 3- 3:** Schematics of Hybrid Testing Software Framework

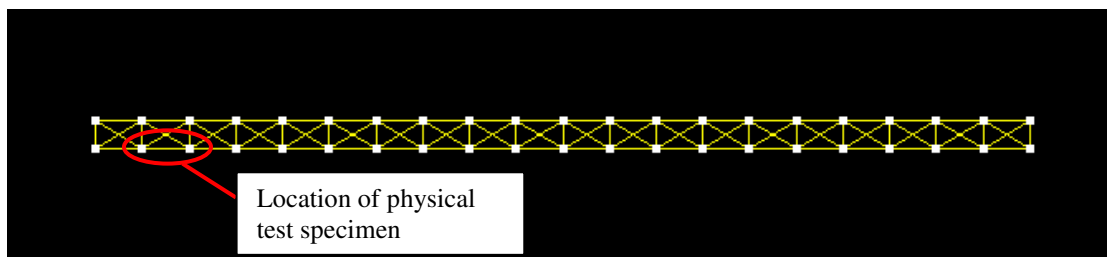


**Figure 3- 4:** Virtual Model #1: Truss Element Model (Elevation View)

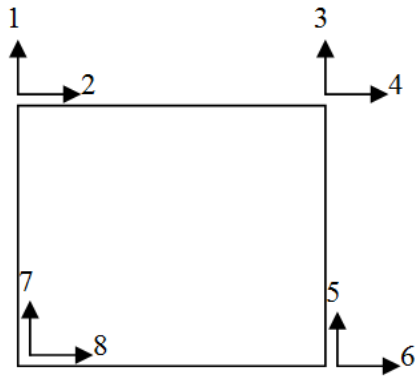


**Figure 3- 5:** Quad Element (Mazzoni, 2009)

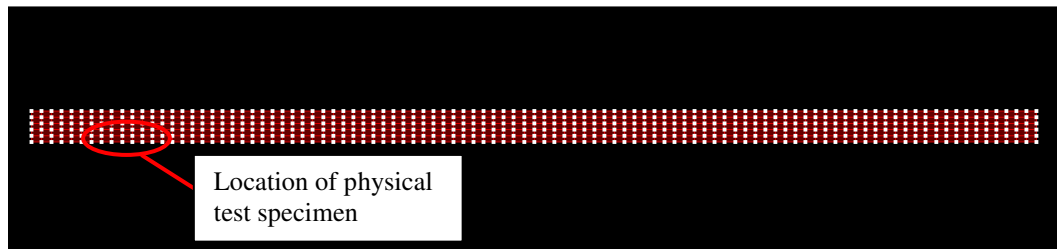


**Figure 3- 6:** Virtual Model #2: Quad Element Model



**Figure 3- 7:** Interface between Lower Flange and Cover plate (Takamori, 2000)



**Figure 3- 8:** Test Specimen (Physical Component)

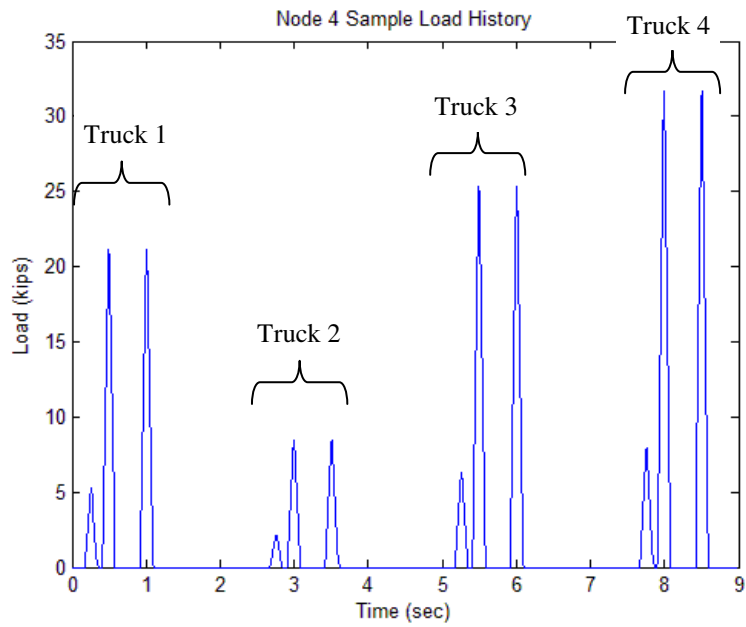


**Figure 3- 9:** Sample Load History for Node 4

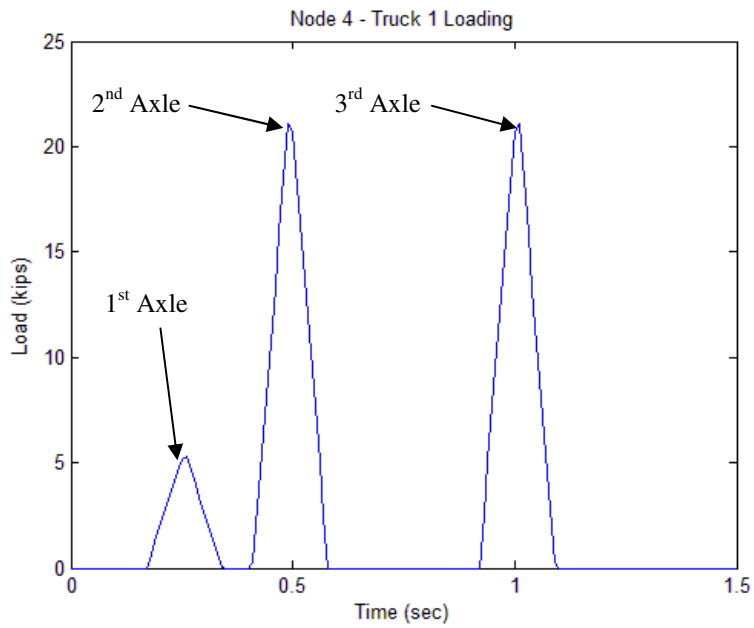


**Figure 3- 10:** Individual Truck Loading

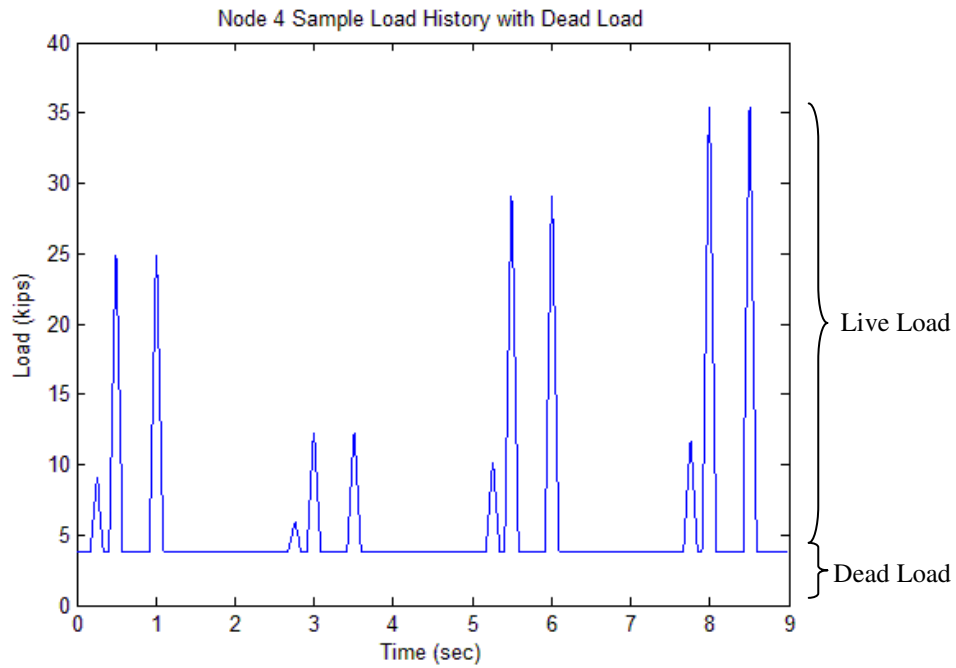


Figure 3- 11: Complete Loading History

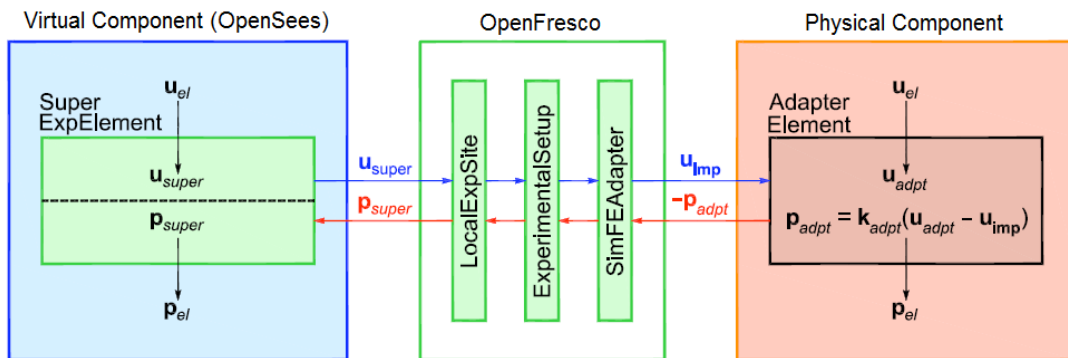


Figure 3- 12: OpenFresco Flow Diagram (Schellenberg, et al., 2009)

## **Chapter 4: Hybrid Testbed for Sensors Characterization**

### ***4.1 Overview***

As described in the previous chapters, a hybrid testing setup demonstrated with a prototype steel I-girder highway bridge was developed. A series of hybrid tests were performed to characterize this sensor characterization testbed. The hybrid tests can be divided into three stages. The first stage is the actual hybrid testing of the Yellow Mill Pond Bridge where realistic traffic loads were generated and applied to the bridge model in the hybrid testing setup. These results are discussed in section 4.2 and are evaluated as to how accurate the hybrid testing setup represents the actual response of the Yellow Mill Pond Bridge subjected to traffic loads. The second stage involves a parametric study into the effects of the various parameters involved in the hybrid testing setup. These parameters include the ramp time of the servo-hydraulic test equipment, the type of virtual model, stress level, experimental drift in repetitive tests, and the effect of an impulse or ramp load in the time history. Each one of these parameters and their effects on the hybrid testing results are evaluated in sections 4.3 through 4.6. The final stage involves hybrid testing with a controlled environmental chamber. In particular, the effects of elevated temperatures on the hybrid tests and various sensors for structural health monitoring (SHM) is discussed in section 4.7.

## ***4.2 Hybrid Testing Results***

A hybrid testing setup was created to validate and characterize infrastructure sensor technology, using a model of the Yellow Mill Pond Bridge as the prototype. This setup consists of two primary components: the virtual component which includes the OpenSees model of the majority of a typical interior girder in the bridge and the physical component which was a 5'-0" fabricated section of the lower flange at the location where the cover plate terminates. A more in-depth description of both the virtual and physical components of the hybrid testing setup is given in Chapter 3. A photo of the physical component of the hybrid testing is shown in Figure 4-1.

From this test setup five types of data were collected: the actual force and displacement the test specimen underwent during the testing, the virtual force and midspan deflection of the virtual OpenSees model, and the nominal strain in the test specimen. The actual force and displacement in the test specimen were measured using a load cell and LVDT installed on the MTS actuator, the virtual force and displacement were available from the OpenSees Program, and the nominal strain was measured by strain gages installed on the test specimen.

The metal foil strain gages (model#: Vishay EP-08-250BF-350) used throughout the test were quarter bridge with 350 ohms resistance and were placed 8" away from the transverse cover plate interface weld so that any "hot spot" stresses near this change in cross section would not affect the strain readings from these strain gages; this way the strain recorded is the nominal strain for the test specimen. A close up view of the location of the strain gages is shown in Figure 4-2.

As described in Chapter 3, AASHTO fatigue trucks were randomly generated using a cumulative distribution function determined from real weigh-in-motion data obtained from the Yellow Mill Pond Bridge site. These fatigue trucks were generated virtually in OpenSees and the forces caused by these fatigue trucks were transmitted throughout the bridge model and later to the test specimen through the hybrid test setup. A typical figure showing the force applied to the test specimen can be seen in Figure 4-3.

Note that Figure 4-3 shows the actual force applied to the test specimen. This force is scaled up in the OpenSees virtual model, since the test specimen was fabricated at a 60% scale. In Figure 4-3, thirty randomly generated AASHTO Fatigue Trucks were applied to the Yellow Mill Pond Bridge. The two sharp peaks for each truck show the response of the structure to the rear two axles of the fatigue truck, which have the heaviest loading. The front axle of the fatigue trucks imparts a considerably smaller force compared to the rear axles and its effect on the loading is less pronounced. A close-up image showing the loading for a single fatigue truck can be seen in Figure 4-4. From the previous two figures the effects of both the dead load and moving load can be seen. The dead load is transmitted immediately at the beginning of loading and is the constant force below the moving truck loading of approximately 5.8 kips. The moving load due to passing trucks is then superimposed to this dead load shown by the peaks in the previous two figures.

The most important results that can be gathered from the previous two figures, however, is the ability of this hybrid testing platform to realistically apply load histories that closely mimic the actual loadings a bridge encounters. The unique load

history shown in the previous figure varies dramatically from the typical constant amplitude loadings that conventional structural testing uses. By virtually specifying load time histories and allowing the finite element model in OpenSees to transmit these loads to the physical test specimen, a more realistic structural response to this loading history can be determined. This is particularly important when trying to validate and characterize sensors, particularly for local SHM purposes such as ultrasonic guided wave sensors for fatigue crack detection. Since the physical test specimen is subject to the loadings shown in Figure 4-3, any sensors placed on this test specimen are also subject to this more realistic loading history and their responses to this type of loading effect (e.g., fatigue crack growth) can be characterized. This type of sensor validation is not available with conventional constant amplitude structural testing.

As described previously, Figure 4-3 shows the actual force applied to the test specimen before it has been scaled up in OpenSees. Since the test specimen is at a 60% scale, the loading seen by OpenSees is larger than the actual force the test specimen experiences. Furthermore, due to the threaded rod at the end of the test specimen, the displacement is also amplified to account for the stiffness of the threaded rod.

In the hybrid testing program, two scale factors need to be set for displacement and force respectively. This is because a 60%-scaled specimen was used in hybrid testing. One of these two factors scales the displacement applied to the test specimen and the other factor scales the force response of the test specimen to be fed back into the OpenSees model. These two factors are related by the similitude of

stresses between the physical test specimen and OpenSees model. Detailed derivation for each of the scale factors used in this hybrid test can be found in Appendix C.

The hysteresis plots of each of the steps used in scaling the force are useful in illustrating how these scaling factors are determined. Figure 4-5 shows the hysteresis loop of the physical test specimen as it was loaded throughout the hybrid test. The slope of this hysteresis plot is the true stiffness of the subassembly comprised of the test specimen and threaded-rod test fixture; however, since the threaded rod portion of the test setup has a much smaller stiffness compared to the portions for the flange and flange with coverplate, the stiffness value determined from Figure 4-5 is largely dominated by the stiffness of the threaded rod (the stiffness from this hysteresis plot is about 100 kips/in). The displacement response of the test specimen will be scaled down when it is fed back into OpenSees to account for the low stiffness of the threaded rod, and the determination of this scaling factor is shown in Appendix C. Note that the hysteresis is not linear for displacements smaller than 0.04 inches. This is due to initial force overcoming any initial slackness or gaps associated with the threaded rod fixture. This initial nonlinearity is only present at the beginning of the test when the dead load is applied and does not impact the portions of the hybrid testing when the vehicle loads are applied.

The force and displacement from the physical test specimen are scaled and fed back into the OpenSees model. The hysteresis showing this response once it has been scaled in the OpenSees model can be seen in Figure 4-6. In this figure the force has been scaled up to account for smaller scale size of the test specimen and the displacement has been scaled down to account for the low stiffness of the rod. As a

result, the slope of this hysteresis is much larger than the test specimen and more closely resembles the actual stiffness of the lower flange of the Yellow Mill Pond Bridge. The stiffness determined from this hysteresis plot is around 14,300 kips/in.

In order to determine the accuracy of the hybrid test scaling between the test specimen and OpenSees, a purely virtual finite element model was loaded using the same load history as the hybrid testing load history, and this theoretical response was compared to the actual response obtained from the hybrid testing. The hysteresis from this purely virtual finite element response can be seen in Figure 4-7. Note that since this response is from a purely virtual model, it is linear throughout the entire response and does not have the initial nonlinearity that the hybrid test hysteresis plots exhibit. In order to verify the hybrid testing scaling factors, the slope of this purely virtual finite element hysteresis (stiffness) should be similar to the slope determined from the hybrid testing (in Figure 4-6). The stiffness from the purely virtual model hysteresis in Figure 4-7 is 13,400 kips/in. This stiffness value is relatively close to the stiffness value from the hybrid testing, which indicates that the response of the physical test specimen after it is scaled up in OpenSees is similar to the theoretical response of the Yellow Mill Pond Bridge. The following table summarizes the stiffness values determined from each of the previous three hysteresis plots.

**Table 4- 1:** Comparison of Stiffness from Hysteresis Plots

Hysteresis Model	Stiffness (kip/in)
Test Specimen	100
OpenSees	14,300
Purely Virtual Model	13,400

Accurately determining the scale factors for the hybrid testing can be very difficult, particularly when an element is present to amplify the displacement (the threaded rod in this hybrid test). The stiffness of this type of element along with other second order type deflections such as out of plane displacement and non-eccentric loading need to be fully considered in order to have accurate results. The calculations in Appendix C provide a theoretical basis for determining these stiffnesses and associated scale factors, however, the best way to determine these stiffnesses is through experimentally loading and unloading these elements to obtain their hysteresis curves as was done above. Using these hysteresis curves, the stiffness of the various components in the test specimen can be accurately determined and used in determining the scaling factors.

The scaling that is performed between the actual loading in the physical test specimen to produce the loading as seen in the virtual OpenSees model can be seen in Figure 4-8. In this figure, the top plot shows the actual force applied to the physical test specimen during the hybrid testing. The bottom plot shows the force after it has been scaled up for the OpenSees virtual model. Even though the force is scaled up between the physical and virtual components, note that the shape of the force applied is the same for both components. The second aspect of Figure 4-8 is the time domain range for both the physical and virtual testing. Note that the loading for the physical test specimen took roughly 650 seconds to complete. However, the virtual time in the OpenSees model indicates the test only took around 52 seconds to complete. This difference in the actual and virtual time ranges shows the effect of the ramp time of the servo-hydraulic test system. For example, in addition to the time consumed by the

controller in communicating with servo-valves and sensors on the actuator, between each load step, the hydraulic pressure in the actuator needs to be ramped up to the level prescribed by OpenSees. This ramp time cannot be too fast in order to ensure the stability of the servo-hydraulic test system. In addition to the hardware-related ramp time, the communication between the OpenSees software and MTS FlexTest 60 controller takes some time as well as the computations performed in OpenSees between each load cycle. The combination of all of these sources causes the actual time to complete the test to be much longer than the actual loading time in the virtual model. A more in-depth look into the effect of the ramp time on the actual time to complete the hybrid testing is presented in Section 4.3.

In addition to measuring the force applied to the test specimen, the midspan deflection of the virtual model was also considered. This midspan deflection was measured at the midspan lower flange node, which is shown in Figure 4-9. The midspan deflection obtained from the virtual part of the bridge structure can be seen in Figure 4-10. Compared to the force response of the test specimen, the midspan deflection is less affected by the individual axles of the fatigue truck. Instead, each fatigue truck creates a general dip in the deflection and the point where each of the axles begins to load the girder cannot easily be distinguished like in Figure 4-3. The reason for this is that the location of the test specimen is relatively far from the midspan deflection location (refer to Figure 4-9) and the midspan deflection is a global response of the finite element model in OpenSees. Overall, the order of magnitude of the midspan deflection (about 1" average deflection) agrees with typical deflection values for bridges of this span.

As was described earlier, in order to verify the accuracy of the hybrid test results, a purely finite element model was loaded using the same load history as the hybrid testing load history, and this theoretical response was compared to the actual response obtained from the hybrid testing. A comparison of the force applied to the test specimen in OpenSees (after the force has been scaled) can be seen in Figure 4-11.

In this figure, the red line represents the purely virtual finite element solution, while the blue line shows the actual force response as measured during the hybrid testing. In general, the experimental results appear to match the general shape of the finite element analysis results with the exception near the peaks and troughs of each of the load cycles. At these locations, the analysis results indicate that the force should be lower at the peaks and higher at the troughs. Differences between these two results can be attributed to several factors. First, since the test specimen was fabricated at 60% scale and incorporates a threaded rod to amplify the displacement, the force applied to the test specimen needs to be scaled up as was shown in Figure 4-8. This scaling takes into account the stiffness of the threaded rod, test specimen scale factor, and similitude of stresses. However, there are other second order effects that can occur during testing, that are difficult to account for in the scale factor estimation. Due to the nature of experimental testing, there is usually some eccentricity in the test specimen. At high loads, this eccentricity can cause out of plane deflections that were not considered between the components. The components in the test setup are also assumed to have rigid connections that do not displace during testing. However, in actuality this is not the case and second order deflections

can occur in these connections. At lower loads, the effect of the displacement from these connections may be negligible, however, at higher loads (such as in the case of hybrid testing), these deflections in the connections between the elements can further impact the results.

The deflections from the connections and the second order displacement from any eccentricity in the test setup may not be fully accounted for in the scale factor for the test specimen. This may account for the difference between the hybrid testing results and the virtual finite element results. The pure finite element solution also has many assumptions in the model, where loads are assumed to act entirely axially with no eccentricity, there are no stress concentrations at the connections between the elements, and all nodes are friction-less pins. Thus, the purely virtual finite element solution contains some assumptions which may lead to differences between the results of the hybrid testing and virtual solutions. Overall, the hybrid test force results are very similar to the expected virtual finite element solution. For most of the loading history, the results are within 5% of each other. Furthermore, the shape of the load histories are same, which indicates that the force the test specimen experienced, closely matched what the actual Yellow Mill Pond girders experienced.

In addition to the force, the midspan deflection was also determined for both the pure finite element solution and the hybrid testing results. This midspan deflection can be seen in Figure 4-10. Unlike the force results, the midspan deflection results were almost identical. In the above figure, the theoretical displacement is shown in red and it almost entirely overlaps the displacement found through the hybrid testing (shown in blue). The reason the hybrid testing results are closer to the

theoretical results for the midspan deflection is because the location of the midspan deflection is relative far away from the test specimen, as seen clearly in Figure 4-9. Since the midspan deflection is dependent upon the responses of all the members in the truss finite element model, small errors in the test specimen displacement would not have a profound impact on the overall midspan deflection according to Saint Venant Principle. There are 100 other truss elements in the OpenSees finite element model that contribute to this midspan deflection.

In addition to measuring the force and midspan deflection during the hybrid testing, strain gages were also installed on the test specimen to verify the nominal strain on the test specimen. These strain gages were installed 8" away from the transverse weld at the cover plate interface in order to reduce the effects of any stress concentrations from the abrupt change in cross section at the cover plate interface. Figure 4-2 shows the location of the strain gages that measure the nominal strain in relation to the location of the transverse weld.

Unlike the data obtained from the load cell on the loading actuator which was accurate to within several decimal points for both the force and deflection, the data from the strain gages typically includes large amounts of noise from various signals around the testing equipment. As a result, the purpose of the strain gages was to validate the order of magnitude of the strains and forces that the test specimen was subject to during testing.

The strain gages also serve as a simple instrumentation for structural health monitoring. It is typical in many states to install strain gages on bridges when severe issues on structural defects or load conditions have been detected on the bridge

structural elements. This is particularly important with bridges that exhibit fatigue defects, since the stress range of the loading history is a critical parameter in determining the cause and remaining life of any fatigue spots in the bridge. Since these strain gages serve as a basic sensor for structural health monitoring (see, e.g., Zhou 2006), the ability of the hybrid testing method to characterize and validate structural health monitoring sensors can be demonstrated using strain gages.

The nominal strain measured in the strain gages compared to the actuator force applied to the test specimen can be seen in Figure 4-13. In this figure, the green line is the strain as measured by the strain gages, while the blue line is the force measured by the load cell on the hydraulic actuator. The main concept this figure shows is the shape of both sets of data. As Figure 4-13 shows, the strain measured by the strain gages closely mimics the shape of the actual force the test specimen was subjected to. Each of the peaks of the force history also appears accordingly in the strain data. The overall shape of both sets of data follows the same pattern, which indicates that the strain gages were accurately installed and properly measuring the strain during the hybrid testing.

The next issue with these strain gages is the overall accuracy of their results compared to the force measured by the load cell. Since the strain measured is the nominal strain, it can be converted to force by multiplying the strain by Young's Modulus and the cross sectional area of the steel plate. A plot showing this calculated force from the strain data compared to the force measured from the load cell can be seen in Figure 4-14.

In this figure, the blue line is the calculated force from the strain measurements from the strain gages, while the red line is the force measured from the force transducer on the actuator. As this figure shows, the overall order of magnitude of the dynamic force (i.e., excluding the static part due to dead load of the bridge) determined from the strain measurements agrees very well with the actual dynamic force measured from the load cell on the actuator. Furthermore, the shape of the force determined from the strain gages is very similar to the shape of the force from the load cell, which again shows that the strain gages were relatively accurate in measuring the strain during the hybrid testing.

The main reason as to why the calculated force from the strain gages differed from the actual force values is the need to overcome the backlash (i.e., initial slackness or gaps associated with the threaded rod fixture) in the beginning of the test when dead load is applied to the test specimen. Other factors could also contribute to the difference. For example, eccentricity may have existed in the loading setup due to difficulty in perfect alignment of the axis of the test specimen with the actuator. If the centerlines of the actuator and the test specimen have a slight eccentricity, this will impart a bending moment on the test specimen causing the nominal strain on the surface of the test specimen to be higher or lower than what was anticipated.

In general, the strain gages were useful in verifying the order of magnitude and shape of the load history on the test specimen. From the perspective of characterizing and validating structural health monitoring sensors, this hybrid test demonstrated how these sensors can be characterized on select locations of a structure through a realistic loading history. The use of these strain gages for the hybrid test

for the Yellow Mill Pond Bridge demonstrated the particular case of how strain gages can be validated and more realistically tested without the need for a full scale structural assembly. Furthermore, characterizing and validating structural health monitoring sensors through hybrid testing is not just limited to strain gages but can be implemented over a wide variety of structural health monitoring sensors including acoustic emission sensors for fatigue, ultrasonic crack detection systems (e.g., OmniScan phased array NDE system), and other non-destructive testing sensors.

This hybrid testing platform demonstrated how structural testing of large scale systems can occur without having to fabricate every portion of system. Furthermore, it was shown how more realistic loading histories can be applied through the use of this hybrid testing platform. However, simply implementing a hybrid testing setup can have a variety of issues. These include the ramp time of the servo-hydraulic testing system, complexity of the virtual model, and experimental drift over long testing periods, just to name a few parameters. The effect of each of these parameters on the hybrid testing method is the subject of the following sections of this chapter.

### ***4.3 Ramp Time***

This section deals with a series of parametric studies related to the hybrid simulation testbed for sensor characterization. While the hybrid testing system is effective in applying realistic loading conditions and combining virtual modeling with physical testing, there are a variety of parameters associated with the hybrid test system which can impact the accuracy of the hybrid testing and results. The first of these parameters is the ramp time, which is the subject of this section.

In section 4.2, Figure 4-8 shows the difference in the virtual (OpenSees) testing time to the actual, physical testing time. Typically, the actual, physical testing time of the test specimen is much longer than the time in the OpenSees model. This means the physical test specimen is being loaded at a rate that is much slower than the actual virtual rate. The reason for this disparity between the virtual and physical components is largely due to the ramp time of the servo-hydraulic hybrid testing system. An extremely short ramp time is often not practical as a hybrid testing system would become unstable under such conditions. For example, in order to load the specimen at a rate where the response is controllable and accurate, often the ramp time is set so that one second of loading history from OpenSees may take over ten seconds for the actuator to apply the load. By using a slower loading rate, the specimen can be loaded in a stable manner. However, the main issue with this is that the rate at which the physical test specimen is loaded does not match the virtual loading history rate, which for the case of the Yellow Mill Pond Bridge is based on the actual loading rate of a truck passing over the bridge at 40 mph. The ratio between the virtual loading time and physical test time (to complete the specified virtual

loading) is called time ratio, which is an important parameter to quantify the real-time testing ability (i.e., how fast a test can be performed) of a hybrid testing system.

In order to manipulate this loading rate, the ramp time value in the hybrid simulation software can be adjusted to a faster or slower rate. However, there is a lower bound value for the loading rate achievable for any given hybrid testing system, which depends on the hydraulic power (pump capacity, hydraulic service manifold flow rate, servo-valve flow rate) in addition to other factors related to computing and data communication. The question that now arises is: What effect would increasing the loading rate by reducing the ramp time have on the results, and what is the limit for the system to be controllable? In order to answer these questions, a baseline ramp time value of 0.1 seconds was set for the system. This ramp time was found to produce very accurate and controllable results, and was used throughout the hybrid test in section 4.2. The force history applied to the test specimen from the actuator for the first fatigue truck passing over the bridge can be seen in Figure 4-15 (note that this force history is for the truss model of the Yellow Mill Pond Bridge, and also includes the initial ramp).

Note that in the OpenSees virtual model, this first fatigue truck loading history is less than 4 seconds, however, due to the very slow ramp time, it physically takes the actuator around 45 seconds to apply the force history to the physical test specimen. This is roughly a 11:1 time ratio for the hybrid testing. Now that this baseline value has been established, the effect of several other ramp times can be compared.

Figure 4-16 shows the effect of reducing the ramp time for the truss model of the Yellow Mill Pond Bridge. In this figure, it can be seen that as the ramp time decreases, the time for the first fatigue truck to complete its load history also decreases as expected. However, the time it takes for the first fatigue truck to complete its loading is not linearly related to the ramp time. This is evident from Figure 4-16, since the green line (ramp time of 0.01 seconds) takes a much smaller amount of time to complete its loading compared to the red line (ramp time of 0.1 seconds). However, the cyan line (ramp time of 0.001 seconds) is not that much shorter of a time period than the green line. Furthermore the blue line (ramp time of 0.0001 seconds) is almost identical to the cyan line. Thus, there is a limit as to how fast the ramp time can be for the actuator, which approximately corresponds to a time ratio of 2.5:1. This limit is illustrated as the asymptote in Figure 4-17.

In this figure, the time to complete the entire hybrid test (thirty fatigue trucks passing over the bridge) is plotted for each of the ramp times for the truss model. Note that there is a large decrease initially in the time to complete the test when the ramp time is reduced. However, after a ramp time of 0.005 seconds, the time to complete the test converges upon about 130 seconds. Note that the time to complete the loading in the virtual OpenSees model is about 52 seconds. Thus, the maximum ratio of the loading rates is about 1:2.5 meaning for every one seconds of loading in the virtual component, it takes about 2.5 seconds for the hybrid testing system to apply this loading. A summary of the ramp times versus the time to complete the hybrid testing can be found in the following table:

**Table 4- 2:** Test Duration for Truss Model at Various Ramp Times

Ramp Time (sec)	Time to Complete Test (sec)	Time Ratio
0.1	644	12.4: 1
0.05	390	7.5:1
0.01	184	3.5:1
0.005	138	2.7:1
0.001	133	2.6:1
0.0001	129	2.5:1

As the results show, the truss model is controllable for any practical ramp time (ramp times below 0.0001 are impractical). Furthermore, the time to complete the test converges upon a constant value after a ramp time of 0.005 seconds. Thus, after a ramp time of 0.005 seconds, the rate at which the system is applying the loading to the test specimen is limited by factors other than the ramp time in the hydraulic system. Two other factors include the communication time between the virtual model, MTS FlexTest60 controller, and servo-valves of the loading actuator and the numerical computational time in OpenSees. These two factors are independent of the hydraulic-related ramp time, and as long as the same OpenSees model is used, these factors will remain constant. Thus, for the truss model of the Yellow Mill Pond Bridge, the fastest loading ratio that can be achieved is 2.5:1. The question that now arises is: Is this limit on the loading ratio constant for any type of OpenSees model or is it dependent on the type and complexity of the model?

To answer this question, a second, more sophisticated finite element model using a refined mesh of 2-D quad finite elements was used for the girder web which was subject to the same parametric study of various ramp times. An illustration of this refined mesh Yellow Mill Pond Bridge OpenSees model can be seen in

Figure 4-18. Unlike the previous truss model used to represent the Yellow Mill Pond Bridge, this refined mesh model has hundreds of smaller quad elements throughout the web of the girder. This more sophisticated finite element model should yield more accurate results compared to the truss model, however, it is computationally more involved and time consuming compared to the much simpler truss model. A typical force loading on the test specimen for this refined mesh model can be seen in Figure 4-19.

Unlike Figure 4-15 for the truss model, Figure 4-19 does not have as smooth of results. At locations of large changes in force, the refined mesh model takes several cycles to converge on the solution and this is shown through some of the oscillations that occur particularly at the largest peak of the previous figure. Since the finite element model of the Yellow Mill Pond Bridge with the refined mesh is much more complex than the truss model, the solution algorithm is more involved and takes several cycles to converge upon the solution. For a ramp time of 0.1 seconds, these oscillations are transmitted to the physical test specimen at a relatively slow rate so that there is no issue with controlling the force during these oscillations. However, at smaller ramp times, these oscillations could become a control stability issue.

Several other ramp times were also implemented for the refined mesh model and their results compared to the 0.1 second ramp time is shown in Figure 4-20. From this figure, it appears that as the ramp time decreases, the time to complete the loading from the first fatigue truck appears to get smaller at a linear rate related to the ramp time. However, below a ramp time of 0.03 seconds, the system became unstable and the hydraulic actuator was not able to control the force during the

testing. As the ramp time decreased, the previous figure shows that the oscillations become more and more pronounced throughout the load history. This is shown in a close up view given in Figure 4-21. In this figure, the plot on the left (ramp time 0.05 seconds) has a much crisper force history than the plot on the right (ramp time 0.03 seconds), which has large oscillations throughout its force history. These oscillations are particularly pronounced when the force is decreasing.

Note that a ramp time of 0.03 seconds was the smallest, controllable ramp time at which the test was still stable. Below this ramp time, the actuator was unable to control the force in the test specimen. This control issue is shown in Figure 4-22 where a ramp time of 0.02 seconds was applied to the model. In this figure, the oscillations are very pronounced throughout the entire duration of the load history. Furthermore, these large oscillations are at a very high frequency, which cause large vibrations in the testing equipment. These large vibrations cannot yield accurate results. For a ramp time of 0.02 seconds, the testing equipment could have finished the test, however, large vibrations would have been present throughout the test. Ramp times below 0.02 seconds, however, have a stability issue rather than a vibration issue.

A stability issue refers to the inability of the testing setup to converge upon a solution at the beginning of the test, which can cause the force to grow wildly and uncontrollably. This instability is shown in Figure 4-23. As this figure shows, for a ramp time of 0.01 seconds, the hydraulic actuator was not able to control the force at the beginning of the test. The force began to oscillate uncontrollably around 3 seconds into the test before it tripped the lower bound for the force shortly after 4.5

seconds. Unlike the large vibrations and oscillations that caused inaccuracies of the results for a ramp time of 0.02 seconds, when the ramp time is set at or below 0.01 seconds, the issue is not with vibration but instability of the force. Thus for the refined mesh model considered in this research, there is three phases to the response: ramp times at or above 0.03 seconds are stable and have low vibrations and still yield reasonable results, ramp times around 0.02 seconds have very large vibrations and have inaccurate results, and for ramp time at or below 0.01 seconds the system is unstable and cannot complete the hybrid test. Figure 4-24 summarizes the effect of the ramp time on the actual time to complete the hybrid test. The numerical values for Figure 4-24 are summarized in the table below:

**Table 4- 3:** Test Duration for Refined Mesh Model at Various Ramp Times

Ramp Time (sec)	Time to Complete Test (sec)	Time Ratio
0.1	725	14:1
0.05	468	9:1
0.04	405	8:1
0.03	357	7:1
0.02 and Below	Unstable or High Vibrations	N/A

Unlike the truss model for the Yellow Mill Pond Bridge, the refined mesh model becomes unstable at lower ramp times. This indicates that the stability and ability to control the force is not solely dependent on the hydraulic-related part of the ramp time. Instead, the complexity of the virtual model and numerical integration algorithm also have a large impact on the overall stability of the hybrid testing system as the ramp time decreases. For the case of the truss model with a very simple finite element model and integration algorithm, there were no issues with stability for any

ramp times and the maximum rate at which the test could be conducted was 2.5:1 (2.5x the virtual time). The refined mesh model however could only achieve a loading rate ratio of 7:1 (7x the virtual time) and still have a stable, accurate solution. While neither of these models is able to apply the force at real time (1:1 loading rate ratio), both of these loading rates provide a baseline value as to how fast the hybrid test can be performed given a virtual loading history. Furthermore, these results also show that the fastest rate a hybrid test can be performed at and still obtain accurate results, also depends on the complexity and numerical integration algorithm of the virtual model for a given hydraulic system comprised of hydraulic pump, servo-valves and hydraulic service manifolds.

### ***4.3 Model Type***

The hybrid testing system consists of two major components: the virtual and physical testing components. The latter of these two components, the physical testing component is limited to the actual testing equipment (hydraulic system and test frames) available in a structural testing lab. This component remains constant through all the tests and cannot be easily changed. However, the virtual component of the testing is a model based on the OpenSees software platform within the OpenFresco framework. Since this component is virtual, it can be easily changed and modified from test to test. Furthermore, as sections 4.2 and 4.3 showed, the choice and complexity of the virtual model can have a dramatic effect on the accuracy and stability of the results. This section deals with the different types of models that can be implemented in OpenSees to perform the hybrid testing, the limitations of each of these model types, and the accuracy of their solutions.

Four different model types were created to show the effect of the model type on the hybrid testing results for the Yellow Mill Pond Bridge. The most basic of these model types is the truss model (shown earlier in Figure 4-9) where a typical interior girder of the Yellow Mill Pond Bridge had been simplified into a truss model. This basic model is the computationally simplest model and was the model used for the hybrid testing in section 4.2.

A second truss model was made with the same geometry as the basic truss model, however mass was added to each of the upper chord nodes to represent the mass from the girders and concrete deck. By adding mass, this second truss model could incorporate the dynamic effects due to the mass as well as any damping effects.

Rayleigh damping was chosen to model the damping in the bridge and a viscous damping coefficient of 0.01 was assigned to the first two modes of the structure.

The third model used was much more sophisticated and was based on using a refined mesh of quad elements to represent the web of the girder. An image of this refined mesh model can be seen in Figure 4-18. This refined mesh model was also used in section 4.3 in evaluating the ramp time of a computationally complex virtual model. By using 2-D quad elements to represent the web that are meshed at very small dimensions, the goal is to create a more accurate solution compared to the truss model. There is no damping assigned in this model.

The fourth and final model used is based off the refined mesh model geometry. The only difference is that mass has been assigned to all of the quad elements and nodes along the top and bottom flanges to represent the mass from the upper and lower flanges and concrete deck. Similar to the second truss model, this model also incorporated Rayleigh damping where a coefficient of 0.01 was assigned to the first two modes of the bridge structure.

Unlike the hybrid testing shown in section 4.2, only five randomly generated fatigue trucks were generated and used for the loading of each of the four virtual models. Note that all of the following results in this section are for the forces and displacements as seen virtually in OpenSees after they have been scaled up. For the basic truss model and truss model with mass included, the force that was applied to the test specimen can be seen in Figures 4-25 and 4-26. Similar force histories for the refined mesh model with and without mass can also be seen in Figures 4-27 and 4-28.

From these four figures, it is evident that when mass is not included in the model, the force history is smoother and each peak from each of the axle loads can be clearly identified. In both Figures 4-25 and 4-27, a simple linearly elastic solution algorithm was used that did not need to take into account any dynamic mass effects. Figures 4-26 and 4-28, however show the inertia-induced dynamic effects and damping into their force time histories. This is evident by the response oscillating overriding the general waveform of the response without any mass. This is typical for the dynamic response of a bridge structure where the mass effects are included.

A close up view of the effects the mass has on the results can be seen in Figure 4-29. This figure clearly shows how the models with the dynamic effect oscillate about the force histories for the models without any mass. From the perspective of creating realistic loading conditions through the hybrid test setup, these results show how very complex and realistic loadings with vibration effects can be applied to a test specimen. Particularly in the case of models with the dynamic effect included, this force history is much more complex compared to conventional constant amplitude sinusoidal loading that is used frequently in conventional structural fatigue testing. Furthermore, these detailed and complex force histories are applied to the test specimen, and any structural health monitoring sensors placed on the physical test specimen would also be subject to these complex force histories. This enables a much more realistic response characterization of these structural health monitoring sensors, since the loadings they are subject to closely resemble the actual loading histories they will be subject to in the field.

Beyond the force history for the test specimen, data was also collected for the midspan deflection of each of the bridge models throughout the hybrid testing. The midspan deflection for each of the four models is shown in Figures 4-30 through 4-33. In these figures, the waveform of the midspan deflection does not show the distinct time when each axle begins to load the bridge like in the force history, but rather the midspan deflection is a gradual curve for each fatigue truck. As described in section 4.2, this is because the midspan deflection incorporates all the individual member effects of the finite element model in OpenSees. Similar to the force history, the models without dynamic effects have a very smooth deflection history, while the deflection history for the models with dynamic effects appear to oscillate about the deflection waveform of the case without mass. Again, this is anticipated given the dynamic response that the inertia mass induces compared to the static response of the bridge models in which the mass is not assigned.

A figure showing the effect the mass has on the midspan deflection for both the truss and refined mesh model can be seen in Figure 4-34. Similar to the mass effects on the force history, this figure shows how the models that incorporated the dynamic effect have a response that oscillates about the waveform corresponding to the bridge model without mass. As stated in the case for the force history, this deflection history represents a much more complex and realistic midspan deflection history. Compared to conventional load testing with constant amplitude load cycles, the use of this hybrid testing system with detailed virtual models and environmental loading allows for much more realistic structural testing and high fidelity structural response simulation.

The four virtual models have differences in either finite element type or assigned mass at nodes, which accordingly cause their responses to be slightly different from each other. This is evident from the maximum midspan deflection for all four models, as shown in Figure 4-35. From this figure the oscillatory nature of the models with mass can be clearly seen. Also it is noted that the largest midspan deflection occurs when the dynamic mass effects are included, however, note that all four midspan deflections are within 1/10" of each other. The maximum midspan deflection and maximum force in the test specimen that occurs during the hybrid testing have been tabulated in Table 4-4.

**Table 4- 4:** Max Force and Deflection for Each Model Type

Model Type	Max Force (kips)	Max Deflection (in)
Truss	43.82	-1.325
Truss w/mass	44.68	-1.359
Mesh	47.91	-1.281
Mesh w/mass	50.54	-1.359

#### ***4.4 Force Level***

One of the major advantages of hybrid testing is that the magnitude of the loading can be easily adjusted through the virtual component in the testing. However, oftentimes issues can arise when increasing (scaling up) the load from typical levels that are used. In case of the Yellow Mill Pond Bridge hybrid test performed in this research, one major concern was second order effects on the displacement that may have been caused by support conditions for the loading actuators. Since the loading for the hybrid test was performed parallel to the ground, the actuators and test specimen were anchored to a large W-beam, which was assumed to act as a rigid support frame for the test setup due to the large moment of inertia of the W-beam. A picture of this supporting frame comprised of W-beams and the test setup can be seen for reference in Figure 4-36.

One potential issue with this test setup is that as the actuator applies an axial load to the test specimen, the supporting W-beam will be subject to a moment from the actuator. This moment will cause the W-beam to bend, however, for small loads, the bending of the W-beam and deflection at the ends will be negligible and not impact the deflection and results for the test specimen during the hybrid testing.

When initially setting up the hybrid test setup, several cyclic loading patterns at different loading frequencies were applied. At around 2 Hz the loading appears to match the natural frequency of the supporting frame and the ends of the supporting beams were observed to deflect by over one inch due to resonance. A large deflection like this at the ends would have a large impact on the testing results since it is assumed the supports do not move. The loading frequency for the hybrid tests used

throughout this thesis are well below the natural frequency of the supporting frame (2 Hz), however this large deflection at the ends of the supporting W-beam provided the primary motivation for the parametric study of this section. This parametric study is to determine if there is a linear relationship between increasing the loading magnitude and the displacement response of the test specimen. It is possible that at large loading magnitudes, the ends of the beam will deflect beyond a negligible amount and affect the displacement in the test specimen.

The original load specified in the hybrid testing used in the previous sections was scaled at four different levels (1.0 scale, 1.25 scale, 1.50 scale, and 1.625 scale). The 1.625 scale is the largest of the loading that can be scaled without causing yielding of the threaded rod in the test setup, and thus it represents the practical upper limit that the loading can be scaled to for this particular setup. A plot showing the effect of the loading scale level on the force applied to the test specimen can be seen in Figure 4-37. The maximum value of the force history for each scale factor is shown in Figure 4-38. From these two figures, it is evident that as the loading is scaled up, the force history applied to the test specimen also scales up proportionally. This linear proportion relationship is particularly evident from Figure 4-38 where a linear regression line was plotted with the data. The coefficient of determination,  $R^2$  value for this regression line was 0.999, which represents almost a perfect linear fit to the data. This indicates that any deflections that occurred in the support W-beam frame were negligible and did not contribute towards affecting the force history of the test specimen for the load range considered. A similar analysis was made into the

deflection history for the test specimen. The result of scaling the loading on the displacement history is shown in Figures 4-39 and 4-40.

Similar to the results for the force history, the displacement history also followed a linear relationship to the magnitude of the loading applied to the test specimen. A linear regression fitted to the maximum displacement for each loading scale level shown in Figure 4-40 verifies this linear relationship, since the coefficient of determination,  $R^2$  value is 0.999. A summary of the maximum force and displacement in the test specimen for each loading magnitude scale factor can be seen in Table 4-5:

**Table 4- 5:** Summary of Max Force and Displacement at Various Loading Factors

Scale	Max Force (kips)	Max Displacement (inches)
1	16.75	0.184
1.25	21.07	0.228
1.5	25.31	0.274
1.625	27.4	0.297

From these results it is evident that at the low loading frequency of the hybrid testing, scaling up the loading does not affect the accuracy of the test results. Thus the supporting W-beam frame to which the actuator is anchored effectively acts as a rigid frame. However, it should be cautioned that at loading frequencies near the natural frequency of the test setup, resonance can occur and lead to large displacements of the test setup which can lead to inaccurate results. But this problem can be solved by increasing the stiffness of the support frame or anchor the test setup directly to strong floor using strong tie downs. Overall, when evaluating scaling up

the force used in a hybrid test, both the magnitude of the loading and the actual loading frequency of the applied loading to the test specimen need to be considered. However, typically at low loading frequencies, if the support conditions are stiff enough, such as in the case of the hybrid test performed in this research, the effects of any second order displacement from scaling up the force can be neglected.

## ***4.5 Experimental Drift***

Due to the ability of hybrid testing to apply loading histories that are more complex than conventional constant amplitude loading, hybrid testing provides an attractive testing method for performing more realistic long term, high cycle testing. Variable amplitude fatigue may have different behavior from those corresponding to constant amplitude stress range (Albrecht and Lenwari 2009). In the case of fatigue testing, fatigue tests can take millions of cycles to complete. In these fatigue tests, the load is oftentimes simplified to a constant amplitude sinusoidal loading due to the high number of loading cycles applied during a fatigue test. Hybrid testing offers an alternative method of performing high cycle testing where the loading history can be much more detailed and realistic.

In the virtual component of the hybrid testing, each loading cycle contains numerical integration which converge upon a solution for each time step. Each of these integration step may introduce a small roundoff error, which for tests with a short duration, does not have any significant impact on the results. However, for longer duration fatigue tests which can take millions of cycles and months of testing, these small roundoff errors may accumulate and become significant to cause drift in the experimental data. This roundoff error is the subject of this parametric study, which looks into the effect of experimental drift for cyclic loading using a hybrid test setup.

The cyclic loading applied in the hybrid test was a typical fatigue truck scaled at the same level for thirty trucks (approximately 30 minute hybrid test). The displacement applied to the test specimen is shown in Figure 4-41. Theoretically, the

displacement history on the test specimen should be constant for all thirty of the fatigue trucks. However, as mentioned previously, due to the round-off errors of each time step and the overall nature of experimental testing, each loading cycle may have a slightly shifted displacement response. From Figure 4-41, it appears that each of the loading cycles has the same displacement response without any significant drift. However, a more in-depth look at the maximum displacement of each loading cycle will give a clearer picture as to any experimental drift that may have occurred during the hybrid testing. A plot showing the maximum displacement of the test specimen is shown in Figure 4-42. Note the scale on the y-axis is very small compared to Figure 4-41. On this figure, three regression lines have also been plotted. The red line represents the standard linear regression for the data and the two dashed blue lines represent the statistical upper and lower 95% confidence regression lines for the data.

As this figure shows, there is some variability in the maximum displacement for each loading cycle. Furthermore, from the upper and lower 95% confidence regression lines, there is a statistically significant upward trend in the displacement over the loading history. Even though an experimental drift exists, the question is how much will this drift affect the data? For the above figure, the slope of the regression line is  $7.084 \times 10^{-6}$  in/cycle. This is a very small drift error, and for this hybrid test with only 30 loading cycles, the effect is only  $30 \times \text{slope} = 2.125 \times 10^{-4}$  in, which is a negligible effect. However over a longer loading period such as for 1,000,000 cycles, which can be typical for fatigue tests, the experimental drift would be  $1,000,000 \times \text{slope} = 7.084$  in. This drift value is very significant, since a drift of 7.084 inches would be a very significant error and in the case of the Yellow Mill

Pond hybrid test would yield the threaded rod. Thus, for longer duration tests, this experimental drift can become significant. Note that the above results were for the simplified truss model, which has a much simpler and accurate solution algorithm compared to the refined mesh model. Due to the large amount of elements in the refined mesh model, the round-off errors would be expected to be even greater per load cycle. The same loading applied to the truss model in Figure 4-41 was also applied to the refined mesh model and the results can be seen in Figure 4-43. This response appears to be very similar to the response for the truss model. Once again, since the drift that can occur is very small for 30 load cycles, a closer look needs to be made of the maximum displacement that occurs for each load cycle. This maximum displacement for each load cycle in addition to a linear regression line and 95% confidence regression lines are shown in Figure 4-44.

Similar to the figure showing the maximum displacement for the truss model, the maximum displacement for the refined mesh model also has a statistically significantly slope in its linear regression lines. This indicates that experimental drift is also occurring in this refined mesh model where the displacement is slowly increasing each load cycle. The slope on this linear regression line is  $1.360\text{e-}5$  in/cycle. This is one order of magnitude larger than the truss model. For a long term fatigue test which may have 1,000,000 load cycles, the experimental drift in this case would be  $1,000,000 * \text{slope} = 13.6$  in. This is a very substantial displacement and would induce very large errors in the testing equipment and would most likely yield one of the components in the test setup. As the refined mesh results show, as the model gets more complex and the numerical solution methods introduce larger round-

off errors, the experimental drift also gets larger and more pronounced for higher loading cycles. A table summarizing the experimental drift for both the truss and refined mesh models can be found in Table 4-6:

**Table 4- 6:** Experimental Drift for Various Model Types

	Model Type	
	Truss	Refined Mesh
Regression Slope (in/cyc)	7.08E-06	1.36E-05
Upper 95% Slope (in/cyc)	9.96E-06	1.76E-05
Lower 95% Slope (in/cyc)	4.21E-06	9.6E-06
1,000,000 Cycles Drift (in)	7.08	13.6

In addition to the drift in the displacement of the test specimen, there is also the potential for experimental drift to occur in the strain gages on the test specimen. Figure 4-45 shows the nominal strain in the test specimen for the same 30 constant truck loading used in determining the displacement drift. From this figure, it is evident that the data from the strain gages is not as crisp as the data for the displacement of the test specimen. A similar figure can be seen in Figure 4-46 for the refined mesh model.

Similar to the truss strain history, the refined mesh strain history contains noise causing fluctuations in the data obtained. Due to these fluctuations a statistically significant trend in the strain drift of the maximum strain values for each cycle could not be determined. Rather, the maximum strain values appear to be distributed randomly. This is evident from Figures 4-47 and 4-48 which show the maximum strain for each cycle for both the truss and refined mesh models. Note that

linear regression lines have not been added to this figure since there is no statistically significant trend in the strain drift.

Overall, for hybrid tests of short duration, experimental drift of the data can be considered negligible and will not impact the overall accuracy of the results.

However, for longer tests where tens of thousands of loading cycles may be performed, experimental drift caused by round-off errors in the numerical solution algorithm may become significant and impact the accuracy of the results. This drift problem can be overcome by embedding a filter algorithm in the hybrid testing software to remove the drifting trend from the displacement command signal. As shown through comparing both the truss and refined mesh models, the rate at which these experimental drift errors affect the data is largely dependent upon the complexity of the model being used and magnitude of the round-off errors in the numerical solution algorithm. For high cycle fatigue tests further work needs to be done to improve the hybrid testing software capability in filtering out the drift from displacement command signal, which should not be too difficult to implement.

#### ***4.6 Step and Ramp Loading of the Dead Load***

Hybrid testing allows for the use of very complex and dynamic time histories for the dynamic or moving loads applied to a structure. However, one facet of the loading that is often overlooked is the dead load applied to the structure. This dead load should be very easy to apply since it is constant over the entire test period, however, a variety of issues can develop when the dead load is added to the structure in the beginning of the test.

Typically, in Opensees the dead load is applied to all of the nodes simultaneously at the beginning of the testing right before the live load begins to be applied. This instantaneous loading across all nodes of the structures behaves like a step load where the system is shocked by this initial dead load at the beginning of testing. This initial step type loading can cause convergence issues at the beginning of the testing and can affect the results for several loading cycles after the initial dead load has been applied.

The second way to add the dead load involves ramping up the dead load slowly at the beginning of the hybrid test in order to not shock the system. The result is that the entire structure slowly responds to the load instead of the pulsive response that is caused by the step load when the dead load is suddenly applied in its entirety at the beginning of the test. The parametric study of this section looks into the effects of applying the dead load instantaneously versus ramping up the dead load at the beginning of the hybrid test.

Figure 4-49 shows both of the responses for the truss model: when the dead load is applied instantaneously at the beginning of the test (no ramp) and when the

dead load is slowly ramped up at the beginning before the live load is applied. As this figure shows, when a ramp loading is not used (the blue line) there is some convergence issues at the beginning of the test. This is because the system is shocked by the initial dead load applied. This effect of applying the dead load instantaneously at the beginning of the testing only lasts for the first load cycle. This is evident because the blue line completely overlaps the ramp loading response (red line) during the loading from the first truck. Thus, for the case of the truss model, the effect of applying the dead instantaneously at the beginning of the loading only impacts the response a couple of seconds after the load is applied.

In order to see the effect of the ramp loading more clearly, a close up view of the beginning of Figure 4-49 is given in Figure 4-50. The convergence issues for the case in which a ramp loading is not applied can be clearly seen from this figure. The blue line which represents the dead load being instantaneously applied at the beginning of the loading oscillates for several seconds due to free vibration caused by step load applied suddenly to the structure. Furthermore, these initial oscillations cause slight errors in the results for about 10 seconds afterwards until both the blue and red lines almost exactly overlap. From this figure, the advantage of applying the dead load slowly through a ramp loading can be seen. The red line does not have any oscillations at the beginning of the loading and is much more stable as the dead load increases. Note that the above results were for the truss model that has no assigned mass at the nodes. If mass is added to the system and thus dynamic effect is incorporated in the model, the results would differ considerably from the results for the basic truss model.

Figure 4-51 shows the response of the refined mesh model with mass included when the dead load is applied instantaneously at the beginning of the loading. From this figure it is evident that instantaneously applying the dead load at the beginning of the loading cycle can have a dramatic effect on the response for several cycles after the load is applied for models that have mass included. This is evident by the highly oscillatory waveform of the force response in Figure 4-51, particularly during the first load cycle, where the overall shape of the loading can hardly be seen due to the higher frequency and amplitude of the overriding oscillations. This shows the dynamic effect of adding mass to the model. When a load is instantaneously applied at the beginning, it acts as a step load. This step load causes the system to oscillate until the free vibration response has been dampened out, however this time period of dampening out the initial response due to instantaneous loading can take several load cycles, which causes the data in these cycles to be largely inaccurate. In order to obtain more accurate results, the dead load can be applied as a ramp loading slowly at the beginning of the test as was done with the truss model.

The effect of ramping the dead load for a model with mass and dynamic effects included can be seen in Figure 4-52. In this figure, the dead load applied initially through a ramp load can be seen with the red line. The response when the dead load is ramp loaded is as expected, each of the loading cycle peaks can be clearly distinguished. Furthermore, it can be seen that the blue line (instantaneously applied dead loading) appears to oscillate about the solution for the red line (ramp loading). From the above figure, it is also evident that the range of the time domain increases when the dead load is not initially ramped. This is shown from the blue line

which takes roughly 425 seconds to complete its loading compared to the red line which only takes about 400 seconds to complete. This increase in the time to complete the tests shows how the testing takes longer to converge for each load step when the dead load is applied instantaneously causing high oscillations throughout the test.

The first several load cycles for a model with mass when the dead load is ramped up is shown in Figure 4-53 for clarity. As was stated previously, the ramp loading of the dead load does not shock the system and gives the structure time to slowly respond. This is shown in Figure 4-53, where ramp loading occurs until about 25 seconds when the live loading begins. As the figure shows, each of the first three load cycles can be clearly seen without any large oscillations for the initial dead loads affecting the results.

Overall, when dead loads need to be applied to a hybrid test model, the best method to apply these loads is by slowly ramping these loads to their specified levels at the beginning of the testing. For models without any mass, this ramp load is not critical to obtaining accurate results. However, when mass is included and dynamic effects are considered, it is critical to slowly apply the dead load in order to have accurate results for the beginning of the hybrid testing.

#### ***4.7 High Temperature Testing***

In order to demonstrate how controlled, elevated temperature environmental testing can be applied in a realistic manner in the hybrid testing platform, the Yellow Mill Pond Bridge test specimen will be subject to a specified temperature value (e.g., experienced by the bridge in summer). This will showcase how differential temperatures can be applied in a realistic manner in the hybrid testing platform and later it will be shown how these controlled environmental testing conditions can be used to validate and characterize sensors for structural health monitoring purpose.

The goal of this portion of the research is to create a controlled temperature environment around the test specimen that would be similar to the temperatures a bridge girder would experience on a hot day in summer. In order to establish these temperatures around the test specimen, an environmental chamber with a heating control system was constructed for the test specimen. Photos of this environmental chamber can be seen in Figures 4-54 through 4-57.

The environmental chamber works by circulating the air through the chamber and passing it through a heating fan. A thermocouple attached to a temperature control system regulates the temperature in the chamber by turning the heating fan on and off. The walls of the chamber are made of 2" insulation foam to minimize the heat losses that may occur during testing. Finally a front door with plexiglass was installed in the front of the chamber to view the test specimen during testing.

Since the environmental chamber completely encompasses the test specimen and creates a uniform temperature around the specimen, this setup presents the possibility to realistically assess sensors at elevated temperatures before they are

placed in the field. For the test specimen used in this thesis, several types of sensors were attached to the test specimen including strain gages and acoustic emission (AE) sensors for fatigue crack detection. The temperature inside the chamber was then increased to 95°F (hot summer day), and the response of these sensors could be assessed at this higher temperature. In addition, since the environmental chamber fits over the test specimen, the hybrid test loading can still be applied to the test specimen. Thus, the hybrid test was performed at elevated temperatures, and the response of these sensors to the realistic loading from the hybrid test at higher temperatures could be evaluated and compared to the response at lower temperatures.

This demonstrates another major advantage of the hybrid testing testbed for realistic sensor characterization; the virtual model which encompasses the majority of the structure and where the loads are applied is separate from the physical component. Since this physical component is a smaller, critical section of the overall structure in the virtual model, sensors can be evaluated at this critical location of the structure (test specimen) without having to fabricate and test a full scale structure. Furthermore, due to the smaller size of the large scale test specimen, it is easier to apply certain environmental conditions to the test specimen.

As described previously, the goal was to conduct a hybrid test at 95°F and assess the response of the various sensors and the overall structure in the OpenSees model as a whole. This testing was conducted in two steps. The first was increasing the temperature in the chamber without any loading occurring in the test setup. After the desired temperature was reached, the second step of the testing was to apply the hybrid test loading to the specimen at its elevated temperature.

In the first step of this testing, the temperature inside the chamber was increased from the ambient temperature of 50°F in the lab to the desired temperature of 95°F (typical hot summer day temperature). While the temperature inside the chamber was rising, the force inside the test specimen was also monitored. Since the temperature was increasing, it was expected that the test specimen would want to expand and compression would be introduced in the test specimen. A plot showing the force inside the test specimen as the temperature was increased can be seen in Figure 4-58. This figure shows the expected results. As the temperature increased with time, the compressive force (denoted by a negative force in the above figure) also increased. By the time the temperature in the chamber had reached 95°F, a compressive force of almost 100 lbf had developed within the test specimen. Compared to the load amplitude on the order of 20 kips in hybrid testing, this 100lbf is considered insignificant though. This can be attributed to the rod fixture with a small cross-section area that partially releases the thermal induced force in the test specimen. This initial compressive force will eventually be carried over to the hybrid testing. This demonstrates how differential temperature changes can be applied to a structure in the hybrid testing setup; the temperature of the physical components in the test setup can be increased, while the temperature of the virtual components stays constant. Thus, the effect of a temperature change on only certain components of a structure can be evaluated through this hybrid testing method.

The results of the hybrid test performed once the temperature reached 95°F can be seen in Figure 4-59. A close up view of the first loading cycle for this figure can be seen in Figure 4-60. From these two figures, the hybrid test conducted at

elevated temperatures performs similar to the hybrid test at lower temperatures, except that the response is offset by about 0.1 kips (the initial compression induced by the temperature loading). This response is to be expected since the same loading was applied at both temperature levels and the only difference was the initial compressive force within the test specimen.

Beyond the effects of the temperature change on the overall hybrid test model, the largest advantage of this controlled temperature environmental test involves the realistic characterizing and assessing of sensors at elevated temperatures. Several different types of sensors including strain gages and AE sensors were placed on the specimen to characterize the response of these sensors before and after increasing the temperature around the test specimen. In order to demonstrate how these sensors can be assessed under different temperatures in the hybrid test setup, the results from the strain gage characterization will be presented below.

The strain gages were placed on the specimen 8" away from the transverse weld at the cover plate interface in order to measure the nominal strain that occurred in the test specimen during the testing. The location of these strain gages was also well within the environmental chamber to ensure that these sensors would be subject to the temperature changes. The location of the strain gages in relation to the environmental chamber can be seen in Figure 4-61. The results from the strain gage readings during the heating up of the chamber can be seen in Figure 4-62.

Figure 4-62 shows that a compressive strain (denoted by a negative microstrain) developed in the test specimen as the temperature increased within the environmental chamber. This was to be expected given the earlier results showing

the compressive force developing within the test specimen as the temperature increased. Unlike the data for the force, however, the strain data began to have more noise and oscillate at a larger amplitude as the temperature increased. This shows one of the issues with the strain gages, since they are calibrated at the beginning of the test at one temperature, and when large changes occur in the temperature, the strain gages may have a higher uncertainty at higher temperatures.

Strain gage readings were also taken during the hybrid test that was performed under these higher temperatures. The results from the strain gages can be seen in Figure 4-63. Similar to force response to the temperature change, the strain data exhibited the same shape at both temperatures. Furthermore, the higher temperature (95°F) strain data was offset from the ambient temperature (50°F) strain data, similar to force response. The strain data appears to have a larger offset than the force data, which may be associated with the thermal expansion of the strain gages themselves at the higher temperatures. However, due to the large noise and uncertainty in the strain gages, the measurements from these sensors give an overall idea as to how the system is responding to the increase in temperature and they verify the trends shown in the force data.

The main concept to be taken from the above results is the ability of the hybrid testing platform to test sensors in more realistic environmental conditions. Even though the previous results were shown for strain gages, a variety of other sensors can also be assessed at these different environmental conditions. Before sensors can be placed in the field, they must first be evaluated and characterized under these various environmental conditions. Unexpected responses to fluctuations

in temperature and humidity, issues with bonding the sensor to the structural member, or issues with communicating with the sensor are all possible problems that can occur with sensors newly placed in the field. Often these issues cannot be predicted and the hybrid testing platform presents a realistic way to perform controlled environmental tests on these sensors under realistic loading histories. Thus, the hybrid testing method provides a testbed for evaluating responses and potential issues with structural health monitoring techniques and sensors under various environmental conditions before they are subject to these environmental conditions in the field.



**Figure 4- 1:** Yellow Mill Pond Bridge Physical Test Specimen

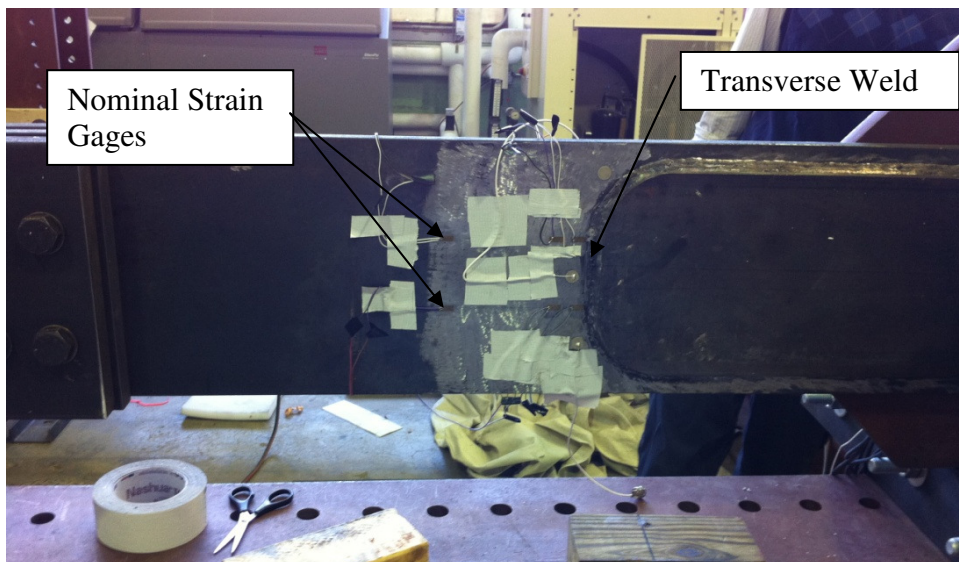


**Figure 4- 2:** Strain Gage Locations on Test Specimen

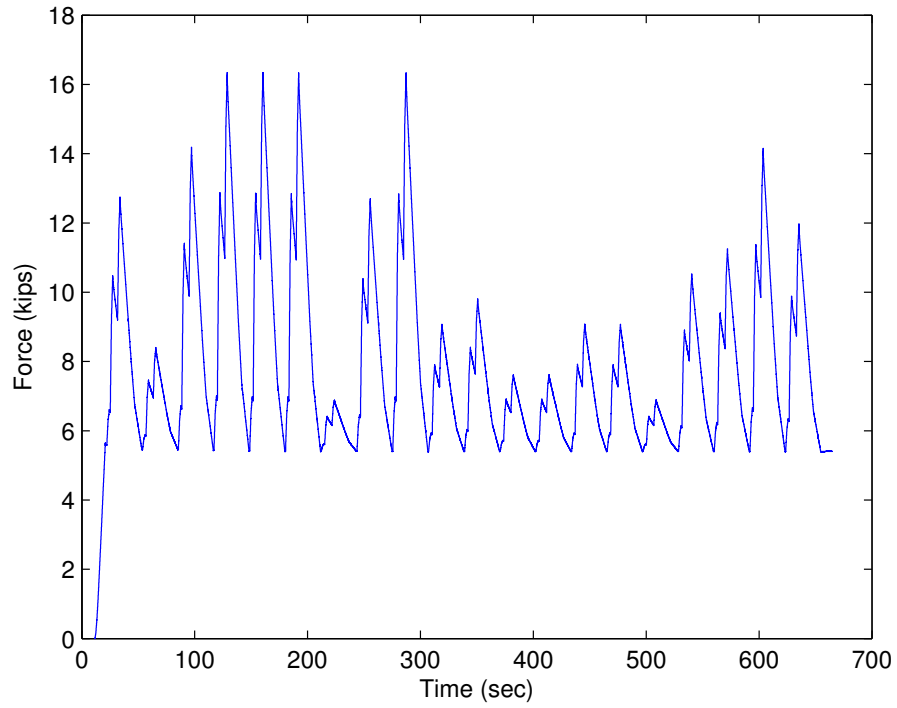


**Figure 4- 3:** Force Applied to Test Specimen During Hybrid Test

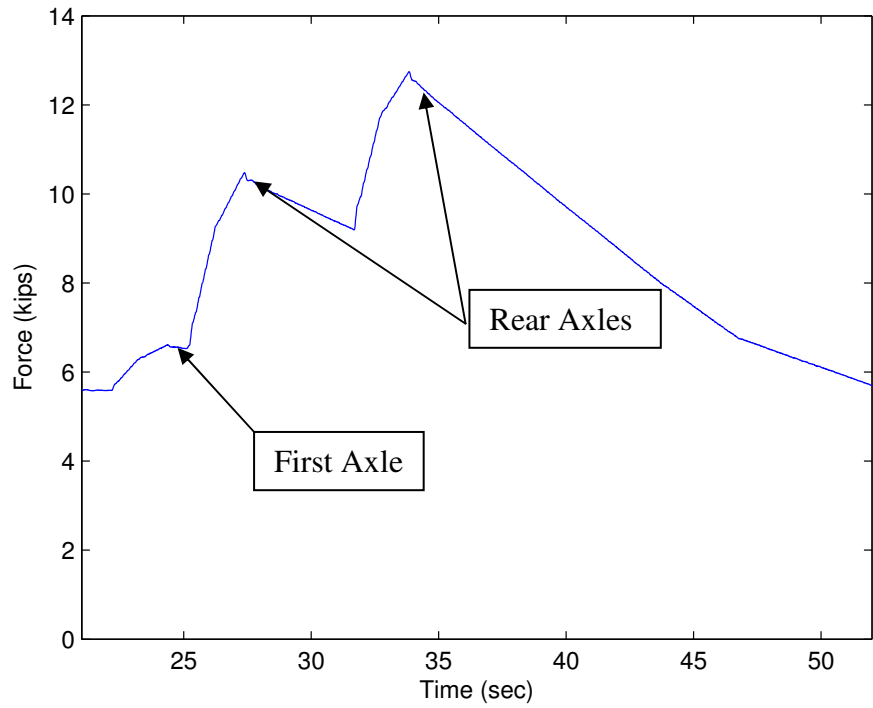


**Figure 4- 4:** Close-up of Loading from Single Fatigue Truck

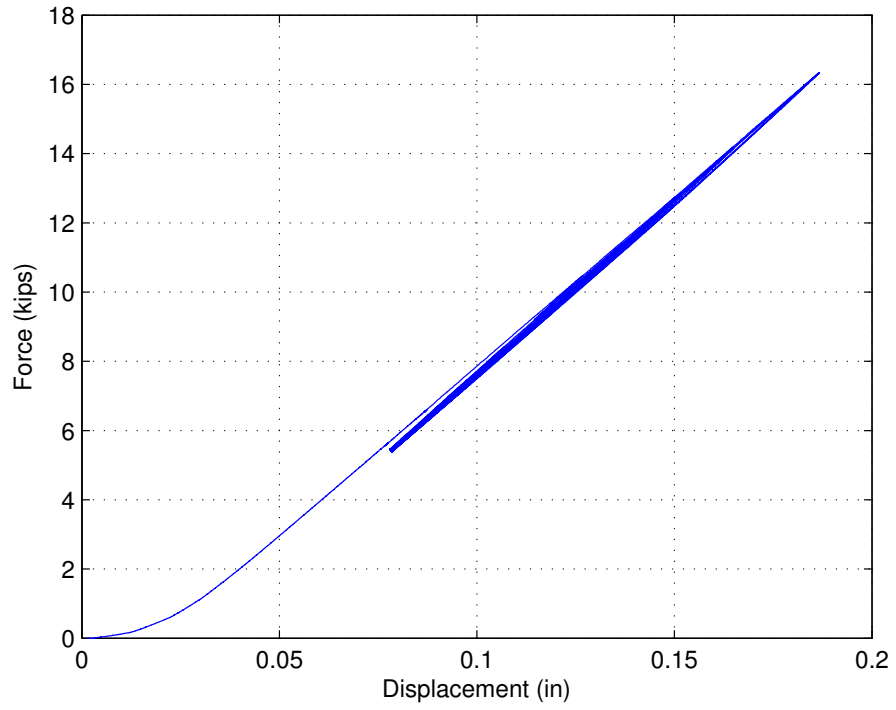


**Figure 4- 5:** Hysteresis of Physical Test Specimen

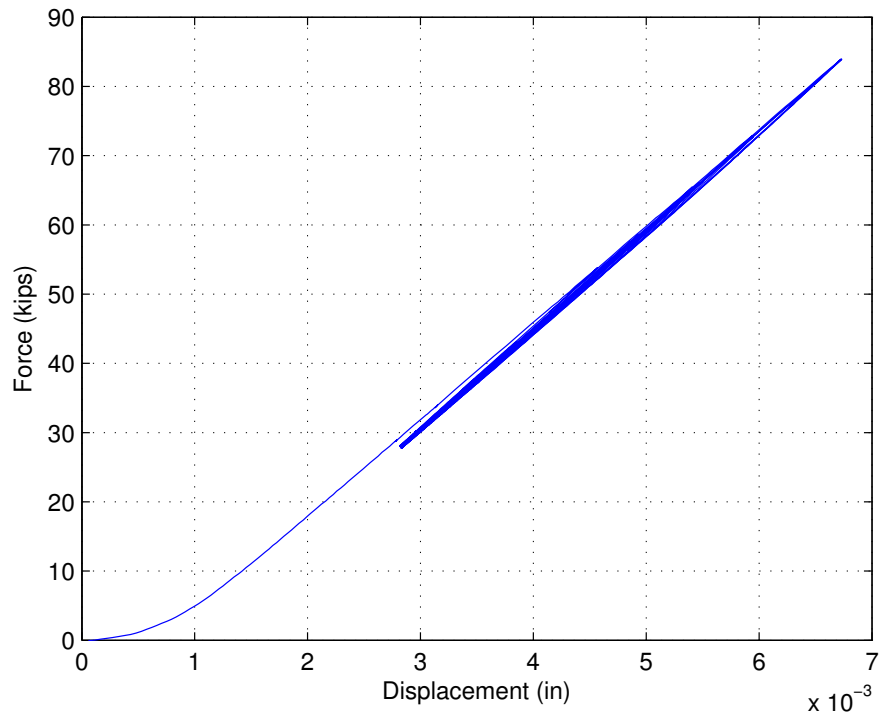


**Figure 4- 6:** Hysteresis of Test Specimen in OpenSees

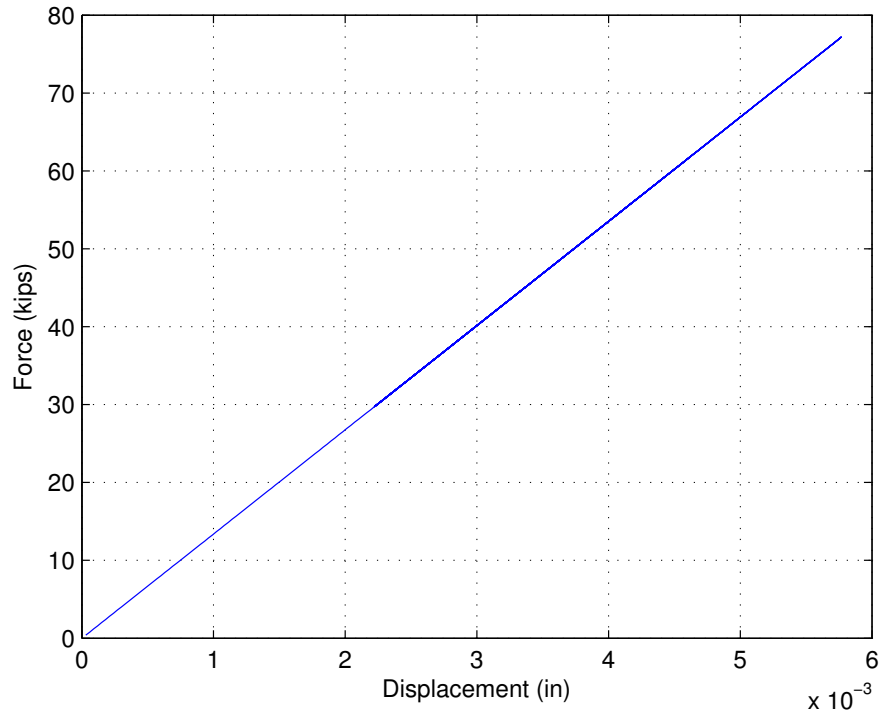


**Figure 4- 7:** Hysteresis of Purely Virtual Finite Element Model

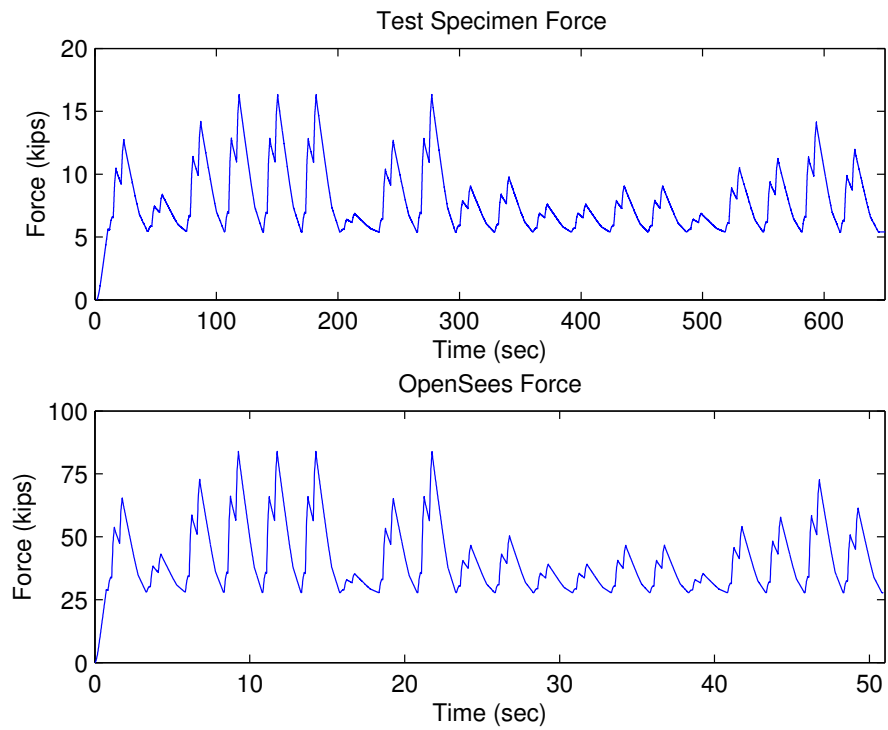


**Figure 4- 8:** Force Scaling Between Physical and Virtual Components

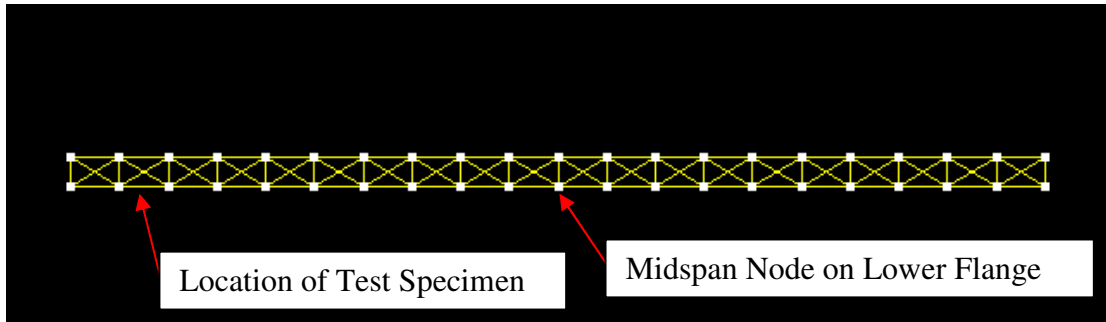


**Figure 4- 9:** Location of Midspan Deflection and Test Specimen in Virtual Model

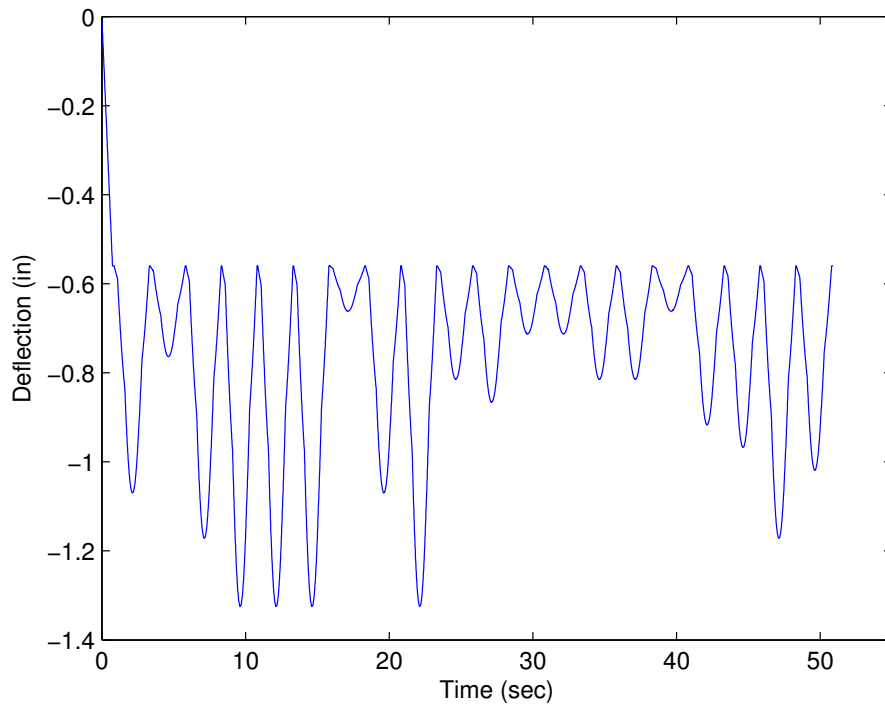


**Figure 4- 10:** Midspan Deflection of OpenSees Model

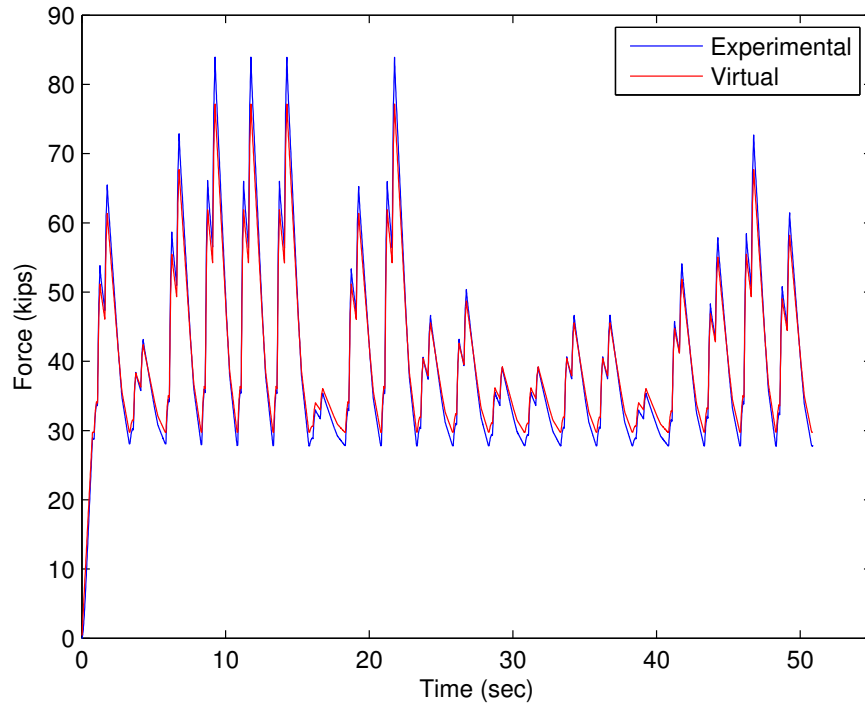


**Figure 4- 11:** Comparison of Virtual to Experimental Force Results

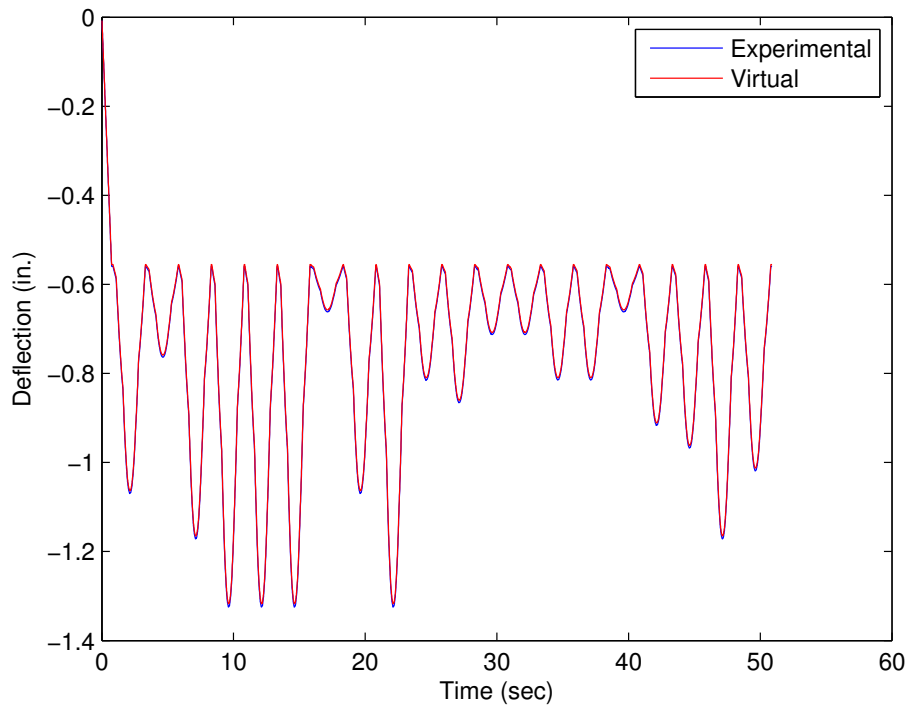


**Figure 4- 12:** Comparison of Virtual to Experimental Deflection Results

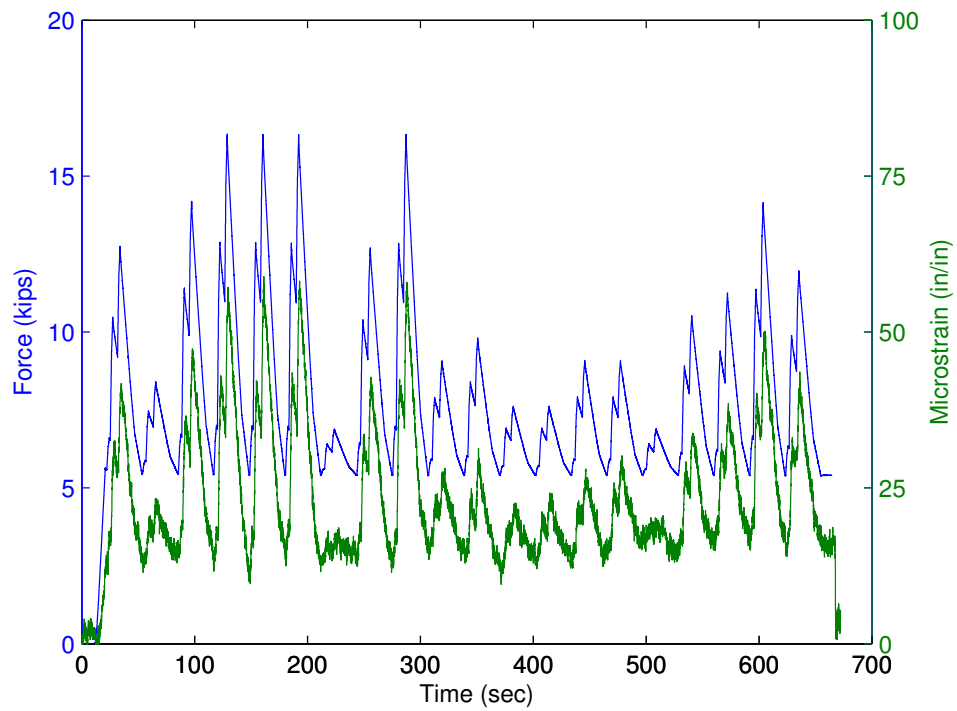


**Figure 4- 13:** Comparison of Strain to Force Measurements

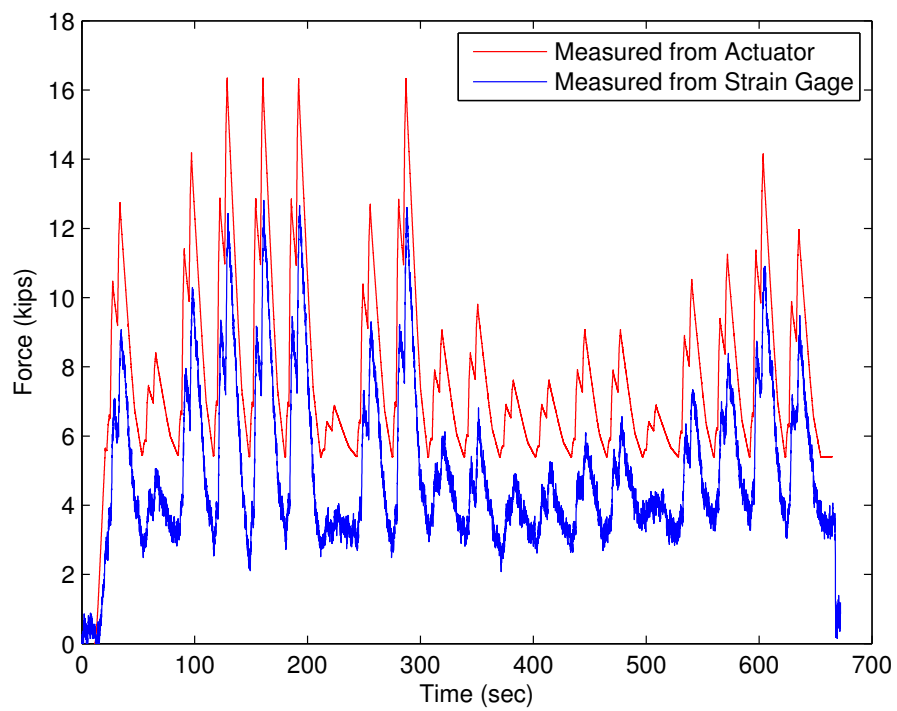


**Figure 4- 14:** Strain Gage Force versus Measured Force

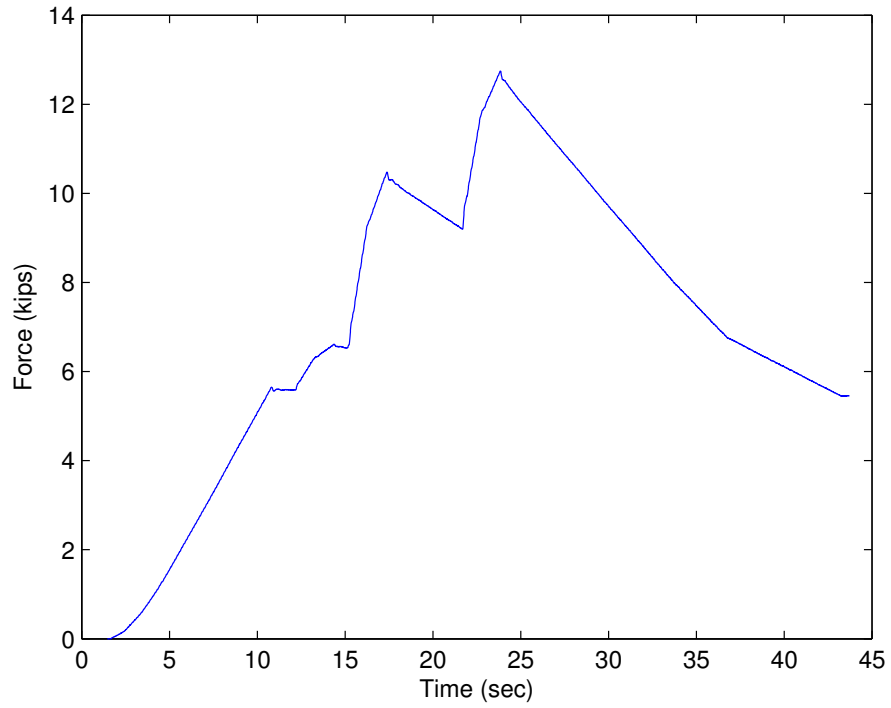


**Figure 4- 15:** Truss Model Force History for 0.1 Second Ramp Time

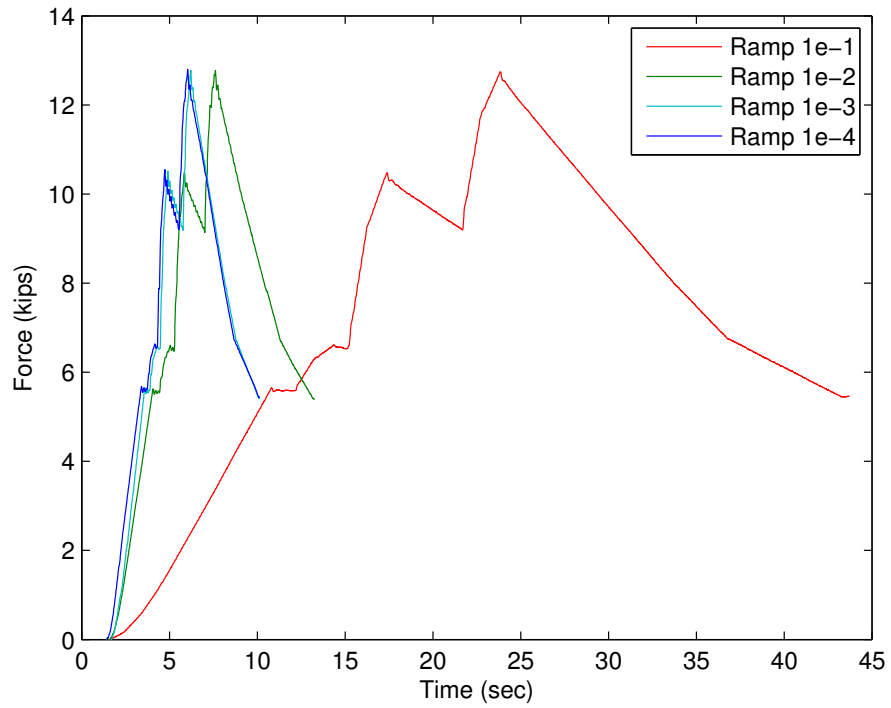


**Figure 4- 16:** Comparison of Ramp Times for Truss Model

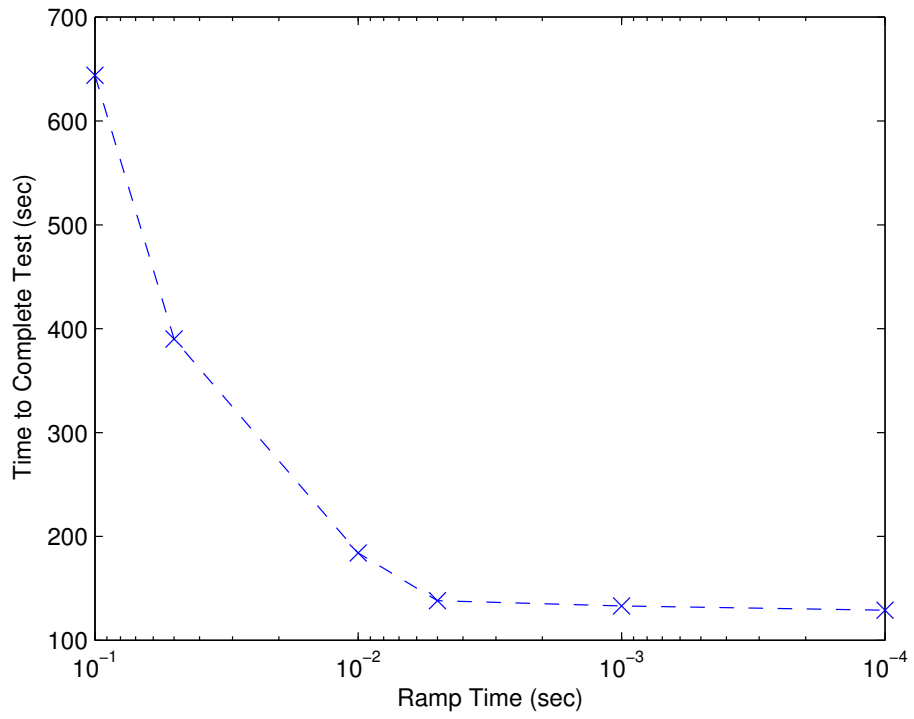


**Figure 4- 17:** Truss Model Total Time to Complete Test vs. Ramp Times

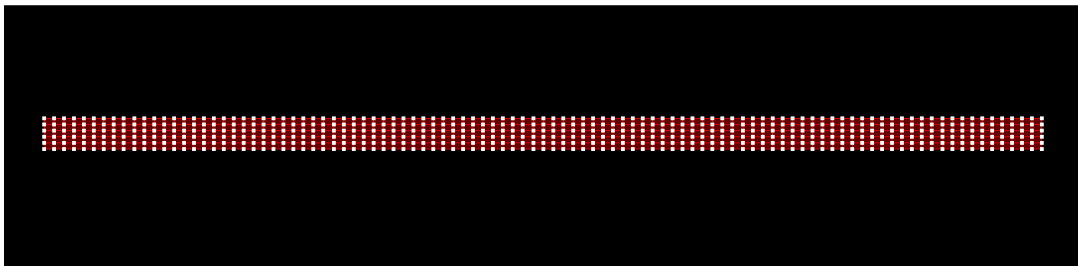


**Figure 4- 18:** Refined Mesh OpenSees Model

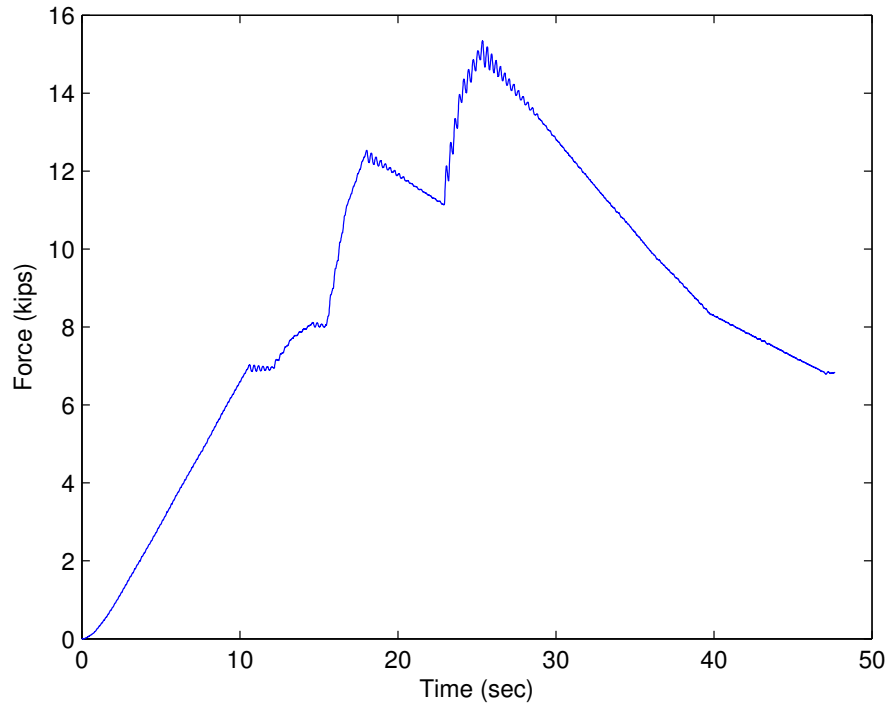


**Figure 4- 19:** Refined Mesh Model Force History for 0.1 Second Ramp Time

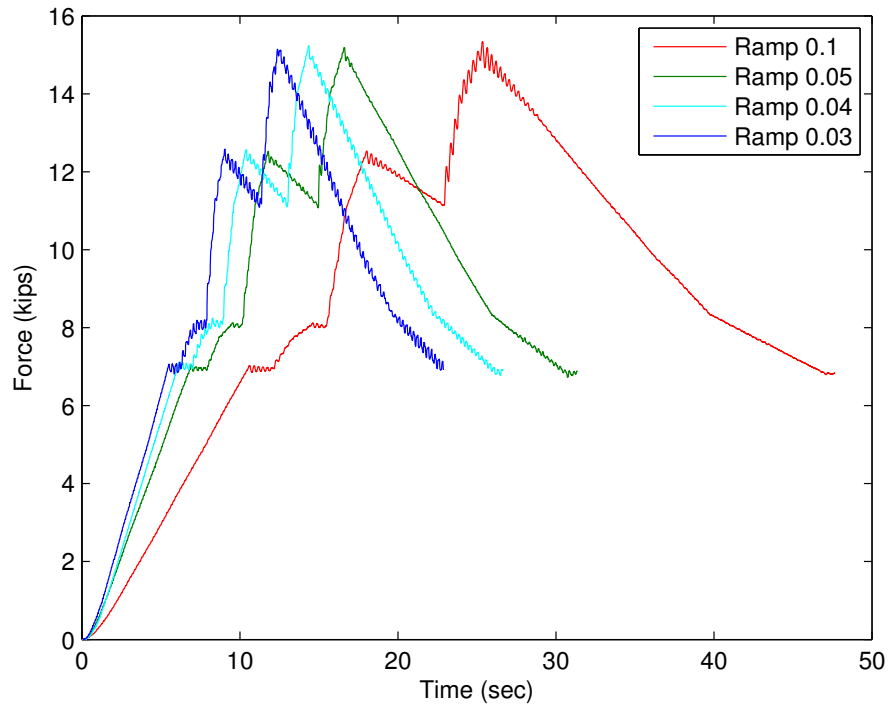


**Figure 4- 20:** Comparison of Ramp Times for Refined Mesh Model

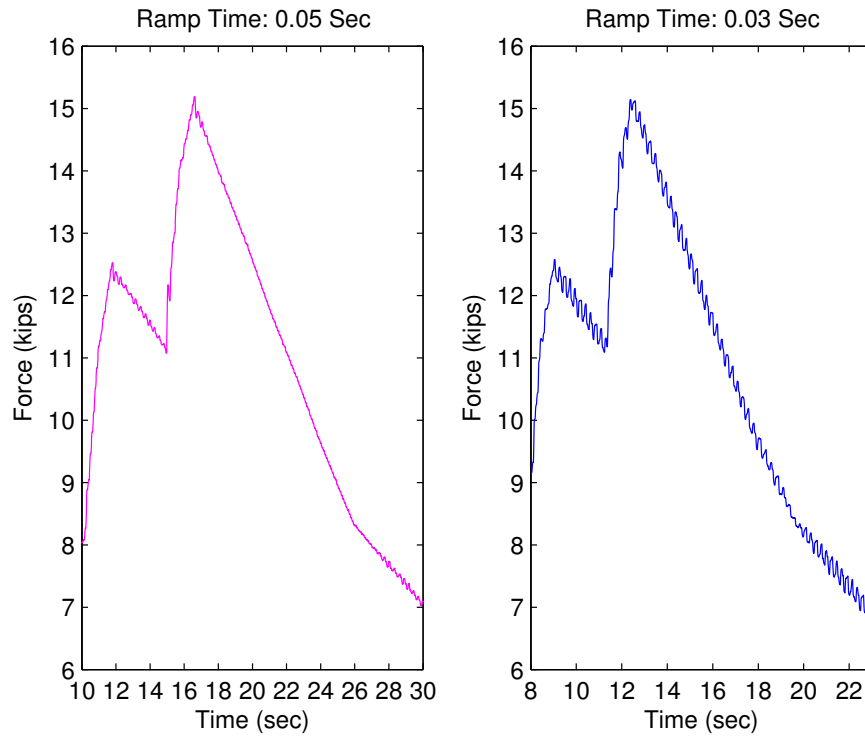


**Figure 4- 21:** Comparison of Oscillations at Different Ramp Times

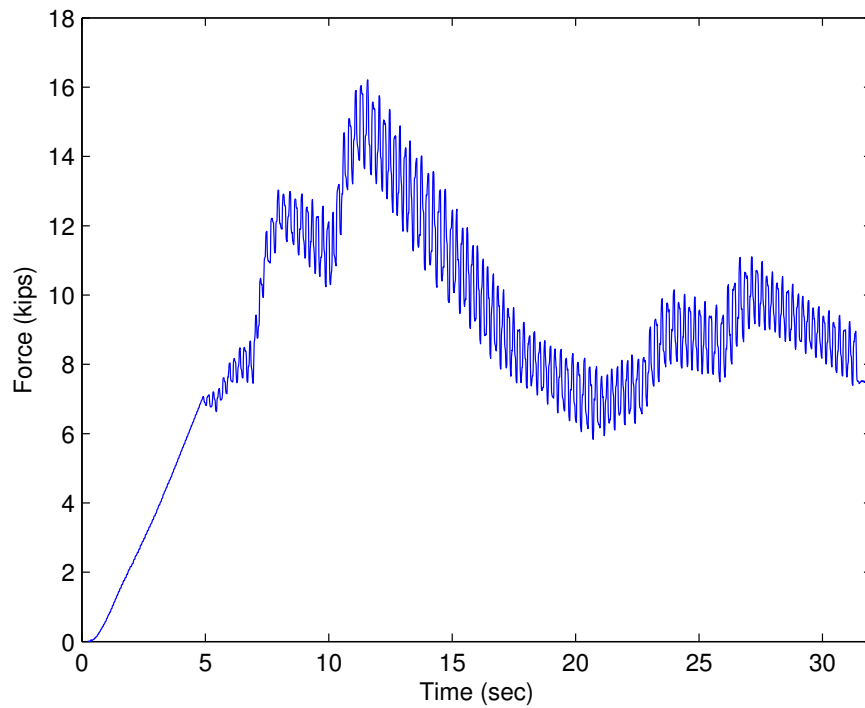


**Figure 4- 22:** High Oscillations at Ramp Time of 0.02 Seconds

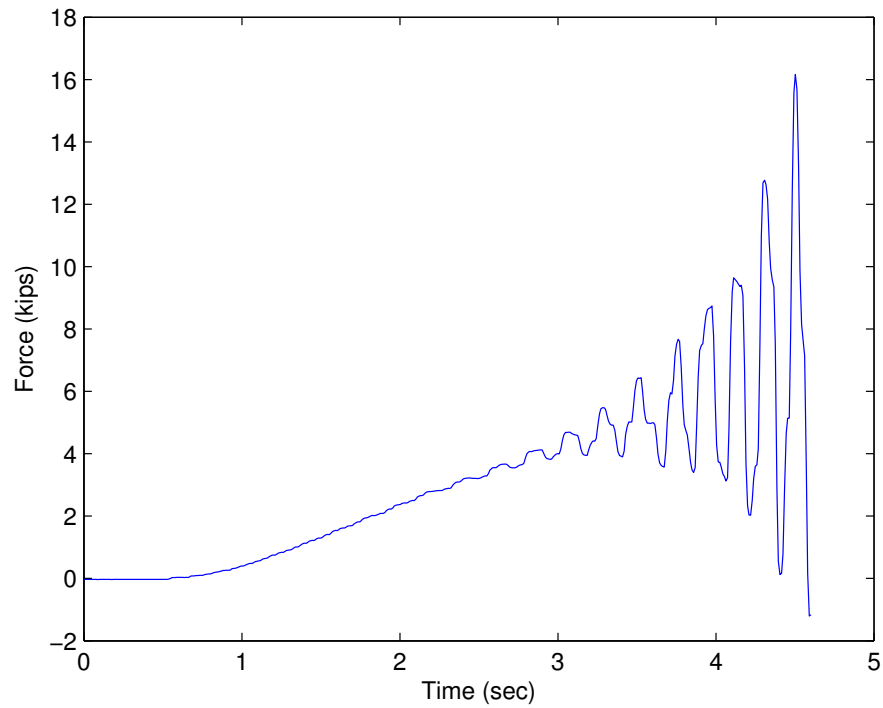


**Figure 4- 23:** Force Instability at Ramp Time of 0.01 Seconds

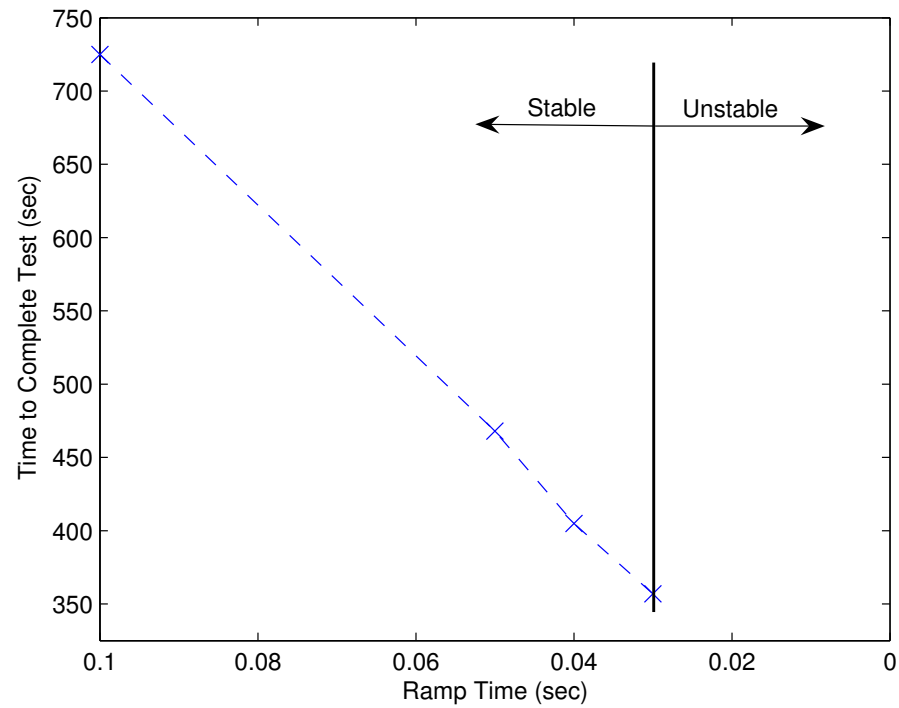


**Figure 4- 24:** Refined Mesh Model Total Time to Complete Test vs. Ramp Times

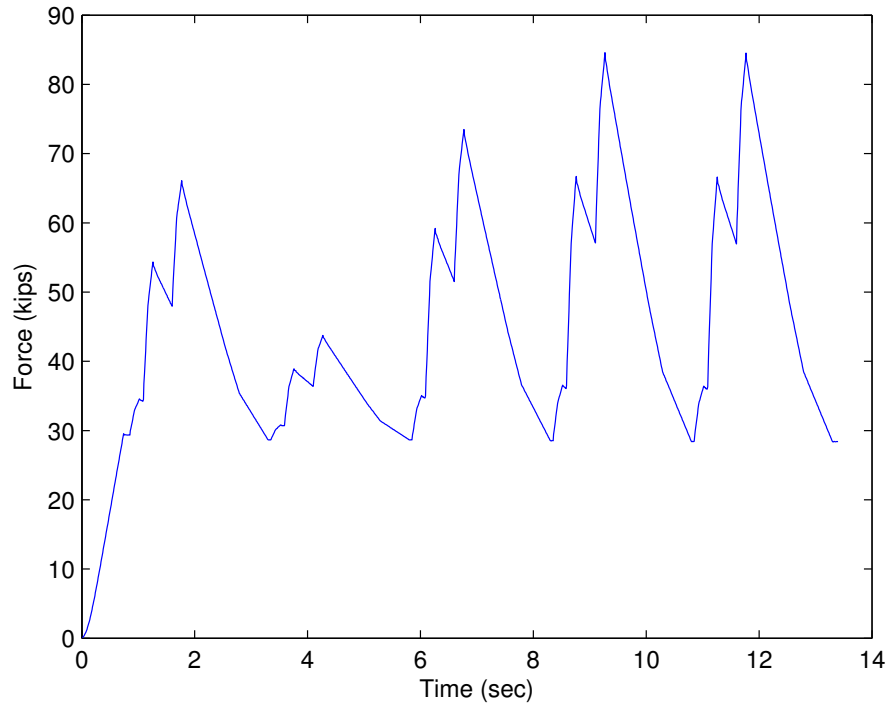


**Figure 4- 25:** Truss Model Force History

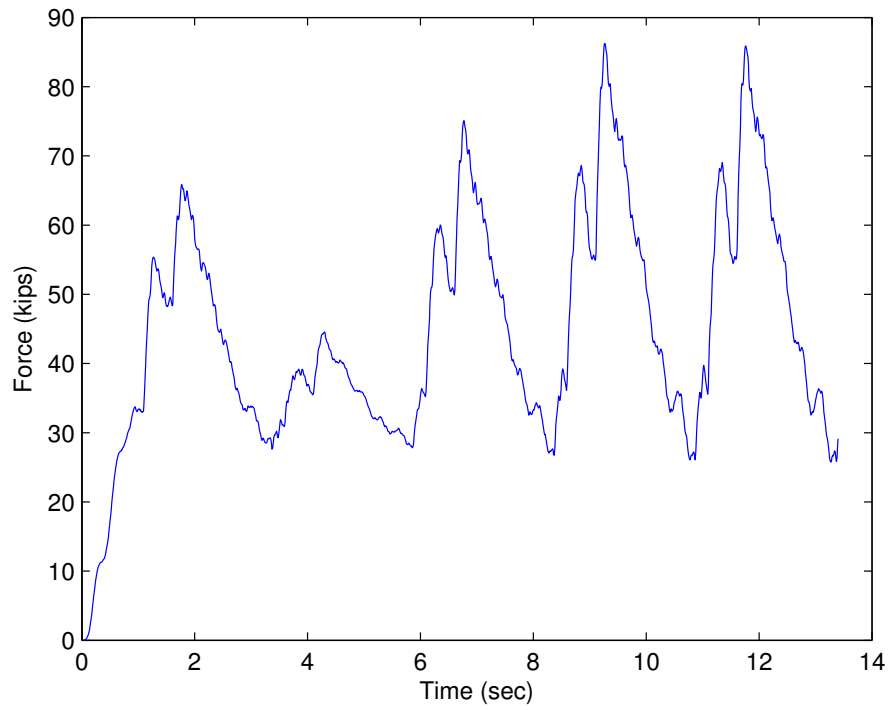


**Figure 4- 26:** Truss with Mass Model Force History

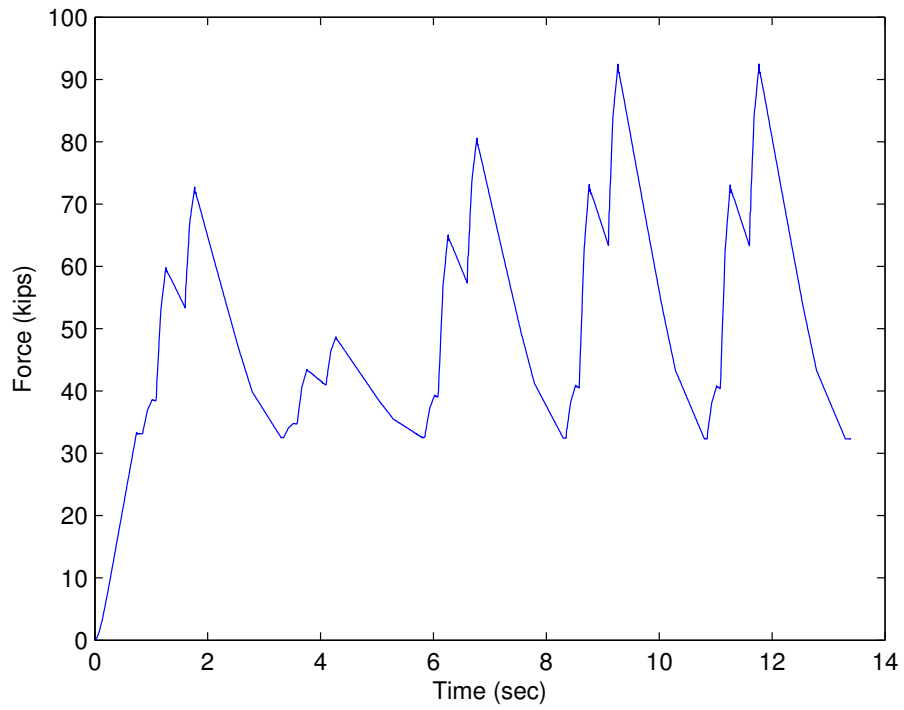


**Figure 4- 27:** Refined Mesh Model Force History

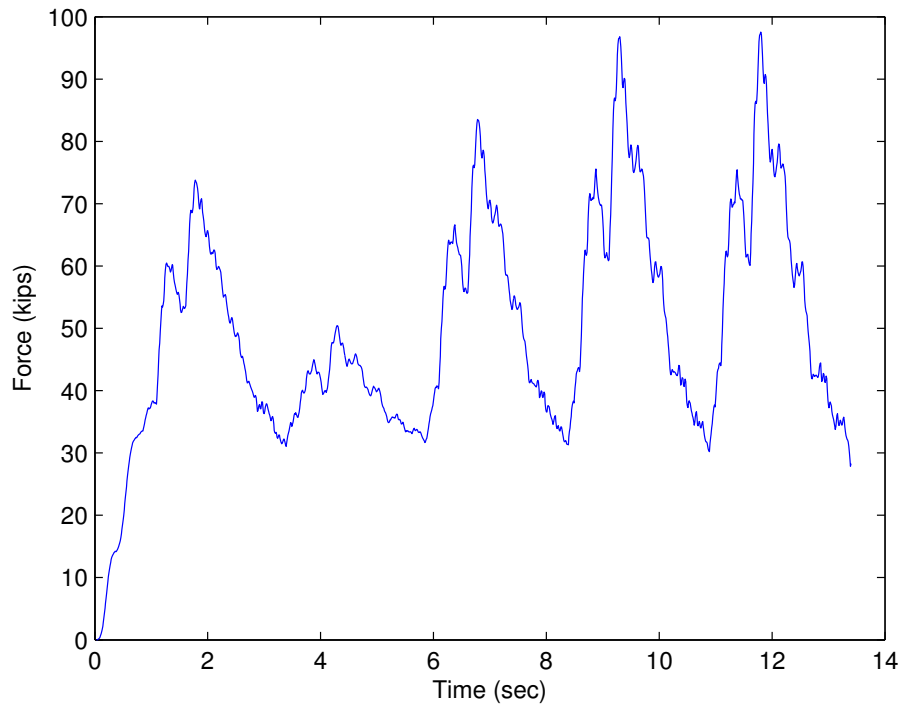


**Figure 4- 28:** Refined Mesh with Mass Model Force History

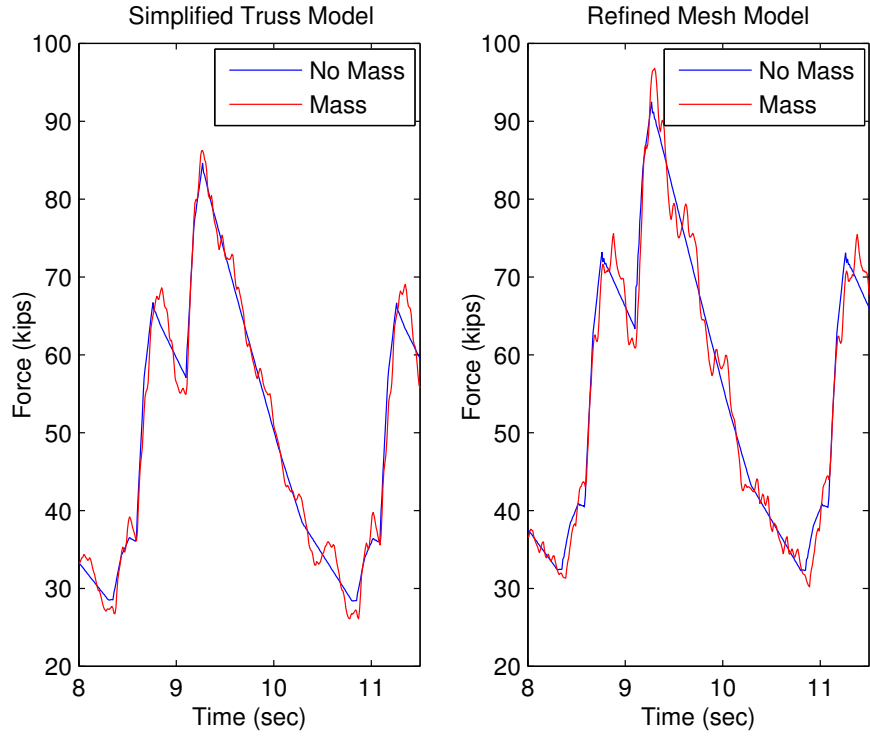


**Figure 4- 29:** Mass Effects on the Force Histories

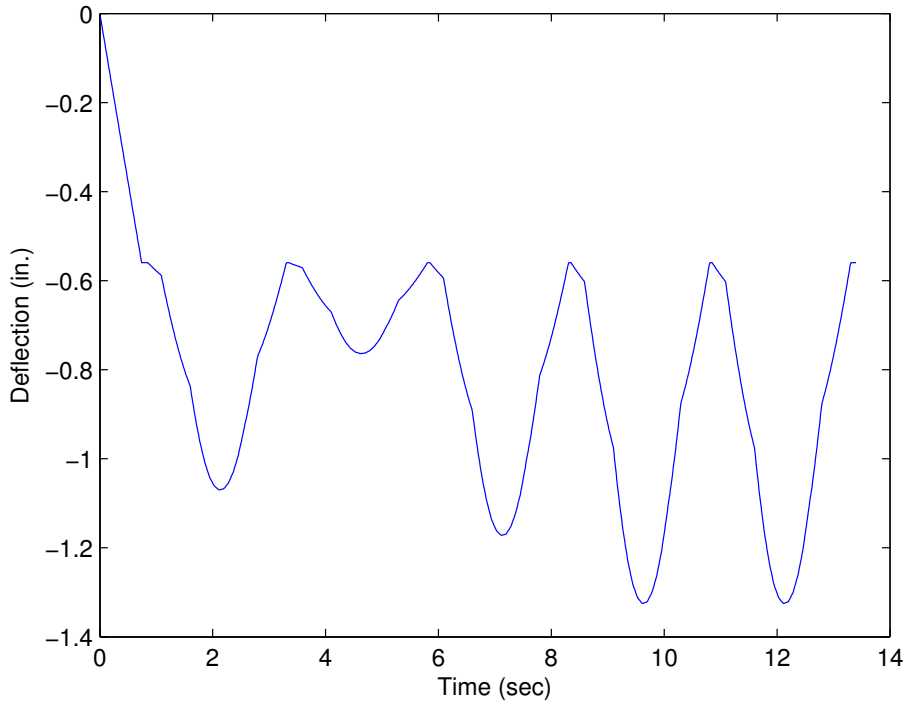


**Figure 4- 30:** Truss Model Midspan Deflection

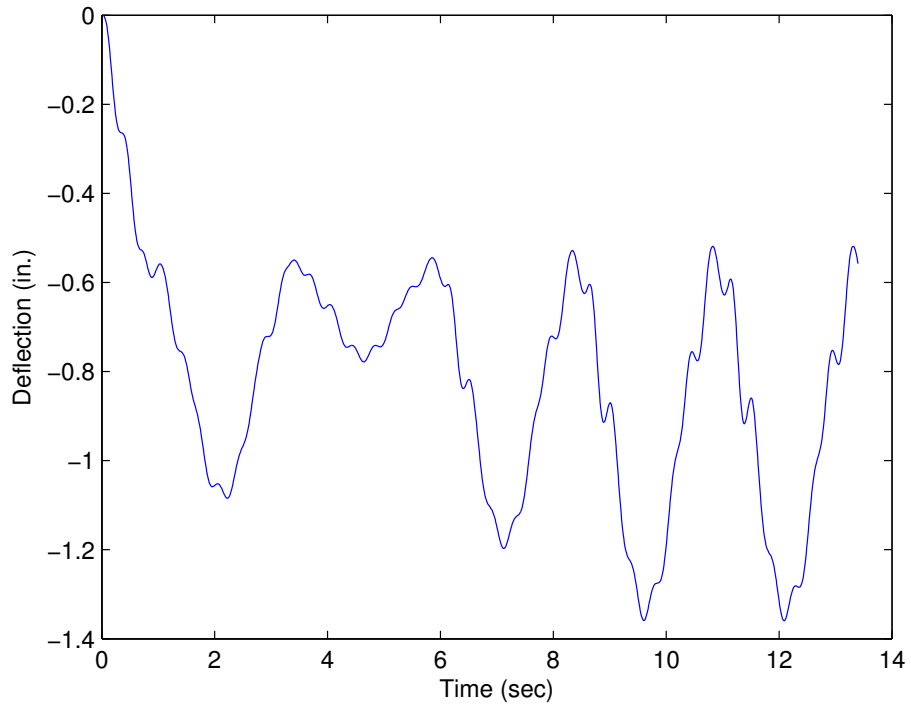


**Figure 4- 31:** Truss with Mass Model Midspan Deflection

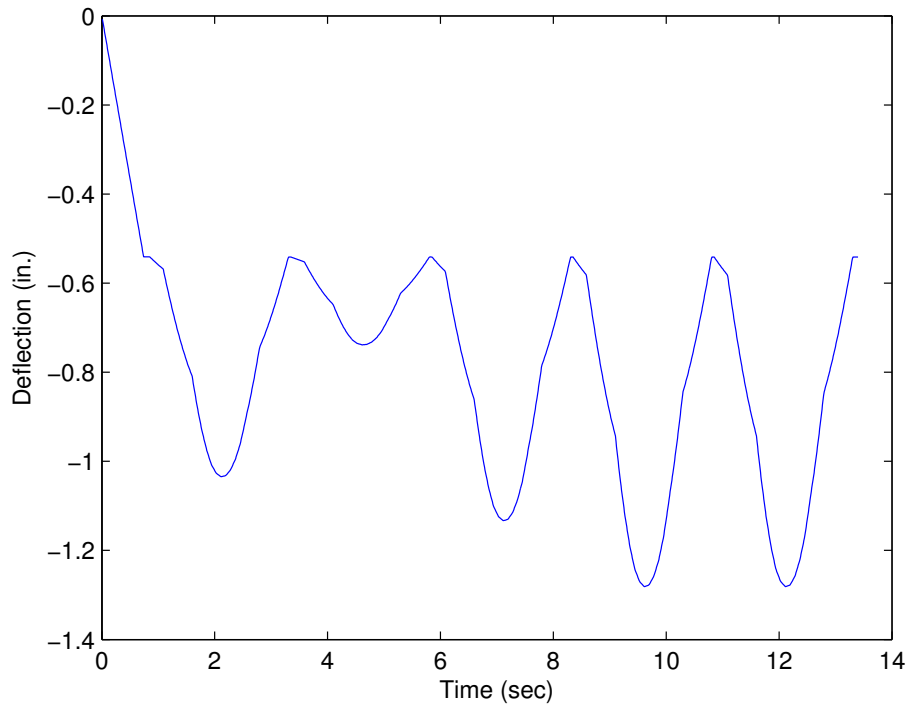


**Figure 4- 32:** Refined Mesh Model Midspan Deflection

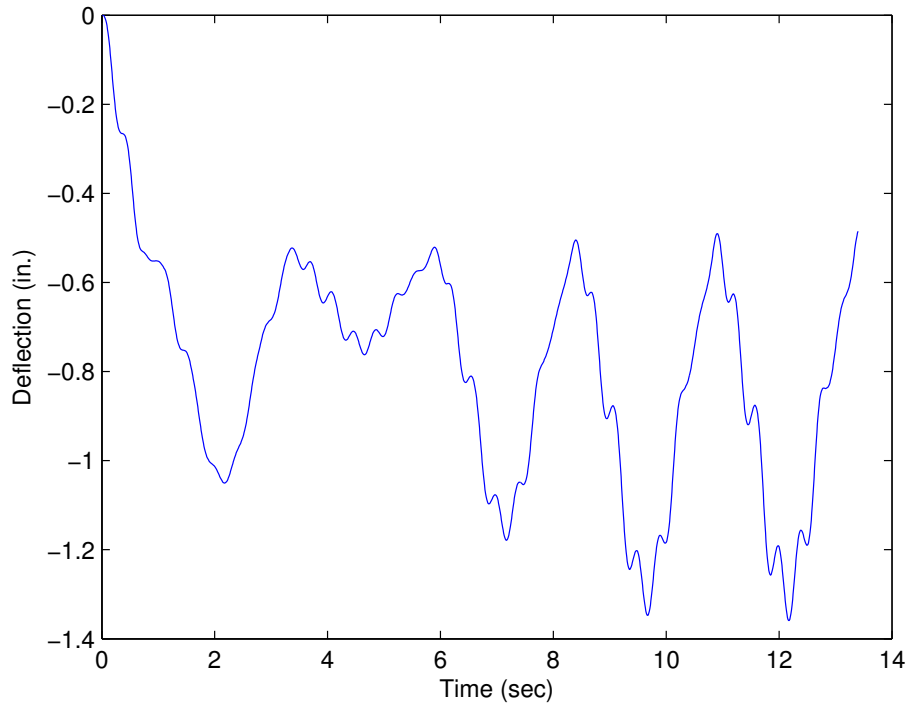


**Figure 4- 33:** Refined Mesh with Mass Model Midspan Deflection

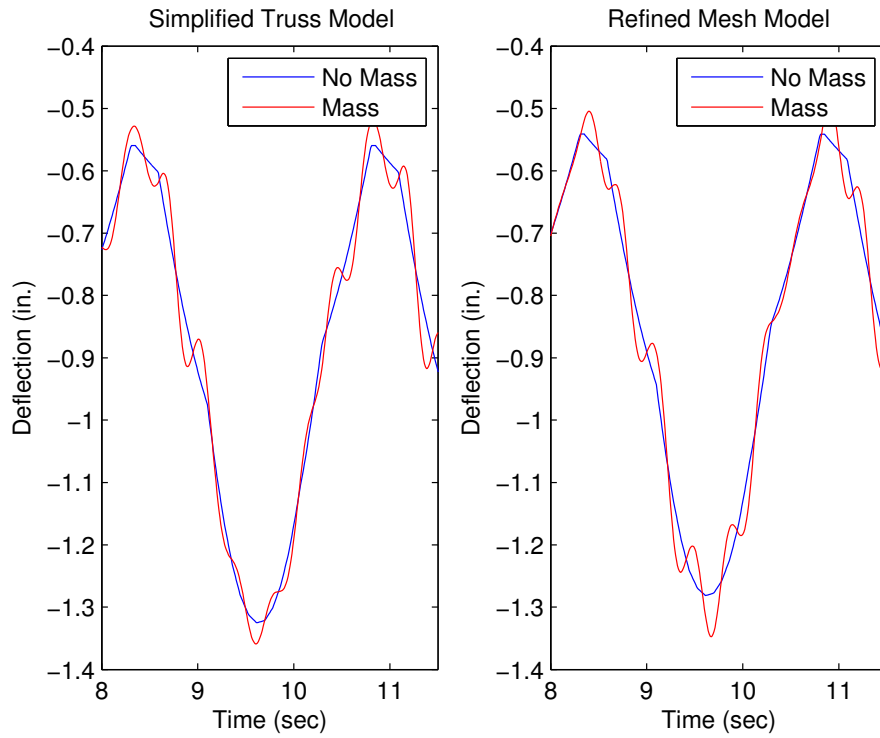


**Figure 4- 34:** Mass Effects on the Deflection History

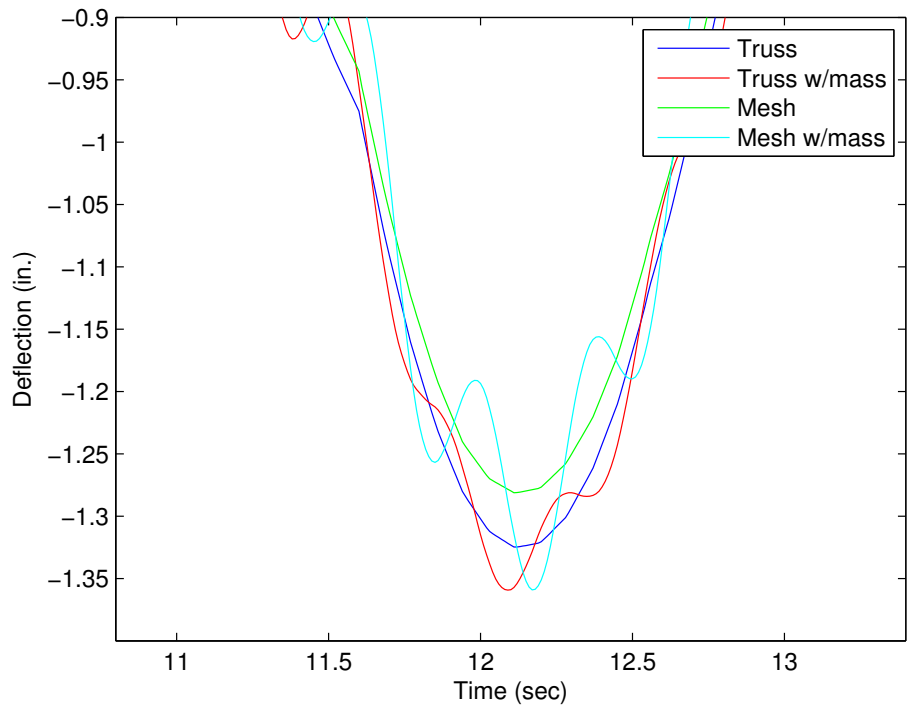


**Figure 4- 35:** Comparison of Max Midspan Deflection for Each Model Type

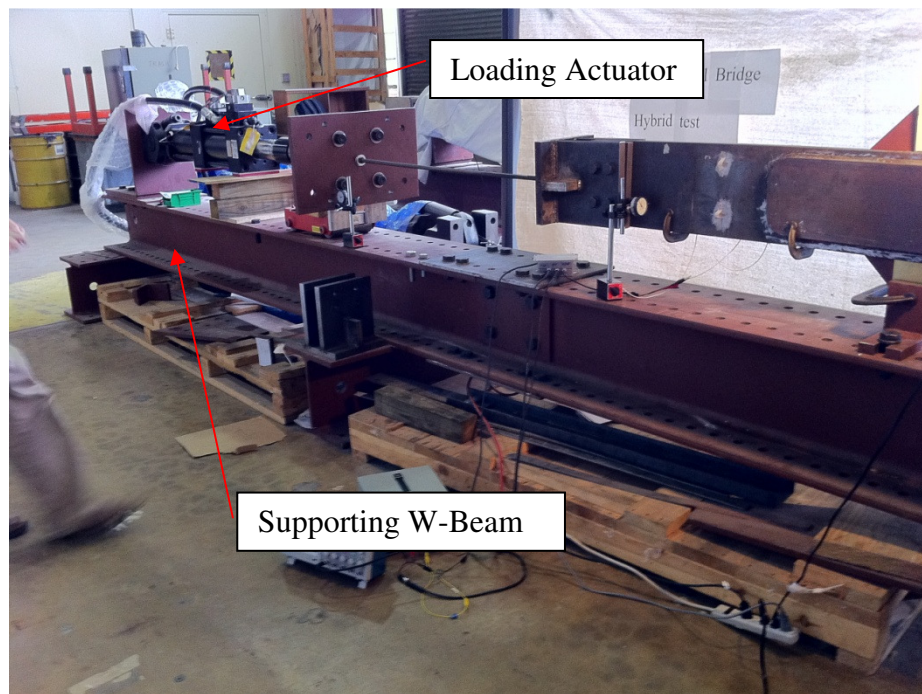


**Figure 4- 36:** Test Setup with Supporting W-Beam

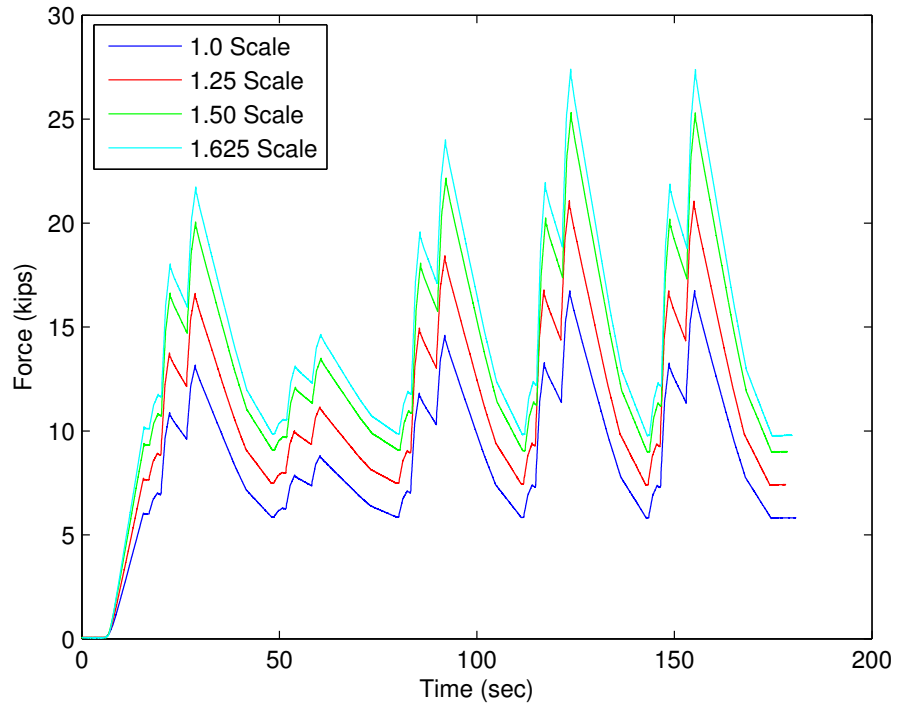


**Figure 4- 37:** Force History Comparison at Different Scale Factors

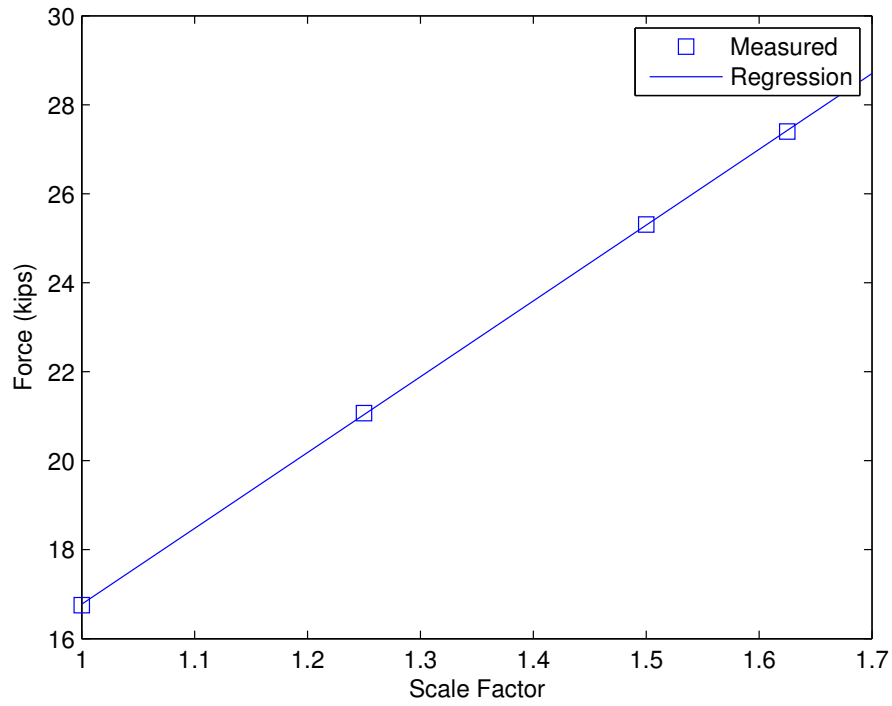


**Figure 4- 38:** Max Force vs Scale Factor

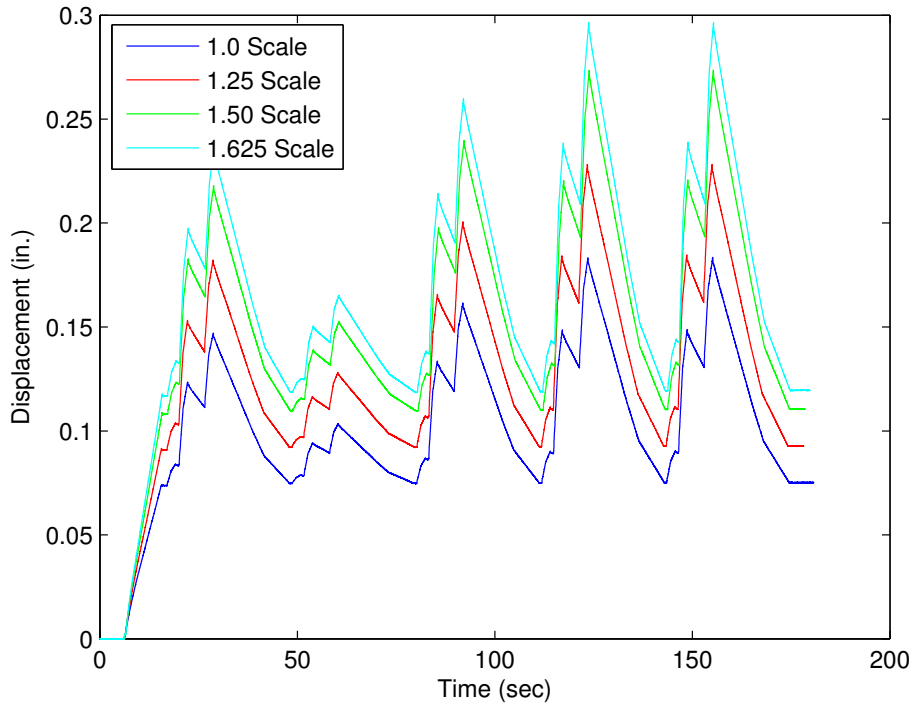


**Figure 4- 39:** Displacement History Comparison at Different Scale Factors

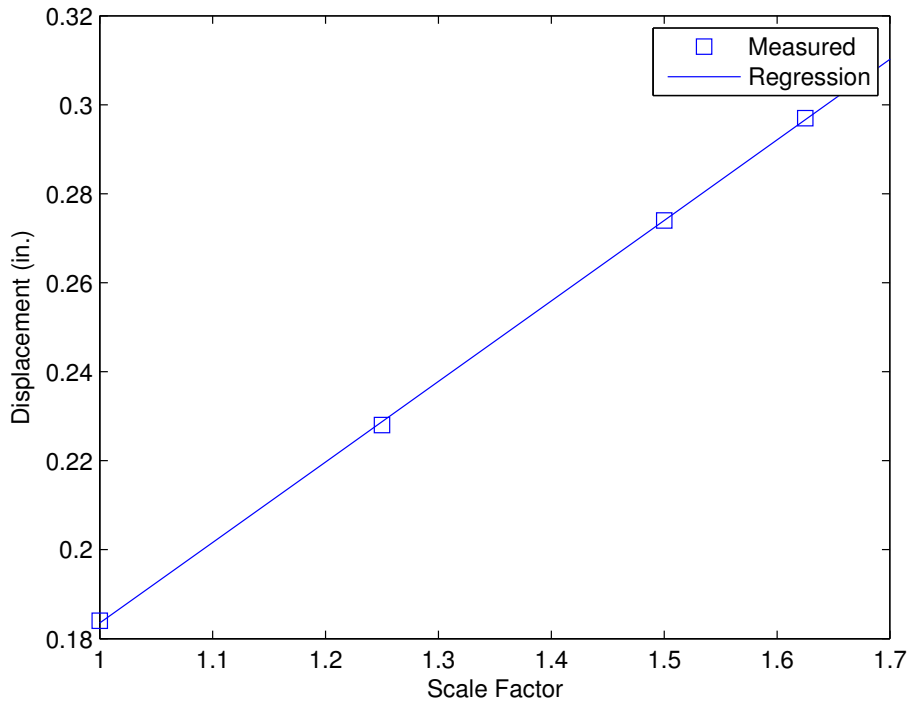


**Figure 4- 40:** Max Displacement vs Scale Factor

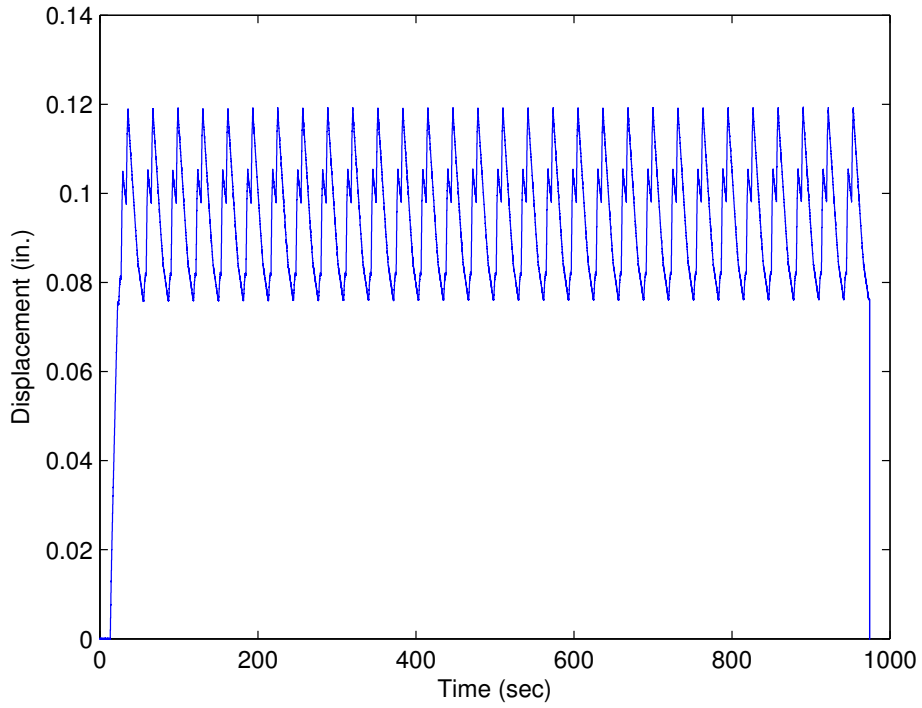


**Figure 4- 41:** Displacement Response to 30 Constant Trucks for Truss Model

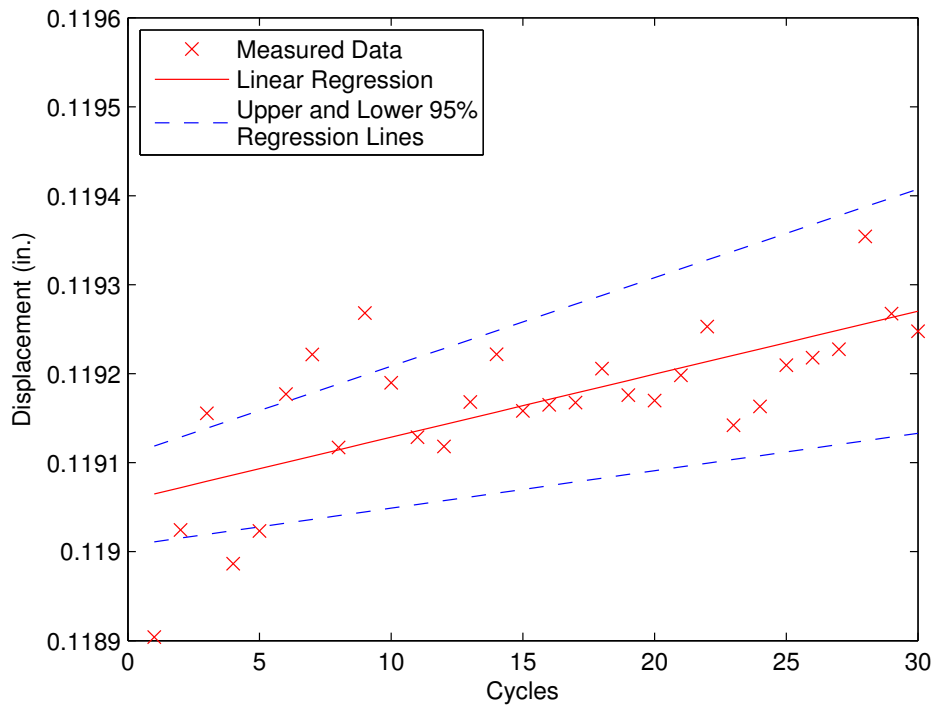


**Figure 4- 42:** Max Displacement for Truss Model at Constant Loading

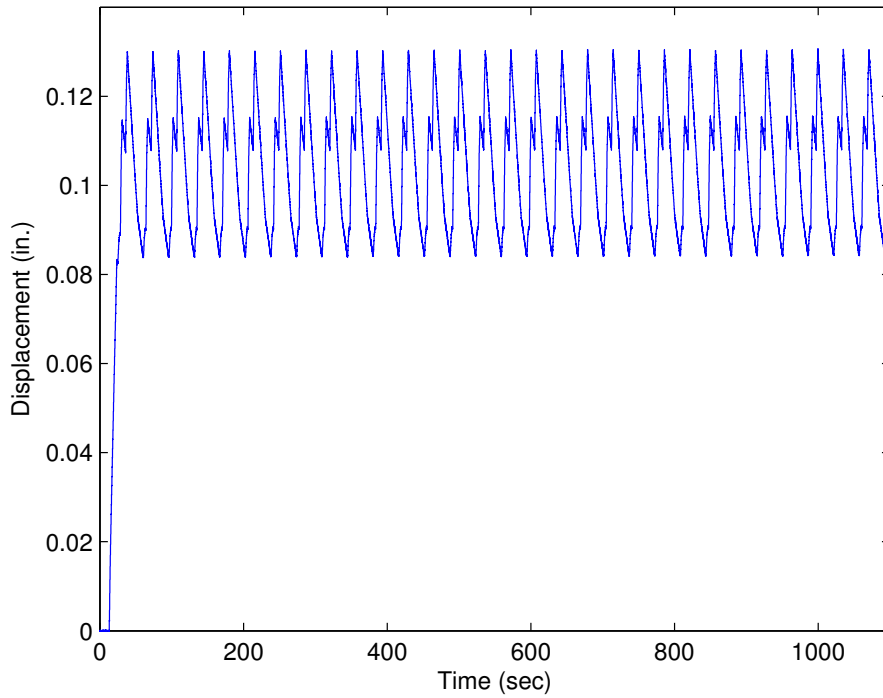


**Figure 4- 43:** Disp. Response to 30 Constant Trucks for Refined Mesh Model

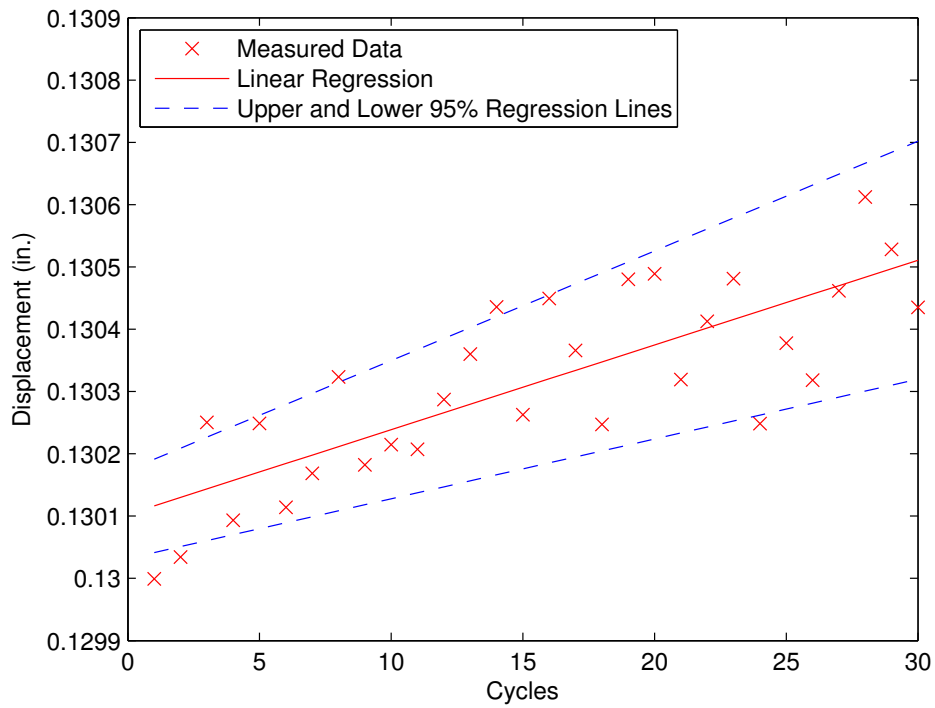


**Figure 4- 44:** Max Displacement for Refined Mesh Model at Constant Loading

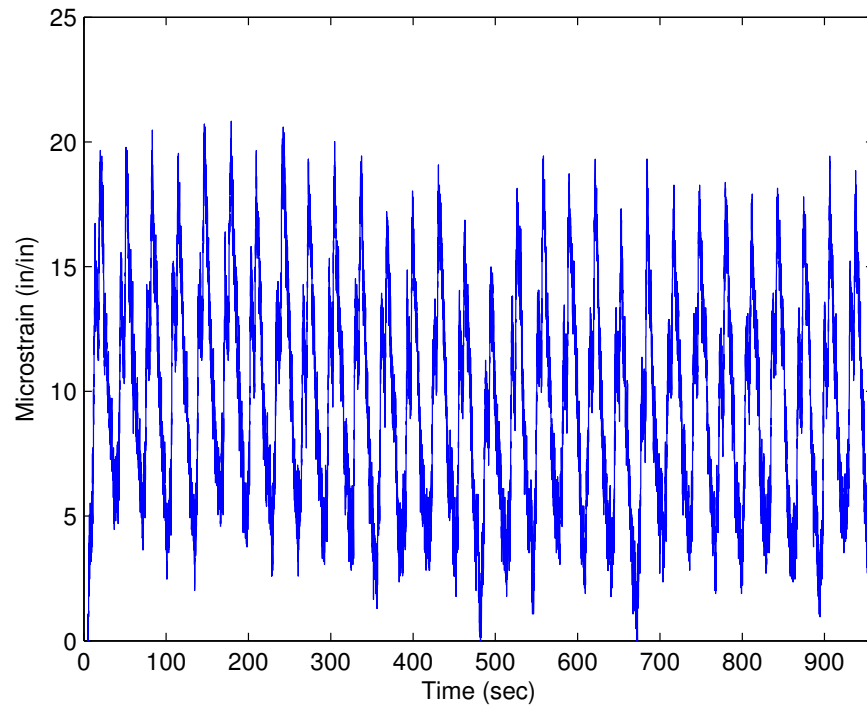


**Figure 4- 45:** Strain History for 30 Constant Trucks for Truss Model

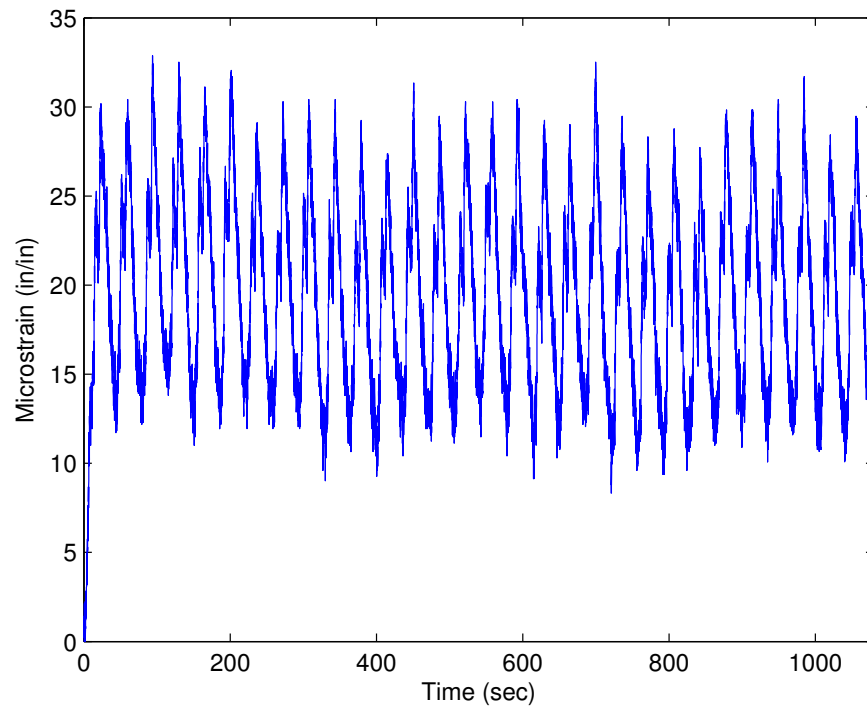


**Figure 4- 46:** Strain History for 30 Constant Trucks for Refined Mesh Model

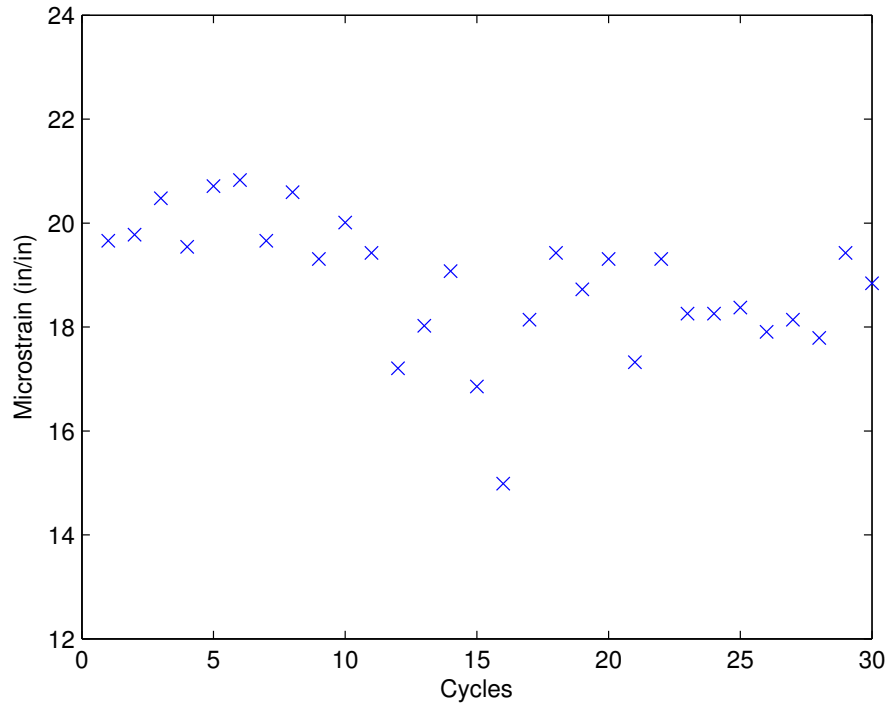


**Figure 4- 47:** Max Strain Truss Model at Constant Loading

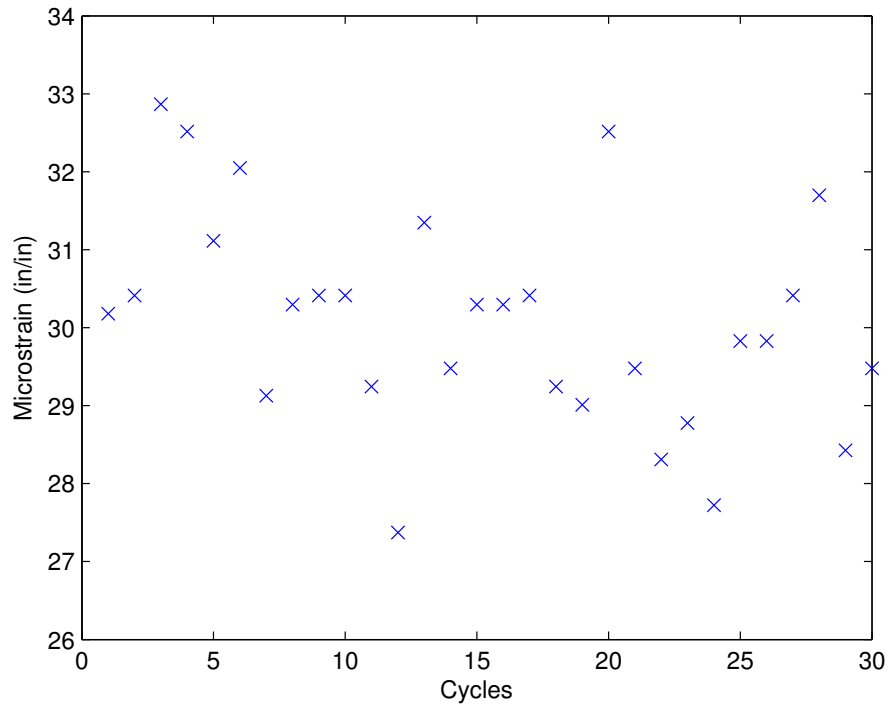


**Figure 4- 48:** Max Strain Refined Mesh Model at Constant Loading

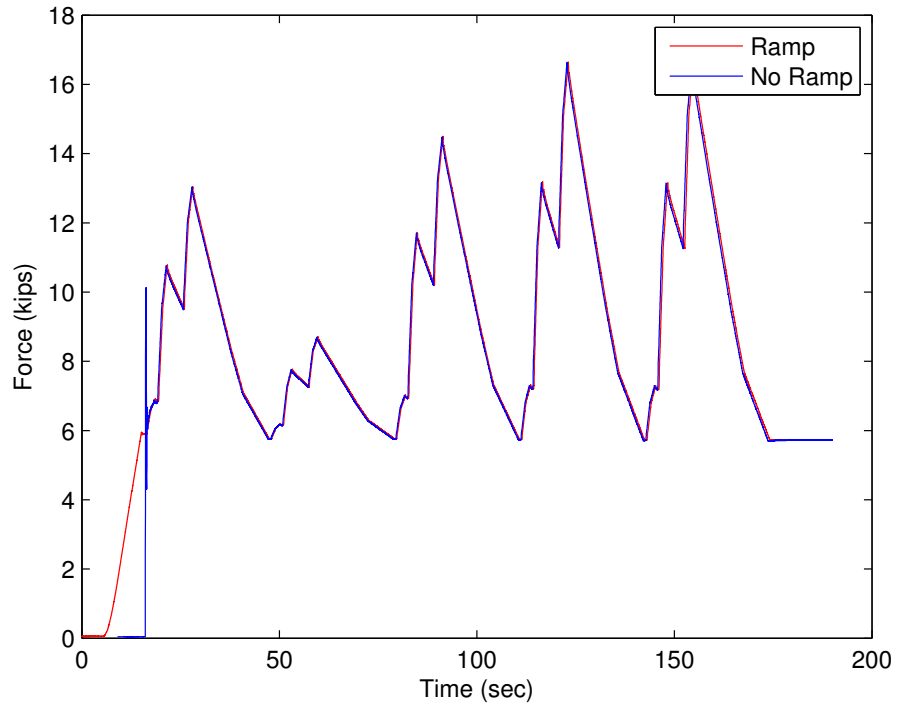


**Figure 4- 49:** Effect of Ramp Loading on Truss Model

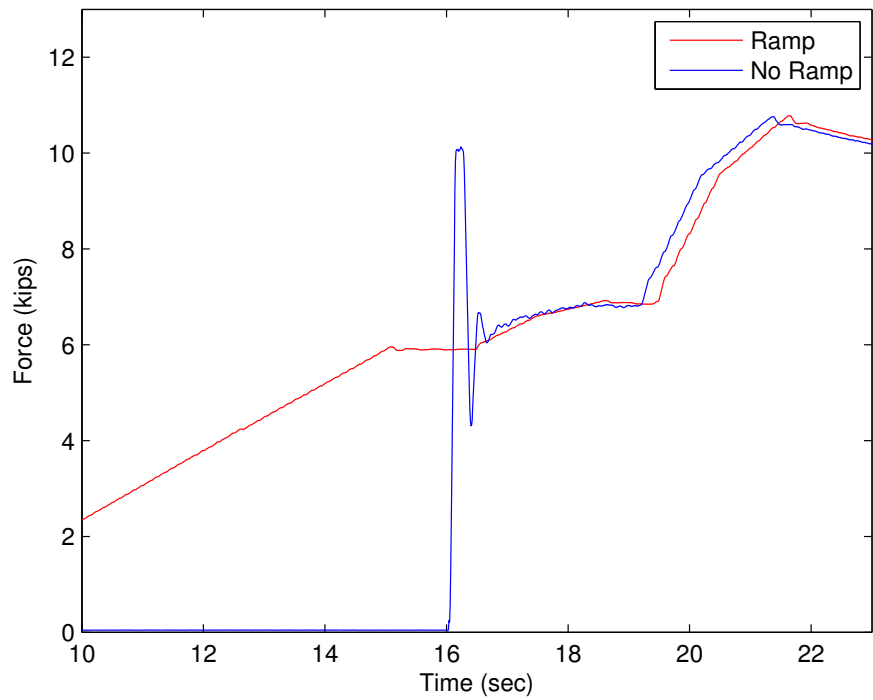


**Figure 4- 50:** Closeup of Ramp Loading for Truss Model

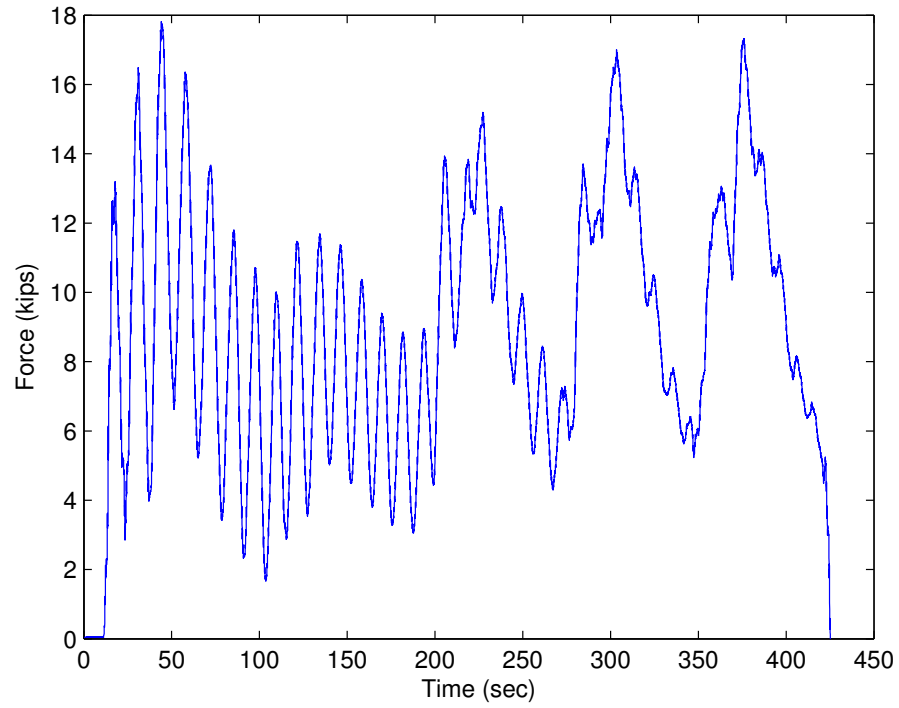


**Figure 4- 51:** Effect of Instantaneous Dead Loading on Model with Mass

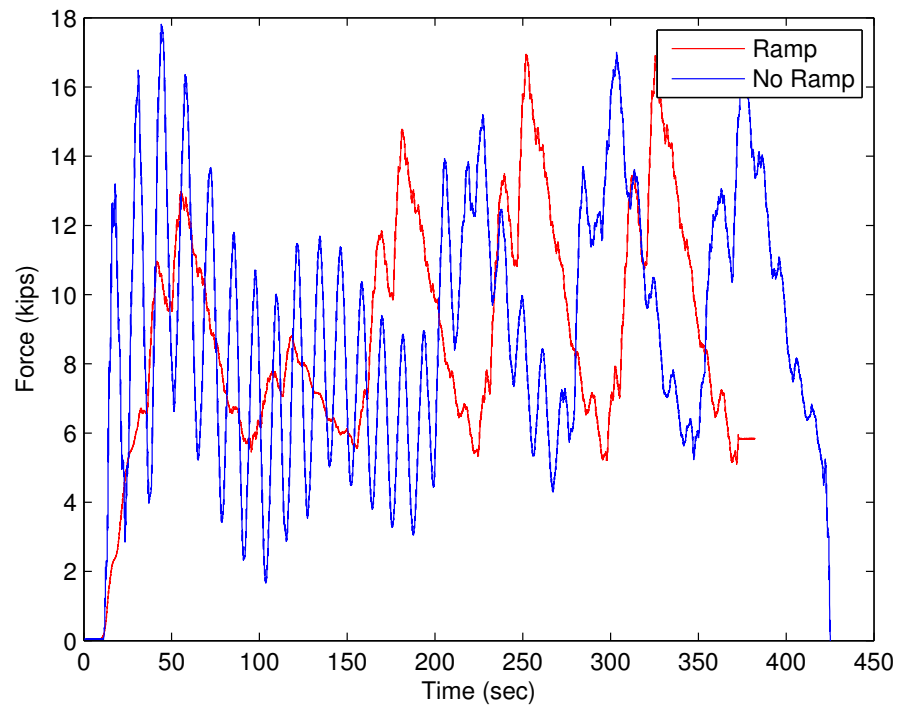


**Figure 4- 52:** Effect of Ramp Loading on Model with Mass

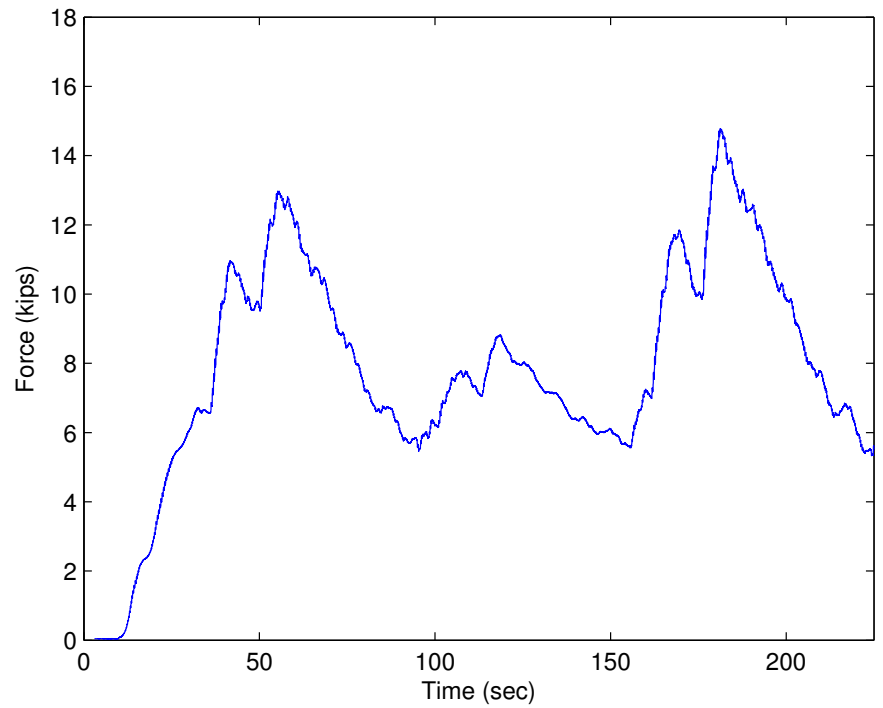


**Figure 4- 53:** Close-up of Ramp Loading on Model with Mass

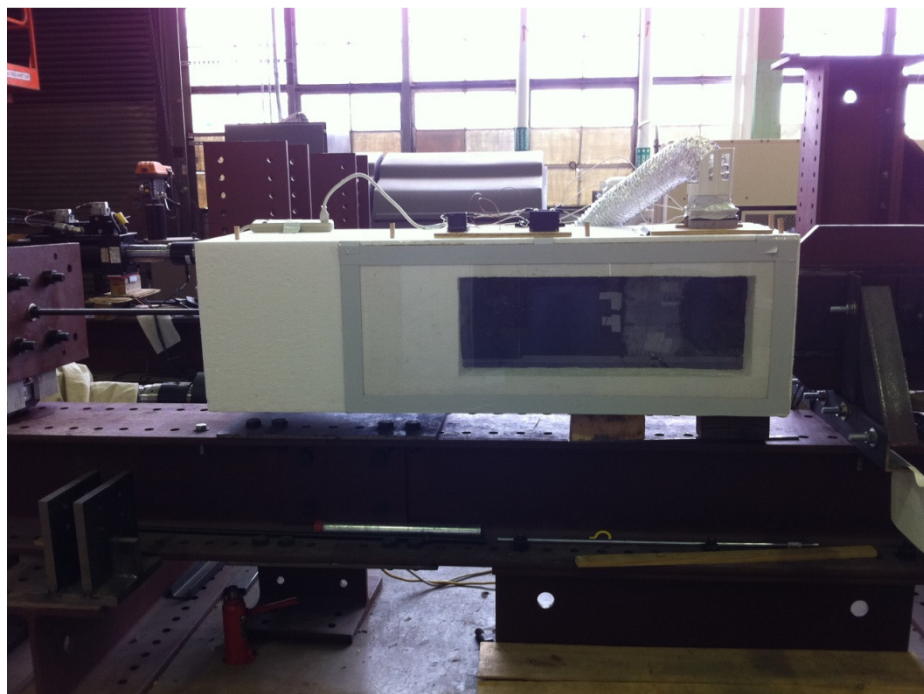


**Figure 4- 54:** Environmental Chamber Front View



**Figure 4- 55:** Environmental Chamber with Front Door Removed

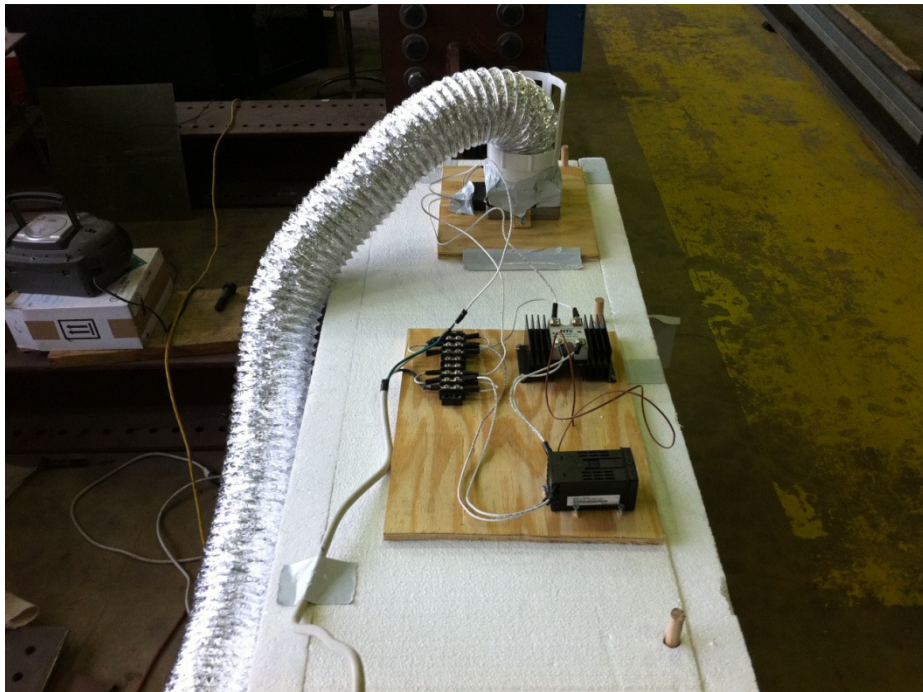


**Figure 4- 56:** Heat Control System for Environmental Chamber

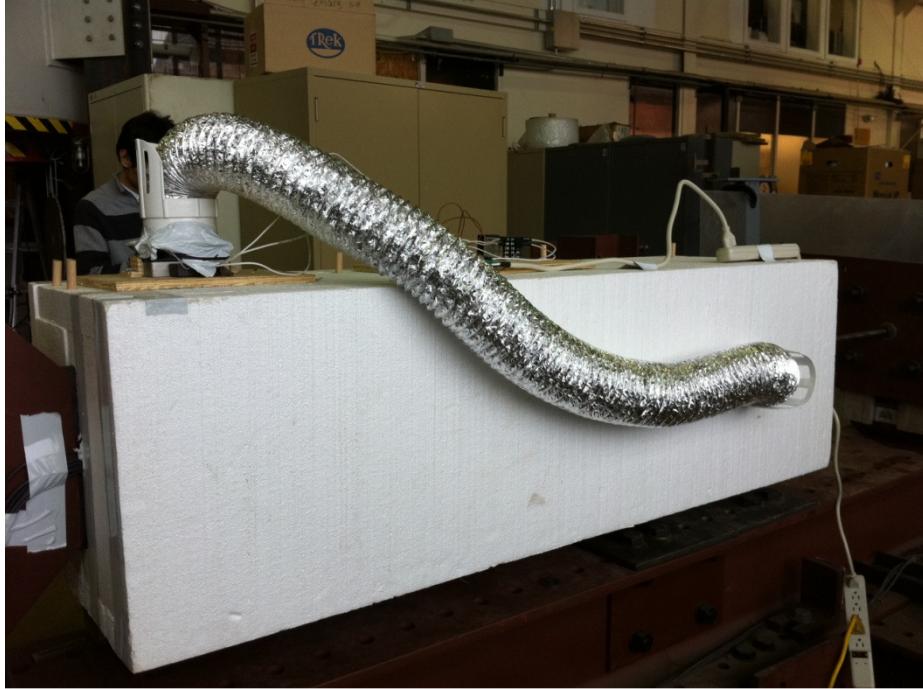


**Figure 4- 57:** Air Circulation Vent in Environmental Chamber

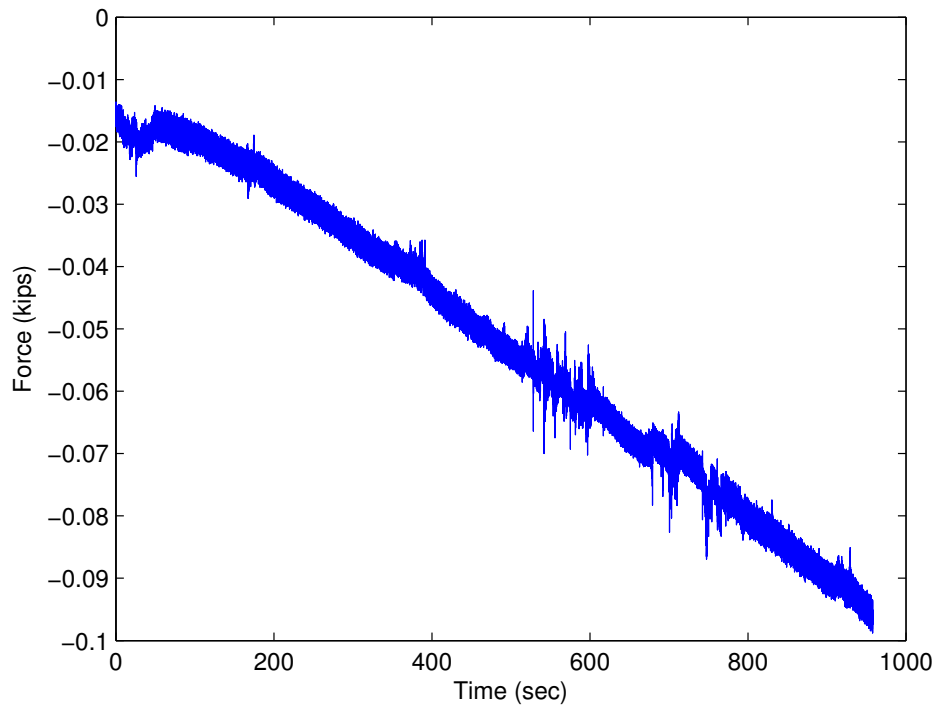


**Figure 4- 58:** Force in Test Specimen as Temperature Increases

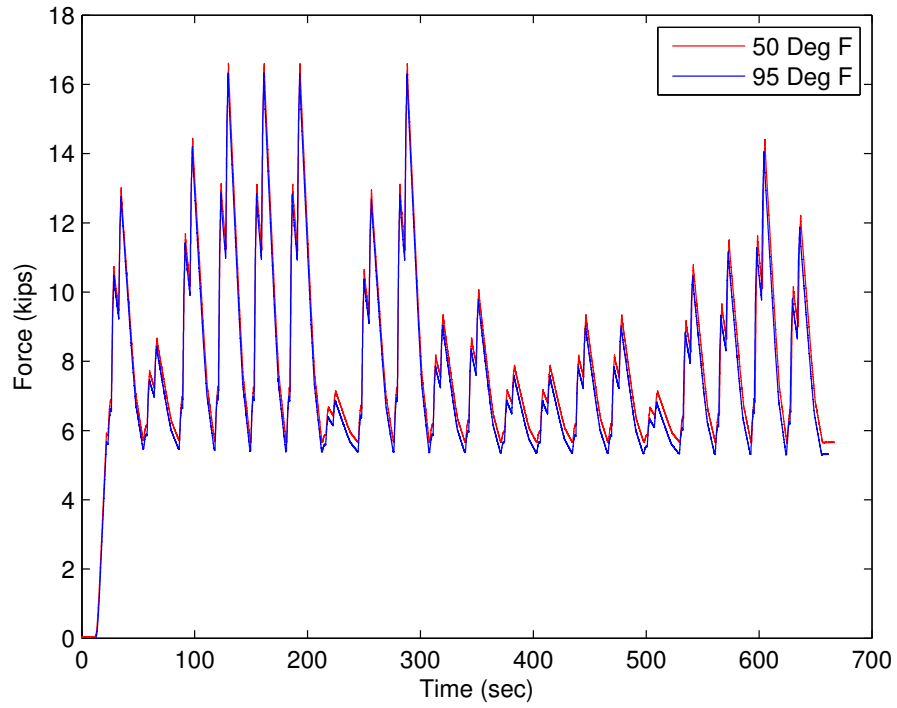


**Figure 4- 59:** Effect of Temperature on Force Applied

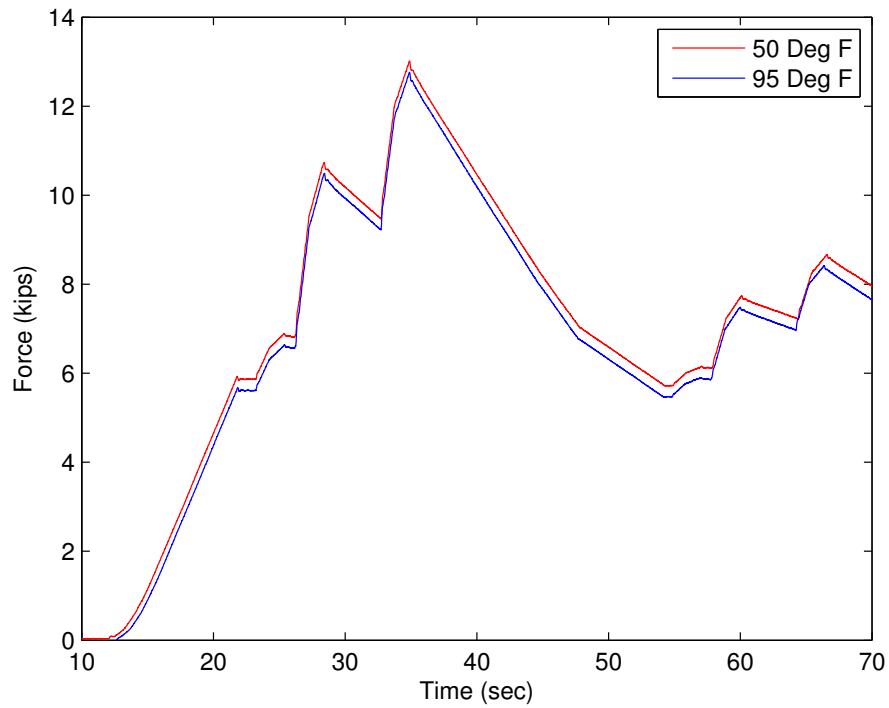


**Figure 4- 60:** Close-up of Temperature Effect on Force History

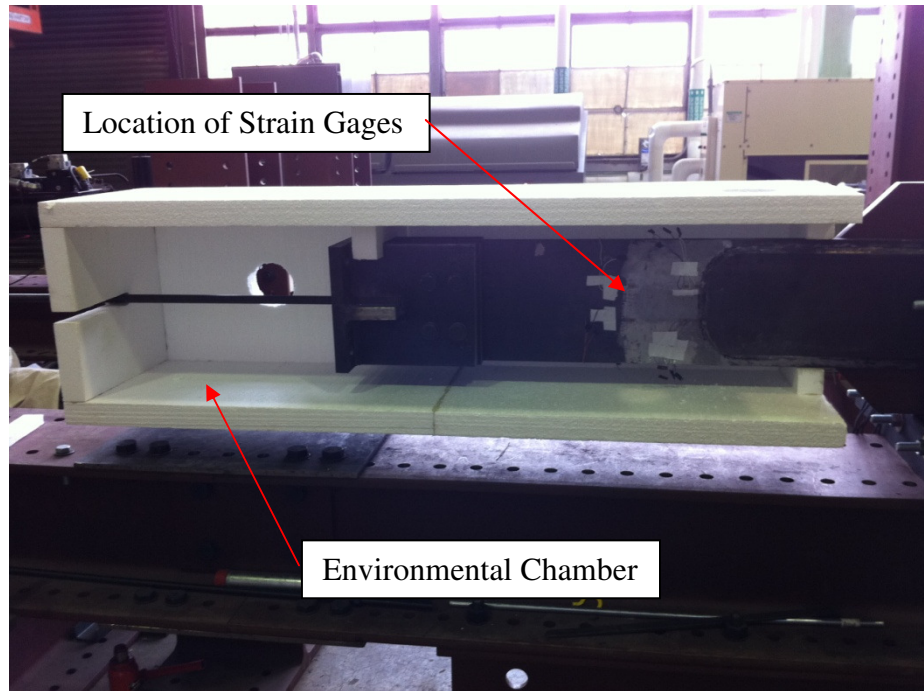


**Figure 4- 61:** Location of Strain Gages in Environmental Chamber

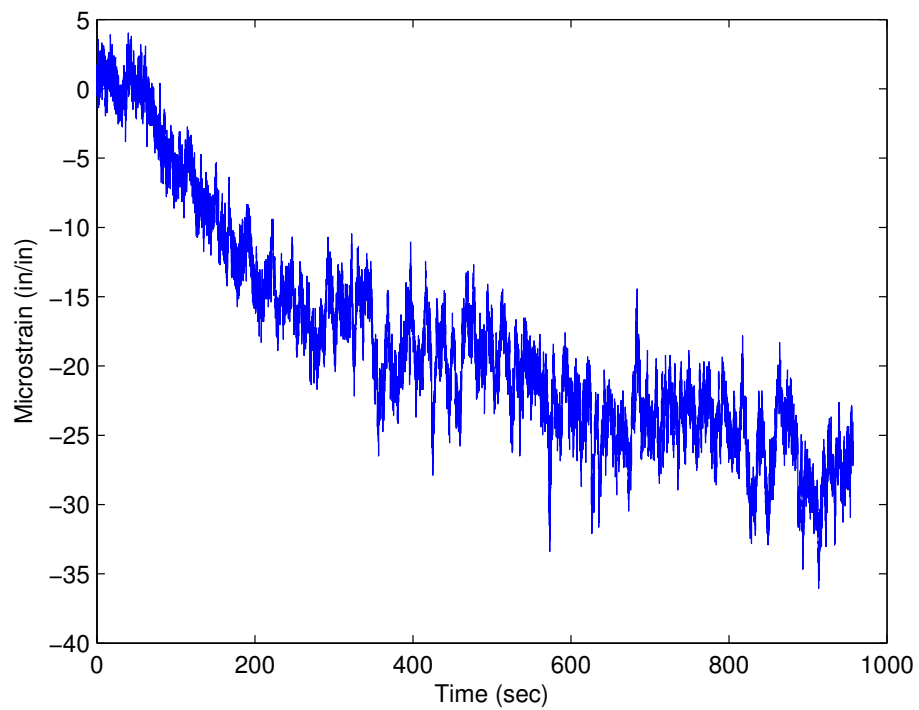


**Figure 4- 62:** Strain Gage Readings as Temperature Increases

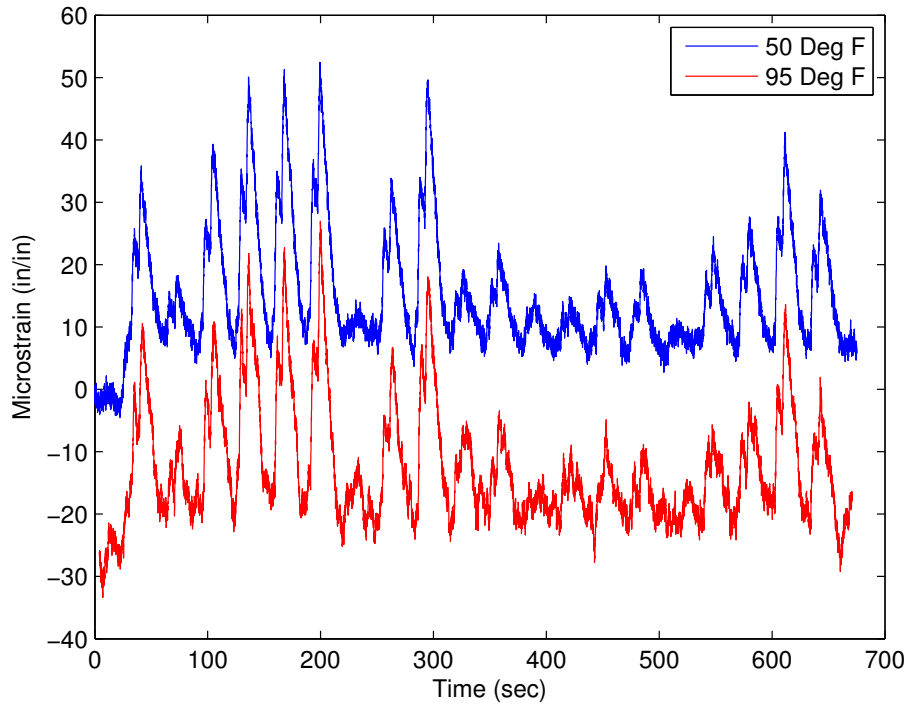


**Figure 4- 63:** Effect of Temperature on Strain Data

## **Chapter 5: Conclusion and Future Work**

### ***5.1 Conclusions***

A hybrid testing setup was implemented based on the Yellow Mill Pond Bridge located on I-95 in Bridgeport, Connecticut. The goal of this hybrid testing setup was to demonstrate how testing of large scale structures could be performed using the hybrid testing methodology and how a hybrid testing platform is ideal for characterizing sensors for structural health monitoring purpose. This hybrid testing method involved combining both physical and virtual models for different components of the bridge and simultaneously combining their responses throughout the testing. Realistic traffic loading was randomly generated based on existing weigh-in-motion data for the Yellow Mill Pond Bridge, applied to this hybrid testing setup, and the overall response of the Yellow Mill Pond Bridge in the this hybrid testing platform was evaluated.

In addition to modeling and performing the hybrid test, a parametric study was undertaken to determine the effects of various parameters on the overall hybrid testing platform. Additionally, controlled environmental testing was also performed on the hybrid test setup for the Yellow Mill Pond Bridge. Elevated temperatures (95°F) were applied to the test specimen to create the temperature environment of a bridge on a hot summer day. It was demonstrated through this elevated temperature testing how the hybrid testing setup creates an effective testbed in evaluating and

validating various sensors at different environmental conditions. Based on these results, the following conclusions can be drawn:

1. The hybrid testing method was successfully implemented to determine the response of an existing highway steel girder bridge subjected to passing traffic loads. From the results of the hybrid testing, the hybrid testing platform can effectively create realistic loading conditions and can physically apply these loading conditions to fabricated, critical locations of the structure at large scale. Furthermore, the overall accuracy of the hybrid testing platform is very close to the expected theoretical results for the response of the Yellow Mill Pond Bridge.
2. By applying realistic loading histories to the test specimen, the hybrid testing platform provides a testbed for evaluating and characterizing structural health monitoring sensors under realistic loading conditions.
3. The stability of the hybrid testing platform at various hydraulic ramp times is dependent on the complexity of the virtual model used.
4. There is an upper bound as to how fast the hybrid test can be performed, and this upper bound is limited by the communication time and computation speed of the components used in the hybrid testing. This upper bound is typically slower than the actual real life loading rate for the hybrid testing facility used in this research.
5. The hybrid testing method can be implemented for a variety of virtual models ranging from basic truss models to complex 2-D refined mesh finite element

models. Furthermore, the dynamic effects of mass and damping can be accurately applied in these virtual models.

6. If a constant dead load is applied throughout the duration of the hybrid test, this dead load should be applied slowly as a ramp load initially before applying the live load. This is particularly important for models that include dynamic effects so that the application of the dead load does not create a step load at the beginning of the testing.
7. The elevated temperature controlled environmental testing demonstrated how the hybrid testing platform can be utilized to create realistic environmental conditions at critical locations of a structure where structural health monitoring sensors will be used. Furthermore, this controlled environmental testing demonstrates how the hybrid testing platform provides the ideal testbed for characterizing and validating structural health monitoring sensors at realistic environmental conditions before these sensors are subject to these conditions in the field.

## ***5.2 Future Work***

The work performed in this research demonstrated how the hybrid testing method can be successfully applied to modeling steel highway girder bridges. Furthermore, it was shown how this testing method could be used to characterize structural health monitoring sensors. However, this is for one specific application of the hybrid testing platform. A variety of other applications exist for which this testing platform could be applied including testing new critical details on bridges and buildings, performing fatigue testing for fatigue critical members of a structure, and evaluating earthquake loadings on a variety of structural details.

At the time of this thesis writing, structural health monitoring sensors are seeing rapid growth in development, but have yet to be widely used across structures in America's transportation infrastructure. For sensors still in their developmental stages, they need to be validated and characterized at a variety of different loading and environmental conditions before full scale field implementation. Future work needs to be performed in validating and characterizing these sensors under various environmental conditions based on the hybrid testing platform demonstrated in this thesis. Furthermore, this thesis focused on elevated temperature environmental testing; further work needs to be undertaken to demonstrate how other environmental conditions including very cold temperatures, humidity, and salt spray can be implemented in this hybrid testing testbed. This will create comprehensive environmental condition testing and validation for structural health monitoring sensors.

It is the author's hope that the use of structural health monitoring sensors will take off within America's infrastructure over the next several decades. These sensors have the potential to help meet the current and future demands to more effectively monitor America's ageing transportation infrastructure and maintain the serviceability and safety of the structures in this system. This thesis shows how to utilize the hybrid testing platform to assess and characterize these structural health monitoring sensors. However, now it is up to other researchers and private corporations to actually develop, assess, and characterize their particular structural health monitoring sensors. Furthermore, opportunities to implement these structural health monitoring sensors need to be created through state DOTs and policy makers in order to promote the widespread use of these sensors. It is the author's hope that one day these sensors are widespread across America's infrastructure and help monitor and maintain this infrastructure into the future.

# Appendix A: WIM Data

Daily GVM versus Class Distribution Summary - Direction 1 Page 1

Date : 10/21/2009 - Wednesday  
 Time : 00:00:00 to 24:00:00  
 Site Identifier : 10504954  
 Site Description : I-95,NB,BETWEEN EXITS 23 & 24,MI.PT.26.31  
 Direction : 1 - I-95,NORTH BOUND  
 Lanes : 1 - SLOW LANE  
           2 - TRAVEL LANE  
           3 - PASSING LANE

Classification : FHWA Classification  
 Mass Units : Kip

GVM	Class00	Class01	Class02	Class03	Class04	Class05	Class06	Class07	Class08	Class09	Class10	Class11	Class12	Class13	Total
7 k	0	4	43338	6945	0	0	0	0	0	1	0	0	0	0	50288
5 k	0	0	5	0	0	7	0	0	0	0	0	0	0	0	12
10 k	0	0	12	1	0	131	0	0	0	0	0	0	0	0	144
15 k	0	0	14	20	0	361	1	0	0	0	0	0	0	0	396
20 k	0	0	11	0	1	379	1	0	44	0	0	0	0	0	436
25 k	0	0	7	0	13	620	5	0	43	1	0	0	0	0	689
30 k	0	0	0	0	5	194	24	0	44	6	0	4	0	0	278
35 k	0	0	0	0	0	6	97	0	23	5	0	1	0	0	139
40 k	0	0	0	0	9	0	175	2	30	8	1	1	0	0	311
45 k	0	0	0	0	26	0	92	0	44	32	0	2	0	0	196
50 k	0	0	0	0	7	0	9	6	77	144	0	3	0	0	246
55 k	0	0	0	0	0	0	0	21	78	352	0	1	2	0	456
60 k	0	0	0	0	0	0	0	14	20	514	0	5	1	0	555
65 k	0	0	0	0	0	0	0	10	4	533	2	32	6	0	587
70 k	0	0	0	0	0	0	0	1	0	593	2	22	11	0	629
75 k	0	0	0	0	0	0	0	0	0	507	4	10	6	0	527
80 k	0	0	0	0	0	0	0	0	0	164	4	3	7	0	178
85 k	0	0	0	0	0	0	0	0	0	10	2	0	5	0	17
90 k	0	0	0	0	0	0	0	0	0	0	0	0	1	0	1
95 k	0	0	0	0	0	0	0	0	0	0	0	0	0	0	0
>95k	0	0	0	0	0	0	0	0	0	0	0	0	0	0	0
Total	0	4	43387	6966	154	1698	406	54	407	2870	15	85	39	0	56085

Daily GVM versus Class Distribution Summary - Direction 1 Page 2

Date : 10/22/2009 - Thursday  
 Time : 00:00:00 to 24:00:00  
 Site Identifier : 10504954  
 Site Description : I-95,NB,BETWEEN EXITS 23 & 24,MI.PT.26.31  
 Direction : 1 - I-95,NORTH BOUND  
 Lanes : 1 - SLOW LANE  
           2 - TRAVEL LANE  
           3 - PASSING LANE

Classification : FHWA Classification  
 Mass Units : Kip

GVM	Class00	Class01	Class02	Class03	Class04	Class05	Class06	Class07	Class08	Class09	Class10	Class11	Class12	Class13	Total
7 k	0	7	57628	9129	0	0	0	0	0	0	0	0	0	0	66764
5 k	0	0	8	0	0	8	0	0	0	0	0	0	0	0	16
10 k	0	0	15	5	0	158	0	0	0	0	0	0	0	0	178
15 k	0	0	10	12	0	495	1	0	0	0	0	0	0	0	519
20 k	0	0	14	0	3	574	4	0	59	1	0	0	0	0	655
25 k	0	0	3	0	17	924	14	0	74	6	0	0	0	0	1038
30 k	0	0	0	0	22	348	25	0	62	10	0	3	1	0	471
35 k	0	0	0	0	15	13	181	1	44	14	0	7	1	0	276
40 k	0	0	0	0	124	0	256	0	39	29	0	1	1	0	450
45 k	0	0	0	0	29	0	114	2	88	77	1	2	1	0	314
50 k	0	0	0	0	4	0	26	13	159	251	1	2	0	0	460
55 k	0	0	0	0	0	0	4	29	108	578	0	14	2	0	735
60 k	0	0	0	0	0	0	1	37	39	988	1	25	6	0	1097
65 k	0	0	0	0	0	0	0	19	2	1131	5	31	9	0	1217
70 k	0	0	0	0	0	0	0	3	0	1163	4	73	14	0	1257
75 k	0	0	0	0	0	0	0	1	0	821	7	36	21	0	896
80 k	0	0	0	0	0	0	0	1	0	368	11	2	13	0	400
85 k	0	0	0	0	0	0	0	0	0	40	4	0	14	0	58
90 k	0	0	0	0	0	0	0	0	0	20	3	0	0	0	23
95 k	0	0	0	0	0	0	0	0	0	0	1	0	0	0	1
>95k	0	0	0	0	0	0	0	0	0	0	0	0	0	0	0
Total	0	7	57678	9146	214	2521	626	106	674	5507	38	220	88	0	76825

Date : 10/23/2009 - Friday  
 Time : 00:00:00 to 10:00:00  
 Site Identifier : 10504954  
 Site Description : I-95,NB,BETWEEN EXITS 23 & 24,MI.PT.26.31  
 Direction : 1 - I-95,NORTH BOUND  
 Lanes : 1 - SLOW LANE  
       : 2 - TRAVEL LANE  
       : 3 - PASSING LANE

Classification : FHWA Classification  
 Mass Units : Kip

GVM	Class00	Class01	Class02	Class03	Class04	Class05	Class06	Class07	Class08	Class09	Class10	Class11	Class12	Class13	Total
7 k	0	4	11570	1929	0	0	0	0	0	0	0	0	0	0	13503
5 k	0	0	0	0	0	2	0	0	0	0	0	0	0	0	2
10 k	0	0	0	1	0	31	0	0	0	0	0	0	0	0	32
15 k	0	0	0	7	0	109	0	0	0	0	0	0	0	0	116
20 k	0	0	1	0	0	128	4	0	8	0	0	0	0	0	141
25 k	0	0	4	0	12	299	4	0	12	3	0	0	0	0	334
30 k	0	0	0	0	9	119	11	0	13	14	0	1	0	0	167
35 k	0	0	0	0	2	3	68	2	8	8	0	0	0	0	91
40 k	0	0	0	0	34	0	94	0	17	13	0	0	0	0	158
45 k	0	0	0	0	9	0	56	0	30	28	0	4	0	0	127
50 k	0	0	0	0	1	0	4	1	67	121	0	4	0	0	198
55 k	0	0	0	0	0	0	0	7	67	244	0	6	0	0	324
60 k	0	0	0	0	0	0	0	3	19	365	0	8	1	0	396
65 k	0	0	0	0	0	0	0	3	3	489	0	48	1	0	544
70 k	0	0	0	0	0	0	0	0	0	554	0	38	9	0	606
75 k	0	0	0	0	0	0	0	0	0	404	0	19	12	0	437
80 k	0	0	0	0	0	0	0	0	0	99	0	1	11	0	116
85 k	0	0	0	0	0	0	0	0	0	15	0	0	2	0	22
90 k	0	0	0	0	0	0	0	0	0	1	0	0	0	0	4
95 k	0	0	0	0	0	0	0	0	0	0	0	0	0	0	0
>95k	0	0	0	0	0	0	0	0	0	0	0	0	0	0	0
Total	0	4	11575	1937	67	691	241	16	244	2358	18	129	38	0	17318

## Appendix B: MATLAB Code

```
function trussarea(h,w,fw,ft,G,E,trussw)
% h = height of girder (ex 60")
% w = thickness of web (ex 1")
% fw = width of flange (ex 12")
% ft = thickness of flange (ex 1")
% G = shear modulus 11200 ksi or 77.2 GPa for steel
% E = elastic modulus 29000 ksi or 200 GPa
% trussw = width of upper chord of truss (ex 60")

%determine deformation on web
A_beam = h*w;
tau = 100/A_beam; %for 100 k load
gamma = tau/G;
deltax = gamma*trussw;
deltax = double(deltax);

%construct model truss
syms A L theta A_vert
C = cos(theta);
S = sin(theta);
C2 = C^2;
S2 = S^2;
CS = C*S;
a = [C2 CS; CS S2];
k=E*A/L*[a -a; -a a];
A_flange = fw*ft;
K_gen=vpa(zeros(8,8));
k_flange=E*A_flange/L*[a -a; -a a];
k_vert=E*A_vert/L*[a -a; -a a];

A_old=A_beam+1; %so initial tolerance is very large
A=A_beam; %upper seed value
upper = A_beam*2;
lower = 0;
tol=1;

%Determine equivalent area of diagonal truss members
while(tol>0.00001)
K = K_gen;
%Element 1
L = trussw;
theta = 0;
map = [1 2 3 4];
k1 = eval(k_flange);
K(map,map) = K(map,map) + k1;

%Element 2
L = h;
theta = pi/2;
map = [3 4 5 6];
k2 = eval(k);
K(map,map) = K(map,map) + k2;
```

```

%Element 3
L = trussw;
theta = pi;
map = [5 6 7 8];
k3 = eval(k_flange);
K(map,map) = K(map,map) + k3;

%Element 4
L = h;
theta = pi/2;
map = [1 2 7 8];
k4 = eval(k);
K(map,map) = K(map,map) + k4;

%Element 5
L = sqrt(trussw^2+h^2);
theta = atan2(h,trussw);
map = [1 2 5 6];
k5 = eval(k);
K(map,map) = K(map,map) + k5;

%Element 6
L = sqrt(trussw^2+h^2);
theta = atan2(h,-trussw);
map = [3 4 7 8];
k6 = eval(k);
K(map,map) = K(map,map) + k6;

%Force vector
remove = [1 2 3 5 7 8];
K(remove,:) = [];
K(:,remove) = [];
P = [50 50]';
d = K\P;
trussdis = double(d(2));
A_old = A;
if (trussdis<deltax)
    upper = A;
    A = (A-lower)/2+lower;
elseif (trussdis>deltax)
    lower = A;
    A = (upper-A)/2+A;
end
tol = abs(A_old-A);
end
A_diagonal_members = A

% Determine effective area of web that should be added to flanges
hw = h-2*ft;
hf = h-ft;
Ae = 0.1875*hw^2*w/hf
A_flange = fw*ft
A_upper_lower_members = Ae+A_flange

```

```

%Deflection at center for beam 20k load

I = 1/12*fw*h^3-1/12*(fw-w)*(h-2*ft)^3
Aweb = (h-2*ft)*w;
l = 720; %in inches, 60 ft
delta_regular = -20*l^3/(48*E*I)
delta_withshear = -20*l^3/(48*E*I)-20*l*l/(4*G*(Aweb+2*fw*ft))

function L=createloadmatrix()
n = 100; %number of trucks
L = zeros(1,3);
for i = 1:n %number of trucks
    t = i*2.5-2.5; %min t for 40mph is 2.45 sec not 4.5 sec
    j = i*3-2;
    L(j:j+2,1) = 40;
    L(j,2) = 1/9;
    L(j+1,2) = 4/9;
    L(j+2,2) = 4/9;
    L(j,3) = t;
    L(j+1,3) = t+0.2386;
    L(j+2,3) = t+0.75;
end
fac=[insert random gross weights determined from probability
distribution function here]; %Factor on loads
for j=1:n
    a=3*j-2;
    b=3*j;
    L(a:b,2)=L(a:b,2).*fac(j);
end
L;

function yellowmillpondloadfile(L,dt)
%This is for the yellow mill pond bridge for opensees. The model has
%already been set up for cars travelling at 40 mph, 100 ft span, and
5 ft
%between 21 nodes.
num = length(L);
v = 40*(5280/60^2); %ft/sec
%size load matrix
total_time = L(num,3)+100/v; %time for last axle to pass completely
over bridge
rem_time = mod(total_time,dt);
mat_length = (total_time-rem_time)/0.01+1; %length of load matrix
M = zeros(21,mat_length); %initialize load matrix
for i = 1:num
    ini_pos = L(i,3)*-v;
    x = ini_pos;
    load = L(i,2);
    t = 0;

```

```

while(x<=100) %100=length of bridge
    if(x>=0 && x<=100)
        x;
        rem = mod(x,5); %remainder
        lower = x-rem;
        upper = lower+5;
        lower_load = (1-rem/5)*load;
        upper_load = (rem/5)*load;
        lower_node = lower/5+1;
        upper_node = lower_node+1;
        %add loads to load matrix
        time=int32(t/dt+1);
        M(lower_node,time) = M(lower_node,time)+lower_load;
        M(upper_node,time) = M(upper_node,time)+upper_load;
    end
    t = t+dt;
    x = x+v*dt;
end
end
M=M+3.76; %3.76 is the dead load in kips

dlmwrite('TimeSeries01.thf', M(1,:), 'delimiter',' ','newline','pc')
dlmwrite('TimeSeries02.thf', M(2,:), 'delimiter',' ','newline','pc')
dlmwrite('TimeSeries03.thf', M(3,:), 'delimiter',' ','newline','pc')
dlmwrite('TimeSeries04.thf', M(4,:), 'delimiter',' ','newline','pc')
dlmwrite('TimeSeries05.thf', M(5,:), 'delimiter',' ','newline','pc')
dlmwrite('TimeSeries06.thf', M(6,:), 'delimiter',' ','newline','pc')
dlmwrite('TimeSeries07.thf', M(7,:), 'delimiter',' ','newline','pc')
dlmwrite('TimeSeries08.thf', M(8,:), 'delimiter',' ','newline','pc')
dlmwrite('TimeSeries09.thf', M(9,:), 'delimiter',' ','newline','pc')
dlmwrite('TimeSeries10.thf', M(10,:), 'delimiter',' ','newline','pc')
dlmwrite('TimeSeries11.thf', M(11,:), 'delimiter',' ','newline','pc')
dlmwrite('TimeSeries12.thf', M(12,:), 'delimiter',' ','newline','pc')
dlmwrite('TimeSeries13.thf', M(13,:), 'delimiter',' ','newline','pc')
dlmwrite('TimeSeries14.thf', M(14,:), 'delimiter',' ','newline','pc')
dlmwrite('TimeSeries15.thf', M(15,:), 'delimiter',' ','newline','pc')
dlmwrite('TimeSeries16.thf', M(16,:), 'delimiter',' ','newline','pc')
dlmwrite('TimeSeries17.thf', M(17,:), 'delimiter',' ','newline','pc')
dlmwrite('TimeSeries18.thf', M(18,:), 'delimiter',' ','newline','pc')
dlmwrite('TimeSeries19.thf', M(19,:), 'delimiter',' ','newline','pc')
dlmwrite('TimeSeries20.thf', M(20,:), 'delimiter',' ','newline','pc')
dlmwrite('TimeSeries21.thf', M(21,:), 'delimiter',' ','newline','pc')

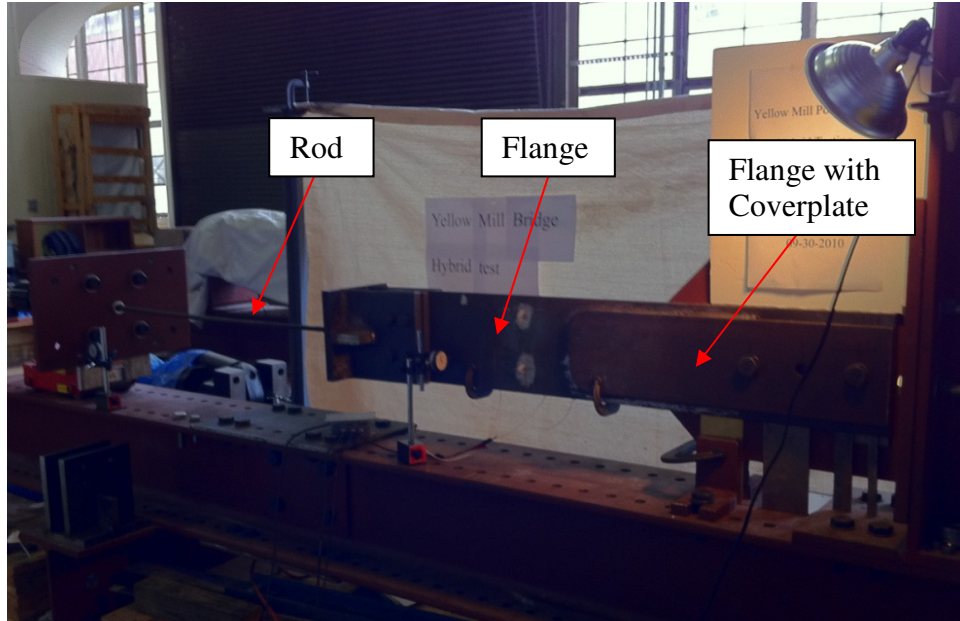
```

## Appendix C: Derivation of Scale Factors

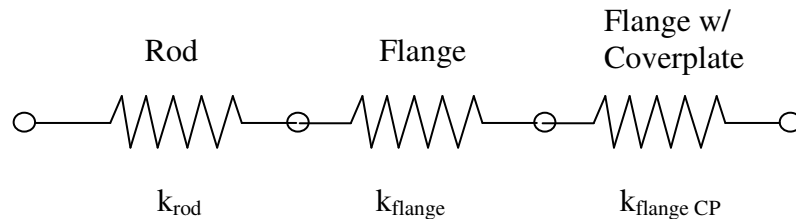
As was described in Section 4.2, due to the 60% scale size of the physical test specimen and the use of a threaded rod fixture to amplify the displacements, it is necessary to apply a scale factor to adjust the test specimen's response during hybrid testing. The basis for these scale factors is that the stress in both the physical test specimen and associated element in the finite element model (i.e., OpenSees here) should be the same. In order for the stress to be the same, the force scale factor must be equal to the ratio of the cross sectional areas for the test specimen and associated element in OpenSees. This force scale factor is denoted below by  $S_{force}$  in the equation below and note that model refers to the OpenSees model and specimen refers to the physical test specimen.

$$S_{force} = \frac{A_{model}}{A_{specimen}} \quad (C-1)$$

The displacement scale factor has to take into account the stiffness from each of the elements in the test specimen. In this hybrid test, a threaded rod fixture was used to amplify the displacement to aid in the data collection. However, this amplified displacement needs to be accounted for in the displacement scale factor. The best way to idealize the test specimen to determine this displacement scale factor is to view the test specimen as a series of springs, which represent each of the elements in the test setup. The following two figures help illustrate this concept:



These three components can be idealized as a series of three springs:



Since all of these components are loaded axially, the stiffness for each of these elements can be determined by  $EA/L$ . With this idealization, the scale factor denoted by  $S_{disp}$  can be derived as follows. Note that  $\delta$  refers to the displacement,  $F$  refers to the force, and  $k$  refers to the stiffness in the following derivation.

$$\begin{aligned}
 S_{disp} &= \frac{\delta_{model}}{\delta_{specimen}} \\
 &= \frac{\frac{F_{model}}{k_{model}}}{\frac{F_{specimen}}{k_{rod}} + \frac{F_{specimen}}{k_{flange}} + \frac{F_{specimen}}{k_{flange\ CP}}}
 \end{aligned}$$

$$= \left( \frac{F_{model}}{F_{specimen}} \right) \cdot \frac{1}{k_{model} \left( \frac{1}{k_{rod}} + \frac{1}{k_{flange}} + \frac{1}{k_{flange CP}} \right)}$$

$$= \left( \frac{A_{model}}{A_{specimen}} \right) \cdot \frac{1}{k_{model} \left( \frac{1}{k_{rod}} + \frac{1}{k_{flange}} + \frac{1}{k_{flange CP}} \right)}$$

Therefore,

$$S_{disp} = (S_{force}) \cdot \frac{1}{k_{model} \left( \frac{1}{k_{rod}} + \frac{1}{k_{flange}} + \frac{1}{k_{flange CP}} \right)} \quad (C-2)$$

From Eqn. C-2, it is evident that both the force scale factor ( $S_{force}$ ) and displacement scale factor ( $S_{disp}$ ) are not independent of each other. In the OpenFresco hybrid testing program for which OpenSees provides the interface, three different parameters need to be specified for the scale factor before the test. These parameters are ctrlDisp, DaqDisp, and DaqForce. The first two parameters, ctrlDisp and DaqDisp, are the displacement scale factors that are applied from OpenSees to the test specimen because displacement control is used in current hybrid testing procedure and from the test specimen response back to OpenSees, respectively. The DaqForce parameter is the scaling factor for the force response from the test specimen for model updating.

The table below summarizes each of these parameters and its value.

Parameter:	Value:
CtrlDisp	$1/S_{disp}$
DaqDisp	$S_{disp}$
DaqForce	$S_{force}$

Note that in the above derivation, the stiffness for each of the components ( $k_{rod}$ ,  $k_{flange}$ , etc.) can be theoretically determined by the axial stiffness of the element  $EA/L$ .

However, often there are other second order displacements of the test specimen that may impact the overall stiffness of the test specimen. Examples include eccentric loading in the components and out of plane displacement during loading. To account for the reduced stiffness these second order effects may cause, the factor  $k_{rod}$  needs to be adjusted to include each of these second order effects. The easiest way to account for these effects is to examine the hysteresis for the test specimen and compare this response and stiffness to the theoretical response found through the previous derivation. This was the method used in this thesis for accounting for the second order displacement effects and was used in determining the scale factors for the results in Section 4.2.

## Bibliography

- Albrecht, P. and Lenwari, A. (2009). "Variable-Amplitude Fatigue Strength of Structural Steel Bridge Details: Review and Simplified Model," *ASCE J. Bridge Engrg.*, 14(4): 226-237.
- American Association of State Highway and Transportation Officials (AASHTO) (2007). *Legal Truck Loads and AASHTO Legal Loads for Posting*. Washington, D.C.
- American Association of State Highway and Transportation Officials (AASHTO) (2007). *Legal Truck Loads and AASHTO Legal Loads for Posting*. Washington, D.C.
- American Association of State Highway and Transportation Officials (AASHTO) (2004). *AASHTO LRFD Bridge Design Specifications*. Washington, D.C.
- American Association of State Highway and Transportation Officials (AASHTO) (1998). *Standard Specifications for Highway Bridges*. Washington, D.C.
- American Association of State Highway and Transportation Officials (AASHTO) (1990). *Guide Specifications for Fatigue Evaluation of Existing Steel Bridges*. Washington, D.C.
- American Society for Metals (ASM) (1976). *Metals Handbook: Failure Analysis and Prevention*, Vol. 10 p. 249. Metals Park, Ohio.
- American Society of Civil Engineers (ASCE) (2009). *2009 Report Card for America's Infrastructure*. Washington, D.C.
- Ayyub, B.M. and McCuen, R.H. (1997). *Probability, Statistics, & Reliability for Engineers*. Chapman and hall/SRC Press, Florida.
- Boresi, Arthur P., and Schmidt, Richard J. (2003). *Advanced Mechanics of Materials*. John Wiley & Sons, Inc., New Jersey.
- Chang, P.C., Flatau, A., and Liu, S.C. (2003). "Review paper: Health monitoring of civil infrastructure." *Structural Health Monitoring*, 2(3), 257-267.
- Chopra, Anil K. (2007). *Dynamics of Structures Theory and Applications to Earthquake Engineering*. Pearson Prentice Hall, New Jersey.
- Chotickai, Piya, and Bowman, Mark D. (2006). "Truck Models for Improved Fatigue Life of Steel Bridges." *Journal of Bridge Engineering*, 11(1), 71-80.

- Chotickai, Piya (2004). "Fatigue Reliability-Based Analysis Methods for Evaluation of Steel Bridge Structures." Ph.D. dissertation, Purdue University.
- Connecticut Department of Transportation: Bureau of Policy and Planning (2009). *Traffic Monitoring and Data Analysis for I-95 Weight Station in Fairfield, Connecticut*.
- Daher, Bassam (2002). "Use of Sensors in Monitoring Civil Structures." Ph.D. dissertation, Massachusetts Institute of Technology.
- Dexter, Robert J., Connor, Robert J., and Mahmoud, Hussam (2005). "Review of Steel Bridges with Fracture Critical Elements." *Transportation Research Record*, 1928, 75-82.
- Fisher, J.W., Kulak, G. L., and Smith, I. F. C. (1998). "A Fatigue Primer for Structural Engineers." National Steel Bridge Alliance, American Institute of Steel Construction.
- Fischer, J.W., Slockbower, R.E., Hausammann, H, and Pense, A.W. (1981). "Long Time Observation of a Fatigue Damaged Bridge." *Journal of the Technical Councils of ASCE*, 107(TC1), 55-71.
- Fraser, M., Elgamal, A., He, X., and Conte, J. P. (2010). "Sensor Network for Structural health Monitoring of a Highway Bridge." *Journal of Computing in Civil Engineering*, 24(1), 11-24.
- Guzda, M., Bhattacharya, B., and Mertz, D. (2007). "Probabilistic Characterization of Live Load Using Visual Counts and In-Service Strain Monitoring." *Journal of Bridge Engineering*, 12(1), 130-134.
- Kim, S., Pakzad, S., Culler, D., Demmel, J., Fenves, G., Glaser, S., and Turon, M. (2007). "Health Monitoring of Civil Infrastructures Using Wireless Sensor Networks." University of California at Berkeley.
- Koerner, Brendan I. (2003). "Intel's Tiny Hope for the Future." *Wired Magazine*, 11.08
- Laman, J.A., and Nowak, A.S. (1996). "Fatigue-Load Models for Girder Bridges." *Journal of Structural Engineering*, 122(7), 726-733.
- Mazzoni, Silvia, et al. (2009). *Open system for Earthquake Engineering Simulation User Command-Language Manual*. Pacific Earthquake Engineering Research Center, University of California, Berkeley.

- McKenna, F.T. (1997). *Object-oriented finite element programming: frameworks for analysis, algorithms and parallel computing*. Ph.D. Thesis, University of California, Berkeley, CA, United States. 1997.
- O'Brien, Eugene, et al. (2006). "Bridge Dynamics and Loading." *Bridge and Infrastructure Research in Ireland: Symposium 2006*.
- Scott, Michael H., and Kidarsa, Adrian (2006). "Rating of Highway Bridges Using OpenSees and Tcl." 13<sup>th</sup> Annual Tcl/Tk Conference. Naperville, Illinois.
- Schellenberg, Andreas, et al. (2009). *OpenFresco Framework for Hybrid Simulation: Simulation Finite Element Adapter Experimental Control Example*. Berkeley, California.
- Schellenberg, Andreas, Kim, H., Mahin, S.A. , Fenves, G.L. "Environment independent implementation of a software framework for fast local and geographically distributed hybrid simulations." The 14th World Conference on Earthquake Engineering, Beijing, Oct 12 2008
- Schellenberg, Andreas, Mahin, Stephen A., and Fenves , Gregory L. "Application of an experimental software framework for international hybrid simulation." 4<sup>th</sup> international conference on earthquake engineering, Taipei, Taiwan, Oct 12, 2006
- Sivakumar, Bala, et al. (2008). *Protocols for Collecting and Using Traffic Data in Bridge Design*. Transportation Research Board of the National Academies.
- Snyder, R.E., Likins, G.E., and Moses, F. (1985). "Loading spectrum experienced by bridge structures in the United States." *Report No. FHWA/RD-85/012*, Bridge Weighing Systems Inc., Warrensville, Ohio.
- Szerszer, M.M., Nowak, A. S., and Laman, J.A. (1999). "Fatigue Reliability of Steel Bridges." *Journal of Constructional Steel Research*, 52, 83-92.
- Takamori, Hiroyuki, and Fisher, John W. (2000). "Tests of Large Girders Treated to Enhance Fatigue Strength." *Transportation Research Record*, 1696 (580093).
- Zhou, Y.E. (2006). "Assessment of Bridge Remaining Fatigue Life through Field Strain Measurement," *ASCE J. Bridge Engrg.*, 11(6): 737-744.